Quantum oscillations and decoherence due to electron-electron interaction in metallic networks and hollow cylinders

Christophe Texier,[1,2] Pierre Delplace,[2] and Gilles Montambaux[2]

[1]*Laboratoire de Physique Théorique et Modèles Statistiques, UMR 8626 du CNRS, Université Paris-Sud, 91405 Orsay, France*
[2]*Laboratoire de Physique des Solides, UMR 8502 du CNRS, Université Paris—Sud, 91405 Orsay, France*

We have studied the quantum oscillations of the conductance for arrays of connected mesoscopic metallic rings, in the presence of an external magnetic field. Several geometries have been considered: a linear array of rings connected with short or long wires compared to the phase coherence length, square networks, and hollow cylinders. Compared to the well-known case of the isolated ring, we show that for connected rings, the winding of the Brownian trajectories around the rings is modified, leading to a different harmonics content of the quantum oscillations. We relate this harmonics content to the distribution of winding numbers. We consider the limits where coherence length L_φ is small or large compared to the perimeter L of each ring constituting the network. In the latter case, the coherent diffusive trajectories explore a region larger than L, whence a network-dependent harmonics content. Our analysis is based on the calculation of the spectral determinant of the diffusion equation for which we have a simple expression on any network. It is also based on the hypothesis that the time dependence of the dephasing between diffusive trajectories can be described by an exponential decay with a single characteristic time τ_φ (model A). At low temperature, decoherence is limited by electron-electron interaction, and can be modeled in a one-electron picture by the fluctuating electric field created by other electrons (model B). It is described by a functional of the trajectories and thus the dependence on geometry is crucial. Expressions for the magnetoconductance oscillations are derived within this model and compared to the results of model A. It is shown that they involve several temperature-dependent length scales.

I. INTRODUCTION

Understanding which processes limit phase coherence in electronic transport is an important issue in mesoscopic physics. Such phenomena such as weak localization or universal conductance fluctuations are well understood to result from phase coherence effects limited at a given time (or length) scale called phase coherence time τ_φ (or phase coherent length L_φ). This explains the interest in studying quantum corrections to the classical conductivity: to provide a powerful experimental probe of phase coherence in weakly disordered metals and furnish some informations on the microscopic mechanisms responsible for the limitation of quantum coherence. This limitation originates from the coupling of electrons to external degrees of freedom such as magnetic impurities or phonons.[1,2] It also results from the interaction among electrons themselves. The physical origin of this decoherence in weakly disordered metals has been understood in the pioneering paper of Altshuler, Aronov, and Khmelnitskii (AAK).[3] In a one electron picture, it is due to the fluctuations of the electric field created by the other electrons. In a quasi-one-dimensional (1D) wire, these authors showed that this mechanism leads to the following temperature dependence of the dephasing time $\tau_\varphi(T) \propto T^{-2/3}$. This power law can be understood qualitatively as follows: the typical dephasing is proportional to the fluctuations of the electric potential, which themselves are known from Nyquist theorem to be proportional to the temperature T and to the resistance of the sample. For an infinite wire, the relevant fluctuations are limited to the scale of the coherence length itself. Consequently, the dephasing time has the structure: $\hbar/\tau_\varphi = k_B T/g(L_\varphi)$, where $g(L_\varphi)$ is the dimensionless conduc-

tance at the length scale L_φ. For a quasi-1D conductor, the conductance is linear in length and the length scales as the square root of time. Therefore the function $g(L_\varphi)$ scales as $\sqrt{\tau_\varphi}$, whence the above power law.

More recently, Ludwig and Mirlin[4] and two of the authors[5] considered the geometry of a ring, and they showed that the damping of magnetoresistance oscillations could be described with a different temperature dependence of the dephasing time $\tau_\varphi(T) \propto T^{-1}$. This new behavior can be qualitatively understood by considering that the diffusive trajectories encircle the ring and all have a length equal to the perimeter L of the ring, so that the relevant resistance is the resistance of the ring itself. As a result: $\hbar/\tau_\varphi = k_B T/g(L)$.

In Ref. 5 we have shown how the dephasing on a ring depends on the nature of the diffusive trajectories: the fluctuations of the electric potential affect differently trajectories which encircle the ring and trajectories which do not encircle it. Within this framework, we have analyzed magnetoresistance experiments performed on a square network of quasi-1D wires, and we have found that indeed two characteristic lengths with two different temperature dependences could be extracted from the data.[6] These recent considerations have led us to the general conclusion that the dephasing depends on the geometry of the system considered.

The purpose of this paper is to analyze the dephasing process and to calculate the weak localization correction in different geometries, where the decoherence induced by electron-electron interaction may have a more complex structure. In order to address this question, it is important to understand that the weak localization correction depends on two ingredients: one is the probability to have pairs of reversed trajectories, which is related to the return probability

$\mathcal{P}(t)$ for a diffusive particle after a time t, the other is the nature of the dephasing process itself. Schematically, the weak localization correction to the conductivity can be written as

$$\Delta\sigma \sim -\int_0^\infty dt\, \mathcal{P}(t)\langle e^{i\Phi(t)}\rangle, \qquad (1)$$

where $\langle e^{i\Phi(t)}\rangle$ is the average dephasing accumulated along a diffusive trajectory for a time t. The return probability has been analyzed in Ref. 7 for various types of networks. Its Laplace transform, the spectral determinant, can be simply calculated from the parameters of the network. More complex is the analysis of the dephasing process itself. A simple and natural ansatz would be to assume an exponential decay $\langle e^{i\Phi(t)}\rangle = e^{-t/\tau_\varphi}$. This assumption is correct when the dephasing is due to random magnetic impurities or electron-phonon scattering. For electron-electron interaction the analysis of the AAK result for a wire shows that time dependence is not exponential:[8] $\langle e^{i\Phi(t)}\rangle_{ee} \neq e^{-t/\tau_\varphi}$. The qualitative reason stands again on the fact that dephasing can be described as due to the fluctuations of the electric potential due to other electrons. Then, one may understand that this dephasing depends on the nature of the trajectories and is not exponential. The main goal of this paper is to describe this dephasing for complex networks and to generalize the known results of the infinite wire and the ring.

The paper is organized as follows: In Sec. II, we recall the physical basis at the origin of this work and in Sec. III we present the general formalism appropriate for our study. In the next sections, we consider successively more and more complex geometries. In Sec. IV, we recall known results for the infinite wire and the ring. In Sec. V, we consider the case of a ring attached to arms and show how the harmonics of the magnetoresistance oscillations are reduced by the existence of the arms. The situation is the same for a chain of rings connected through arms longer than the coherence length. When rings become close to each other the dephasing in one ring is strongly modified by the winding trajectories in the neighboring rings. This is discussed in Sec. VI. The case of an infinite regular network is much more difficult to address since the hierarchy of diffusive trajectories is difficult to analyze, and we have used the limit of the infinite plane as a guideline (Sec. VII). Finally the case of a hollow cylinder (Sec. VIII) is quite interesting since it combines trajectories winding around the axis of the cylinder and two-dimensional (2D) trajectories. Throughout the paper, we shall consider two situations, respectively, denoted by model A and model B: the case where the dephasing has a simple exponential time dependence, and the case where the dephasing is induced by electron-electron interaction. We shall systematically discuss the analogies and the differences between these two situations.

II. BACKGROUND

In a weakly disordered metal, due to elastic scattering by impurities, the classical conductivity reaches a finite value at low temperature, given by the Drude conductivity

$\sigma_0 = ne^2\tau_e/m$, where n is the electronic density and τ_e is the elastic scattering time. Quantum interferences are responsible for small quantum corrections to the Drude result. One important contribution, which survives averaging over the disorder,[9–11] comes from interferences of reversed closed electronic trajectories, and therefore diminishes the conductivity. This quantum contribution to the *average* conductivity is called the *weak localization* (WL) correction. It has been expressed as Eq. (1), where the function $\langle e^{i\Phi(t)}\rangle$ describes dephasing and cut off the large time contributions. A simple exponential decay $\langle e^{i\Phi(t)}\rangle = e^{-t/\tau_\varphi}$ is usually assumed (denoted model A in the present paper). τ_φ is the *phase coherence time*, related to the *phase coherence length* $L_\varphi = \sqrt{D\tau_\varphi}$, where D is the diffusion constant of electrons in the disordered metal. From Eq. (1), we obtain the WL correction in a wire $\Delta\sigma^{(1D)} \sim -\int_{\tau_e}^{\tau_\varphi}\frac{dt}{\sqrt{t}} \sim -\sqrt{\tau_\varphi} \sim -L_\varphi$ and in a plane $\Delta\sigma^{(2D)} \sim -\int_{\tau_e}^{\tau_\varphi}\frac{dt}{t} \sim -\ln(\tau_\varphi/\tau_e)$ (diffusion sets in after a time τ_e, hence the lower cutoff in the integrals). In practice, the WL is a small correction to the Drude conductivity and it can be extracted thanks to its sensitivity to a magnetic field. In the presence of a magnetic field, the contribution of a closed diffusive trajectory $\mathcal{C}$ is multiplied by $e^{2ie\phi_\mathcal{C}/\hbar}$, where $\phi_\mathcal{C}$ is the magnetic flux through the loop. This phase factor comes from the interference of the *two* reversed electronic trajectories, whence the factor 2. After summation over all loops, the additional magnetic phase is responsible for the vanishing of the contributions of loops such that $\phi_\mathcal{C} \gtrsim \phi_0$, where $\phi_0 = h/e$ is the flux quantum. Therefore the magnetic field provides an additional cutoff at time $\tau_\mathcal{B}$ corresponding to diffusive trajectories encircling one flux quantum. In a narrow wire of width w we have $\tau_\mathcal{B}^{(1D)} \sim \phi_0^2/(Dw^2\mathcal{B}^2)$ and in a thin film (plane) $\tau_\mathcal{B}^{(2D)} \sim \phi_0/(D\mathcal{B})$ (see Refs. 1 and 2). The two cutoffs are added "à la Matthiessen"[12,13] as $1/\tau_\varphi \rightarrow 1/\tau_\varphi + 1/\tau_\mathcal{B}$; this leads to a smooth dependence of the WL correction as a function of the magnetic field.

The above discussion concerns homogeneous devices (like a wire or a plane). Another experimental setup appropriate to study quantum interferences and extract the phase coherence length is a metallic ring or an array of rings. In this case the topology constrains the magnetic flux intercepted by the rings to be an integer multiple of the flux per ring ϕ (we neglect for the moment the penetration of the magnetic field in the wires): $\phi_\mathcal{C} = n\phi$ with $n \in \mathbb{Z}$. This gives rise to Aharonov-Bohm (AB) oscillations of the conductance as a function of the flux with period ϕ_0. Disorder averaging is responsible for the vanishing of these ϕ_0-periodic oscillations: only survive the contributions of the reversed electronic trajectories leading to WL correction oscillations, known as Al'tshuler-Aronov-Spivak (AAS) oscillations,[14,15] with a period *half* of the flux quantum. It will be convenient to introduce the harmonics $\Delta\sigma_n$ of the periodic WL correction. An important motivation for considering the harmonic content $\Delta\sigma_n$ in networks, is that it allows to decouple the two effects of the magnetic field:[16] the rapid AAS oscillations ($\Delta\sigma_{n\neq 0}$) and the penetration of the magnetic field in the wires, responsible for a smooth decrease in the MC at large field ($\Delta\sigma_0$). Since the nth harmonic is given by contributions of loops encircling n fluxes we can write

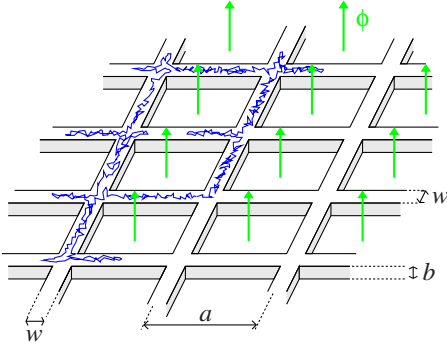FIG. 1. (Color online) A square metallic network submitted to a magnetic field. Schematic picture of a closed diffusive trajectory winding a flux 2ϕ is represented (ϕ is the flux per elementary plaquette).

$$\Delta\sigma_n = -\frac{2e^2 D}{\pi s}\int_0^\infty dt\, \mathcal{P}_n(t)e^{-t/\tau_\varphi}, \qquad (2)$$

where $\mathcal{P}_n(t)$ is the return probability after a time t having encircled n fluxes. s is the cross section of the wires. In an isolated ring of perimeter L, this probability reads $\mathcal{P}_n^{\mathrm{ring}}(t) = \frac{1}{\sqrt{4\pi Dt}}\exp-\frac{(nL)^2}{4Dt}$. Integral (2) gives[14]

$$\Delta\sigma_n^{\mathrm{AAS}} = -\frac{2e^2}{hs}L_\varphi e^{-|n|L/L_\varphi}, \qquad (3)$$

where $L_\varphi = \sqrt{D\tau_\varphi}$ is the phase coherence length. Note that $\Delta\sigma_{-n} = \Delta\sigma_n$ follows from the symmetry under reversing the magnetic field; in the following we will simply consider $n \geq 0$. The exponential decay of the harmonics directly originates from the diffusive nature of the winding around the ring: for a time $t \sim \tau_\varphi$, the typical winding scales as $n_t \sim \sqrt{Dt}/L \sim L_\varphi/L$. The AAS oscillations were first observed in narrow metallic hollow cylinders[17,18] and in large metallic networks.[15,19,20]

Although the simple behavior (3) has been used to analyze AAS or AB oscillations[21] in many experiments until recently (see, for example, Refs. 10 and 22), a realistic description of a network made of connected rings leads to harmonics with a L/L_φ dependence, *a priori* quite different from the simple exponential prediction (3) for two reasons related to the nontrivial *topology* of the networks.

(i) *Winding properties of diffusive loops in networks*. Consider for example the square network of Fig. 1 made of rings of perimeter $L = 4a$. For $L_\varphi \ll L$, an electron unlikely keeps its phase coherence around a ring; therefore AAS oscillations are dominated by trajectories enlacing one ring only and all rings can be considered as independent. In the opposite regime[23] $L_\varphi \gtrsim L$, the interfering electronic trajectories explore regions much larger than the ring perimeter L. In this case, winding properties are more complicated (Fig. 1) and the probability $\mathcal{P}_n(t)$ may strongly differ from the one obtained for a single ring $\mathcal{P}_n^{\mathrm{ring}}(t)$. A theory must be developed to account for these topological effects, which leads to an harmonic content quite different from Eq. (3). This was done in Refs. 25–29 for large regular networks. This theory was later extended in Ref. 30 in order to deal with arbitrary

networks, properly accounting for their connections to contacts.[31]

(ii) *e-e interaction leads to geometry-dependent decoherence*. Not only the winding probability $\mathcal{P}_n(t)$ involved in Eq. (2) is affected by the nontrivial topology of networks, but also $\langle e^{i\Phi(t)}\rangle = e^{-t/\tau_\varphi}$ describing the nature of phase coherence relaxation is replaced by a more complex function. When decoherence is due to *e-e* interaction, the dominant phase-breaking mechanism at low temperature, this relaxation is not described by a simple exponential anymore. This situation will be referred as model B throughout this paper. Such decoherence can be modeled in a one-electron picture by including dephasing due to the fluctuating electromagnetic field created by the other electrons.[3] Therefore the pair of reversed interfering trajectories picks up an additional phase $\Phi[\mathcal{C}]$ that depends on the electric potential V. Averaging over the fluctuations of the potential leads to the relaxation of phase coherence. The harmonics present the structure

$$\Delta\sigma_n \sim -\int_0^\infty dt\, \mathcal{P}_n(t)\langle e^{i\Phi[\mathcal{C}_t^n]}\rangle_{V,\mathcal{C}_t^n}, \qquad (4)$$

where averaging is taken over the potential fluctuations $\langle\cdots\rangle_V$ and over the loops with winding n for time t, $\langle\cdots\rangle_{\mathcal{C}_t^n}$. In a quasi-1D wire, the relaxation of phase coherence involves an important length scale, the *Nyquist length* L_N, characterizing the efficiency of the electron-electron interaction to destroy the phase coherence in the wire. We will see that, in networks also, the Nyquist length is the intrinsic length characterizing decoherence due to *e-e* interaction. It is given by[3,33–36]

$$L_N = \left(\frac{\hbar^2 \sigma_0 D s}{e^2 k_B T}\right)^{1/3} = \left(\frac{\alpha_d}{\pi}N_c \ell_e L_T^2\right)^{1/3}, \qquad (5)$$

where s is the cross section of the wire. We have rewritten the Nyquist length in terms of the thermal length $L_T = \sqrt{\hbar D/k_B T}$, the elastic mean-free path ℓ_e, and the number of conducting channels N_c (not including spin degeneracy); α_d is a dimensionless constant depending on the dimension ($\alpha_d = V_d/V_{d-1}$, where V_d is the volume of the unit sphere in dimension d).[37] In the following we will set $\hbar = k_B = 1$. In the infinite wire, the decaying function $\langle e^{i\Phi}\rangle_{V,\mathcal{C}_t}$ can only involve the unique length L_N. A precise analysis of the magnetoconductance (MC) of the wire shows that, in this case, the calculation of Eqs. (2) and (4) for the infinite wire, for which $\mathcal{P}(t) \propto 1/\sqrt{t}$, leads to almost indistinguishable results provided[2,41] $L_\varphi \to \sqrt{2}L_N$. Therefore the analysis of the MC of the wire suggests that the sophisticated calculation of Eq. (4) can be replaced by the simpler one (2) with $e^{-t/\tau_\varphi} \to e^{-t/2\tau_N}$, where $\tau_N = L_N^2/D \propto T^{-2/3}$ is the Nyquist time. However this is *a priori* not true anymore as soon as we consider networks with a nontrivial topology *because electric potential fluctuations depend on the geometry, and therefore the decoherence is geometry dependent*.

Let us formulate this idea more precisely. Being related to the potential as $\Phi \sim \int' V$, fluctuations of the phase Φ picked by the two reversed electronic trajectories can be related to the power spectrum of the potential, given by the fluctuation-dissipation theorem: $\frac{d}{dt}\langle\Phi^2\rangle_{V,\mathcal{C}_t} \sim e^2 T \mathcal{R}_t \sim \frac{e^2 T}{\sigma_0 s}x(t)$, where

$\mathcal{R}_t = x(t)/(\sigma_0 s)$ is the resistance of a wire of length $x(t)$. The average $\langle \cdots \rangle_{V,\mathcal{C}_t}$ is taken over potential fluctuations and closed diffusive trajectories $\mathcal{C}_t$ for a time scale t. The length $x(t)$ is the typical length probed by electronic trajectories. For an infinite wire it scales like $x(t) \sim \sqrt{Dt}$; therefore $\langle \Phi^2 \rangle_{V,\mathcal{C}_t} \sim (t/\tau_N)^{3/2}$, where $\tau_N = L_N^2/D \sim T^{-2/3}$ is the Nyquist time. On the other hand, in a ring, diffusion is constrained by the geometry: harmonics of the MC of a ring involve winding trajectories for which the length scale probed is therefore the perimeter $x(t) \sim L$, leading to $\langle \Phi^2 \rangle_{V,\mathcal{C}_t} \sim (t/\tau_c)$, where $\tau_c \sim T^{-1}$. Therefore, in a ring, depending on their winding, trajectories probe different length scales: $L_N \propto T^{-1/3}$ or $L_c \propto T^{-1/2}$.

Let us summarize. At the level of Eqs. (2) and (3), L_φ is a phenomenological parameter put by hand. The modelization of decoherence due to *e-e* interaction of AAK shows that, in an infinite wire, the WL correction probes the Nyquist length $L_N \propto T^{-1/3}$ (the only length scale of the problem). This shows that, in the MC of the infinite wire, the phenomenological parameter L_φ must be replaced by $L_\varphi \to L_N \propto T^{-1/3}$. On the other hand the MC of a ring involves a new length scale $L_c = L_N^{3/2}/L^{1/2}$ combination of the Nyquist length and the perimeter. In this case, *assuming* the simple AAS behavior $\Delta\sigma_n \propto e^{-nL/L_\varphi}$, the phenomenological parameter should be substituted by $L_\varphi \to L_c \propto T^{-1/2}$.

Geometry-dependent decoherence in ballistic rings. It is worth pointing out that such a geometry-dependent decoherence can also be observed in ballistic systems: potential fluctuations responsible for decoherence depend on the precise distribution of currents inside the device, which are affected by the way the current is injected through different contacts.[42] Depending whether the measurement is local or nonlocal, different phase coherence lengths have been extracted from the damping of AB oscillations.[43] The different τ_φ are probed by changing the contact configuration (current/voltage probes),[44] whereas in the diffusive ring, the different length scales are probed by considering different harmonics.

III. GENERAL FORMALISM

We first recall the basic formalism and apply precisely the ideas given in the introduction. We will consider the reduced conductivity $\tilde{\sigma}$, defined by

$$\sigma = \frac{2e^2}{hs}\tilde{\sigma}, \tag{6}$$

where s is the cross section of the wire. The reduced WL correction has the dimension of a length. As mentioned above, it is a sum of contributions of interfering closed reversed electronic trajectories, which can be conveniently written as a path integral,

$$\Delta\tilde{\sigma}(x) \equiv -2P_c(x,x)$$
$$= -2\int_0^\infty dt \int_{x(0)=x}^{x(t)=x} \mathcal{D}x(\tau)\exp\left[-\int_0^t d\tau\left(\frac{1}{4}\dot{x}^2 + 2ie\dot{x}A(x)\right)\right]$$
$$\times e^{i\Phi[x(\tau)]}. \tag{7}$$

$P_c(x,x)$ is the so-called *Cooperon*. Summation over diffusive

paths for time t involves the Wiener measure $\mathcal{D}x(\tau)\exp{-\int_0^t d\tau\frac{1}{4}\dot{x}^2}$ (we have performed a change in variable $t \to t/D$ so that "time" has now the dimension of a squared length). Each loop receives a phase proportional to the magnetic flux $2\int_0^t d\tau\dot{x}A(x)$ intercepted by the reversed interfering trajectories, where $A(x)$ is the vector potential. The factor 2 originates from the fact that the Cooperon measures interference between two closed electronic trajectories undergoing the same sequence of scattering events in a reversed order. Finally we have introduced an additional phase $\Phi[x(\tau)]$ to account for dephasing: dephasing due to penetration of the magnetic field in the wires[12] or decoherence due to electron-electron interaction. In this latter case the phase Φ depends also on the environment dynamics over which one should average.

The x dependence of $\Delta\tilde{\sigma}(x)$ in Eq. (7). In a general network, in the absence of translational invariance, the WL correction to the conductance was shown to be given by an integration of $\Delta\tilde{\sigma}(x)$ over the network, with some nontrivial weights attributed to the wires. Let us write the classical dimensionless conductance as $g^{\text{class}} = \alpha_d N_c \ell_e / \mathcal{L}$, where the effective length $\mathcal{L}$ is obtained from addition (Kirchhoff) laws of classical resistances (dimensionless parameter α_d was defined above: $\alpha_3 = 4/3$, $\alpha_2 = \pi/2$, and $\alpha_1 = 2$). Then the WL correction to the conductance is[30]

$$\Delta g = \frac{1}{\mathcal{L}^2}\sum_i \frac{\partial\mathcal{L}}{\partial l_i}\int_{\text{wire } i} dx\,\Delta\tilde{\sigma}(x), \tag{8}$$

where the summation runs over all wires of the networks and l_i is the length of the wire i. Equation (8) was demonstrated in Ref. 30 for the conductance matrix elements of multiterminal networks with arbitrary topology. This result relies on a careful discussion of current conservation (derivation of current conserving quantum corrections can be found in Refs. 45–48). This point will play a relatively minor role in the present paper. Equation (8) may be used in order to calculate geometry-dependent prefactors.

Magnetoconductance oscillations and winding properties. In an array of metallic rings of same perimeter, the magnetic flux is an integer multiple of the flux ϕ per ring $\int_0^t d\tau\,\dot{x}A(x) = \phi \times \mathcal{N}[x(\tau)]$, where $\mathcal{N}[x(\tau)] \in \mathbb{Z}$ is the winding number of the closed trajectory (the number of fluxes encircled). This makes the WL correction a periodic function of the flux $\phi = \theta\frac{\phi_0}{4\pi}$, where $\phi_0 = h/e$. The nth harmonic of the MC

$$\Delta\tilde{\sigma}_n = \int_0^{2\pi}\frac{d\theta}{2\pi}\Delta\tilde{\sigma}(\theta)e^{-in\theta} \tag{9}$$

involves trajectories with winding number n. We can write the harmonics as

$$\Delta\tilde{\sigma}_n(x) \equiv -2P_c^{(n)}(x,x) = -2\int_0^\infty dt$$
$$\times \int_{x(0)=x}^{x(t)=x} \mathcal{D}x(\tau)\delta_{n,\mathcal{N}[x(\tau)]}\exp\left(-\int_0^t d\tau\frac{1}{4}\dot{x}^2\right)e^{i\Phi[x(\tau)]}, \tag{10}$$

where the Kronecker symbol selects only trajectories for a

given winding number n. Let us introduce the probability for a diffusive particle to return to its starting point after a time t, with the condition of winding n fluxes,

$$\mathcal{P}_n(x,x;t) = \int_{x(0)=x}^{x(t)=x} \mathcal{D}x(\tau) \, \delta_{n,\mathcal{N}[x(\tau)]} \exp\left(-\int_0^t d\tau \, \frac{1}{4}\dot{x}^2\right).$$

(11)

For example, in an isolated ring of perimeter L, this probability is simply given by

$$\mathcal{P}_n^{\text{ring}}(x,x;t) = \frac{1}{\sqrt{4\pi t}} e^{-(nL)^2/4t}.$$

(12)

Then, we can rewrite the harmonics as

$$\Delta\tilde{\sigma}_n(x) = -2 \int_0^\infty dt \, \mathcal{P}_n(x,x;t) \langle e^{i\Phi[\mathcal{C}_t^n]} \rangle_{\mathcal{C}_t^n},$$

(13)

which is the structure given in Eq. (4). In Eq. (13) we have introduced the notation $\mathcal{C}_t^n \equiv (x(\tau), \tau \in [0,t] | x(0) = x(t) = x; \mathcal{N}[x(\tau)] = n)$ for a closed diffusive path winding n times. $\langle \cdots \rangle_{\mathcal{C}_t^n}$ designates averaging over all such paths, with the measure of the path integral (11). The phase $\Phi[\mathcal{C}]$ accounts for dephasing and eliminates the contributions of diffusing trajectories at large time. We now discuss two possible modelizations for this function, denoted by "A" and "B."

A. Model A: exponential relaxation

The simplest choice is an exponential relaxation, with a dephasing rate $\gamma = 1/\tau_\varphi = 1/L_\varphi^2$,

$$\langle e^{i\Phi[\mathcal{C}_t]} \rangle_{\mathcal{C}_t} = e^{-\gamma t}.$$

(14)

This simple prescription correctly describes dephasing due to spin-orbit coupling, magnetic impurities,[13,49] effect of penetration of the magnetic field in the wires,[12] or decoherence due to electron-phonon scattering.[1,50] Using Eqs. (12) and (13) with this exponential decay yields the familiar result (3) for the isolated ring.

B. Model B: geometry-dependent decoherence from electron-electron interaction

It turns out that the simple exponential relaxation does not describe correctly the decoherence due to electron-electron interaction, the physical reason being that this decoherence is due to electromagnetic field fluctuations that depend on the geometry of the system. AAK have proposed a microscopic description[3,33] that we can rephrase as follows. In Eq. (7), the phase Φ picked up by the reversed trajectories depends on the environment (the potential V created by the other electrons due to electron-electron interaction): $\Phi_V[\mathcal{C}_t] = \int_0^t d\tau [V(x(\tau),\tau) - V(x(\tau),t-\tau)]$. Averaging over the Gaussian fluctuations of V leads to $\langle e^{i\Phi_V[\mathcal{C}_t]} \rangle_V = e^{-1/2\langle \Phi_V[\mathcal{C}_t]^2 \rangle_V}$, where the fluctuation-dissipation theorem (written for $\omega \ll T$ describing classical fluctuations) $\langle V(r,t)V(r',t') \rangle_V \simeq \frac{e^2 T}{\sigma_0} \delta(t-t') P_d(r,r')$ gives $\frac{1}{2}\langle \Phi_V[\mathcal{C}_t]^2 \rangle_V = \Gamma[\mathcal{C}_t]t$ with[52]

$$\Gamma[\mathcal{C}_t]t = \frac{2}{L_N^3} \int_0^t d\tau \, W(x(\tau), x(t-\tau)),$$

(15)

$$\Gamma[\mathcal{C}_t]t = \frac{k_B T}{\hbar} \frac{2\pi}{R_K} \int_0^t d\tau \, \mathcal{R}(x(\tau), x(t-\tau)),$$

(16)

where $R_K = h/e^2$ is the quantum of resistance. The function $W(x,x')$ is related to the diffusion, solution of $-\Delta P_d(x,x') = \delta(x-x')$, by

$$W(x,x') = \frac{P_d(x,x) + P_d(x',x')}{2} - P_d(x,x').$$

(17)

This function has a physical interpretation discussed in Appendix E: it is proportional to the equivalent resistance $\mathcal{R}(x,x')$ between the points x and x' (Fig. 21). With this remark, we see that Eq. (16) can be understood as a local version of the Johnson-Nyquist theorem relating the potential fluctuations to the resistance.

In Eqs. (15) and (16) we have introduced a decoherence rate $\Gamma[\mathcal{C}_t]$, which depends not only on the time but on the trajectory itself. Therefore the decay of phase coherence is now described by

$$\langle e^{i\Phi_V[\mathcal{C}_t]} \rangle_{V,\mathcal{C}_t} = \langle e^{-\Gamma[\mathcal{C}_t]t} \rangle_{\mathcal{C}_t}.$$

(18)

Within this framework, relaxation of phase coherence is not described by a simple exponential decay like in Eq. (14) but is controlled by a *functional of the trajectories*[54] $x(\tau)$. Therefore the nature of decoherence depends on the network, through the resistance $\mathcal{R}(x,x')$ between x and x', and on the winding properties of the trajectories.

The central problem of the present paper is to compute the path integral

$$\Delta\tilde{\sigma}_n(x) = -2 \int_0^\infty dt \, e^{-\gamma t} \int_{x(0)=x}^{x(t)=x} \mathcal{D}x(\tau) \, \delta_{n,\mathcal{N}[x(\tau)]}$$
$$\times \exp\left(-\int_0^t d\tau \left[\frac{1}{4}\dot{x}^2 + \frac{2}{L_N^3} W(x(\tau),x(t-\tau))\right]\right)$$

(19)

for the different networks. Such a calculation has been already performed in two cases: the infinite wire[3] and the isolated ring.[4,5]

The logic of the following sections is the following: first we study the winding properties in the network. For that purpose we first compute the WL correction $\Delta\tilde{\sigma}_n^{(A)}$ within model A, Eq. (13) with Eq. (14). The probability $\mathcal{P}_n(x,x;t)$ can be extracted from an inverse Laplace transform with respect to the parameter γ. Having fully characterized the winding properties, we use this information in order to study the harmonics $\Delta\tilde{\sigma}_n^{(B)}$ within model B describing decoherence due to electron-electron interaction, Eq. (13) with Eq. (18).

IV. WIRE AND THE RING

We first recall known results within the framework of model B concerning the simplest geometries that will be useful for the following.
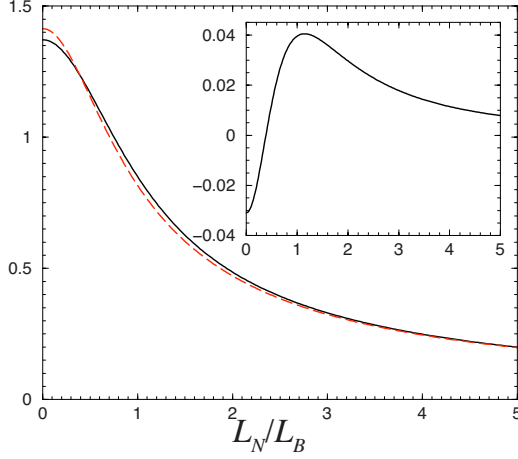
FIG. 2. (Color online) Comparison between $-\mathrm{Ai}(x^2)/\mathrm{Ai}'(x^2)$ (black continuous line) and $1/\sqrt{1/2+x^2}$ (red dashed line). Relative difference (inset) does not exceed 4%.

A. Phase coherence relaxation in an infinite wire

The case of an infinite wire was originally solved in Ref. 3. In this case we have $W_{\mathrm{wire}}(x,x')=\frac{1}{2}|x-x'|$ and the path integral

$$\Delta\tilde{\sigma} = -2\int_0^\infty dt\, e^{-\gamma t} \int_{x(0)=x}^{x(t)=x} \mathcal{D}x(\tau)$$
$$\times \exp\left(-\int_0^t d\tau \left[\frac{1}{4}\dot{x}^2 + \frac{1}{L_N^3}|x(\tau)-x(t-\tau)|\right]\right) \quad (20)$$

can be computed thanks to translational invariance [as pointed out in Ref. 62, using the symmetry of the path integral we can perform the substitution $x(\tau)-x(t-\tau)\to x(\tau)$, provided that the starting point of the path integral is set to $x\to 0$, see Appendix A]. Combining exponential relaxation (model A) and decoherence due to e-e interaction (model B) allows to extract the function (18) with an inverse Laplace transform of the AAK result,[3,33,35,2]

$$\Delta\tilde{\sigma} = -\int_0^\infty \frac{dt}{\sqrt{\pi t}} e^{-\gamma t} \langle e^{i\Phi_V[\mathcal{C}_t]}\rangle_{V,\mathcal{C}_t}, \quad (21)$$

$$\Delta\tilde{\sigma} = L_N \frac{\mathrm{Ai}(\gamma L_N^2)}{\mathrm{Ai}'(\gamma L_N^2)}, \quad (22)$$

where $\mathrm{Ai}(z)$ is the Airy function.[63] As mentioned above, this expression is very close to[2,41] $\Delta\tilde{\sigma}\simeq -(\frac{1}{L_\varphi^2}+\frac{1}{2L_N^2})^{-1/2}$, the result obtained by performing the substitution $\langle e^{i\Phi_V[\mathcal{C}_t]}\rangle_{V,\mathcal{C}_t} \to e^{-t/2L_N^2}$ (see Fig. 2).

The inverse Laplace transform of Eq. (21) was computed in Ref. 8 with residue's theorem,

$$f_{\mathrm{wire}}(t/\tau_N) = \langle e^{i\Phi_V[\mathcal{C}_t]}\rangle_{V,\mathcal{C}_t}, \quad (23)$$

$$f_{\mathrm{wire}}(t/\tau_N) = \sqrt{\frac{\pi t}{\tau_N}} \sum_{m=1}^\infty \frac{1}{|u_m|} e^{-|u_m|t/\tau_N}, \quad (24)$$

where u_m are zeros of $\mathrm{Ai}'(z)$. In particular $u_1 \simeq -1.019$ and $u_m \simeq -[\frac{3\pi}{2}(m-\frac{3}{4})]^{2/3}$ for $m\to\infty$. The limiting behaviors are

$$f_{\mathrm{wire}}(t/\tau_N) \simeq 1 - \frac{\sqrt{\pi}}{4}\left(\frac{t}{\tau_N}\right)^{3/2} \quad \text{for } t\ll\tau_N, \quad (25)$$

$$f_{\mathrm{wire}}(t/\tau_N) \simeq \frac{1}{|u_1|}\sqrt{\frac{\pi t}{\tau_N}} e^{-|u_1|t/\tau_N} \quad \text{for } \tau_N\ll t. \quad (26)$$

Note that the short time behavior can be obtained by expanding $f(t/\tau_N)=\langle e^{i\Phi}\rangle_{V,\mathcal{C}_t}=\langle e^{-1/2\langle\Phi^2\rangle_V}\rangle_{\mathcal{C}_t} \simeq 1-\frac{1}{2}\langle\Phi_V[\mathcal{C}_t]^2\rangle_{V,\mathcal{C}_t}$. This limit can be simply obtained by noticing that in the wire $W(x(\tau),x(t-\tau))\sim x(\tau)\sim \sqrt{t}$; therefore $\Gamma[\mathcal{C}_t]t\sim Tt^{3/2} \sim (t/\tau_N)^{3/2}$ where we recover that the Nyquist time scales as $\tau_N \propto T^{-2/3}$.

B. Phase coherence relaxation in the isolated ring

For the isolated ring of perimeter L, we have $W_{\mathrm{ring}}(x,x')=\frac{1}{2}|x-x'|(1-\frac{|x-x'|}{L})$. The path integral (19) can be computed exactly[5] (see Appendix A). Up to a dimensionless prefactor, we obtain

$$\Delta\tilde{\sigma}_n \sim -L_N e^{-(\pi/8)n(L/L_N)^{3/2}} \quad \text{for } L_N\ll L, \quad (27)$$

$$\Delta\tilde{\sigma}_n \sim -T^{-1/3}e^{-nL^{3/2}T^{1/2}}. \quad (28)$$

This result can be simply understood as follows: in the ring, trajectories with finite winding necessarily explore the whole ring. This "ergodicity" implies that $W(x(\tau),x(t-\tau))\sim x(\tau) \sim L$ and therefore the decoherence rate $\Gamma[\mathcal{C}_t]t\sim TLt\sim t/\tau_c$ involves the different time scale $\tau_c\sim 1/(TL)$, according to the physical argument given in Sec. II. As a consequence Eq. (13) indeed leads to[4]

$$\Delta\tilde{\sigma}_n \sim -L_N e^{-(\pi/8)nL/L_c}, \quad (29)$$

where

$$L_c = \frac{L_N^{3/2}}{L^{1/2}}. \quad (30)$$

Phase coherence length: $L_\varphi \propto T^{-1/3}$ or $L_\varphi \propto T^{-1/2}$? Note that the introduction of a new length scale[4] L_c might appear arbitrary since the harmonics may be written uniquely in terms[5] of L and L_N. The difference between Eqs. (27) and (29) is a matter of convention and may be related to the experimental procedure. The usual method extracts the phase coherence length from the analysis of MC harmonics. Then it is natural to see how the winding number n scales with the phase coherence length, or more properly how the length nL scales with L_φ and therefore assume the form $\Delta\tilde{\sigma}_n \propto f(nL/L_\varphi)$. From Eq. (29) we see that the function is simply the exponential, $f(x)=e^{-x}$, with a *perimeter-dependent* phase coherence length $L_\varphi \to L_c \propto (TL)^{-1/2}$. Another procedure may consist in studying the harmonics content as a function of the perimeter L, that is, for different samples. The experiment is

then analyzed with the form $\Delta\tilde{\sigma}_n \propto f_n(L/L_\varphi)$. Equation (27) gives $f_n(x) = e^{-nx^{3/2}}$ with the *geometry-independent* phase coherence length $L_\varphi \to L_N \propto T^{-1/3}$.

The temperature dependence $\Delta\sigma_n \sim e^{-L^{3/2}T^{1/2}}$ was first predicted in Ref. 4 using instanton method (with a different pre-exponential dependence) and studied in details in Ref. 5, where the path integral (19) was computed exactly for the isolated ring.[64] The effect of the connecting arms was clarified in Ref. 65. The fact that the pre-exponential factor is L_N is related to the fact that the smooth part of the MC, due to the penetration of the field in the wire, probes the same length scale as in the infinite wire.

It is worth pointing out the recent work[53] in which the crossover to the zero-dimensional limit is studied in a ring weakly connected. In this case the authors get a crossover from $\tau_\varphi \propto T^{-1}$ (diffusive ring) to $\tau_\varphi \propto T^{-2}$ (ergodic) for temperature below the Thouless energy. This latter behavior coincides with the result known for quantum dots in the same regime.[66]

C. Penetration of the magnetic field in the wires of the ring

Networks are made of wires of finite width w. The penetration of the magnetic field in the wires is responsible for fluctuations of the magnetic flux enclosed by trajectories with the same winding number but different areas. In the weak magnetic field limit, this effect is described by introducing an effective dephasing rate[12]

$$\gamma \to 1/L_{\mathcal{B}}^2 = \frac{1}{3}\left(\frac{e\mathcal{B}w}{\hbar}\right)^2. \quad (31)$$

The question of how to combine the two decoherence mechanisms (models A and B) in the ring was discussed in Ref. 5. It was shown that the WL correction of the ring presents the structure

$$\Delta\tilde{\sigma}_n \simeq L_N \frac{\mathrm{Ai}(L_N^2/L_{\mathcal{B}}^2)}{\mathrm{Ai}'(L_N^2/L_{\mathcal{B}}^2)} e^{-nL/L_\varphi^{\mathrm{osc}}(L_c,L_{\mathcal{B}})} \quad (32)$$

for $L_N \ll L$, with

$$L_\varphi^{\mathrm{osc}}(L_c, L_{\mathcal{B}}) = \frac{L_c}{\eta(L_c^2/L_{\mathcal{B}}^2)}, \quad (33)$$

where $\eta(x) = \left(\frac{1}{4}+x\right)\arctan\frac{1}{2\sqrt{x}} + \frac{\sqrt{x}}{2}$.

Prefactor. In Eq. (32), the pre-exponential factor coincides with the result obtained for an infinite wire.[3] The ratio of Airy functions can be approximated as[2,41] $\frac{\mathrm{Ai}(x)}{\mathrm{Ai}'(x)} \simeq -(\frac{1}{2}+x)^{-1/2}$ (Fig. 2). In other terms, we may write the zero harmonic (i.e., the result for the infinite wire) as

$$\Delta\tilde{\sigma}_0 \simeq -L_\varphi^{\mathrm{env}}, \quad (34)$$

where

$$L_\varphi^{\mathrm{env}} = \left(\frac{1}{2L_N^2} + \frac{1}{L_{\mathcal{B}}^2}\right)^{-1/2}. \quad (35)$$

This combination expresses that, in a wire of width w, the penetration of the magnetic field provides the dominant cut-
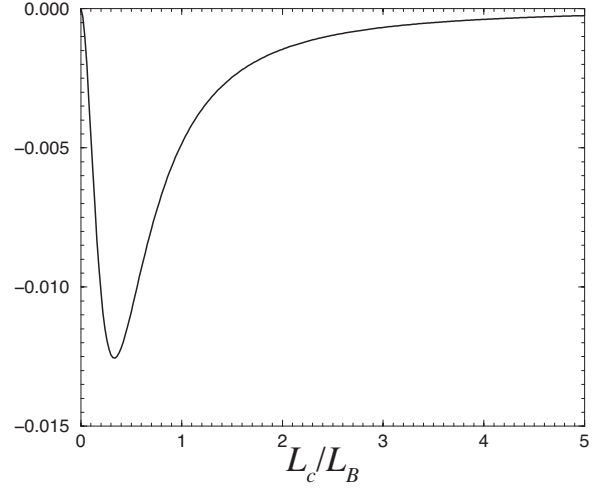

FIG. 3. The relative difference $[1-\eta(x^2)/\sqrt{(\pi/8)^2+x^2}]$ between the effective length L_φ^{osc}, Eq. (33), and its approximation, Eq. (36), does not exceed 1.5%.

off when typical trajectories enclose more than one quantum flux $L_\varphi w\mathcal{B} \gtrsim \phi_0$ (here $L_\varphi \sim L_N$ for trajectories with winding $n=0$).

Exponential damping. In the exponential of Eq. (32), the effective length interpolates between $L_\varphi^{\mathrm{osc}} \simeq \frac{8}{\pi}L_c$ for $L_{\mathcal{B}} \gg L_c$ and $L_\varphi^{\mathrm{osc}} \simeq L_{\mathcal{B}}$ for $L_{\mathcal{B}} \ll L_c$. Its overall behavior is well approximated by

$$L_\varphi^{\mathrm{osc}} \simeq \left[\left(\frac{\pi}{8L_c}\right)^2 + \frac{1}{L_{\mathcal{B}}^2}\right]^{-1/2} = \left(\frac{\pi^2 L}{64L_N^3} + \frac{1}{L_{\mathcal{B}}^2}\right)^{-1/2}, \quad (36)$$

which differs with Eq. (33) by less than 1.5% (Fig. 3). When $L_{\mathcal{B}}$ is the shortest length, the decay of AAS oscillations $\sim e^{-nL/L_{\mathcal{B}}}$ can be understood from the fact that modulations of the flux enclosed by trajectories with finite winding become larger than the quantum flux $nLw\mathcal{B} \gtrsim \phi_0$. Equation (36) was used in the analysis of the recent experiment.[6]

These two remarks show that the magnetic length $L_{\mathcal{B}}$ probes two different length scales: in the pre-exponential factor $L_{\mathcal{B}}$ probes the Nyquist length $L_N \propto T^{-1/3}$, whereas in the ratio of harmonics $\Delta\tilde{\sigma}_n/\Delta\tilde{\sigma}_0$, the magnetic length $L_{\mathcal{B}}$ probes the length scale $L_c \propto T^{-1/2}$.

D. How to analyze MC experiments in networks

In order to understand the implications of this remark, let us discuss the structure of the typical MC curve of a network. The following discussion applies to the case $L_N \lesssim L$, where Eq. (32) holds. Figure 4 represents a typical MC curve, here for a chain of rings. It exhibits rapid AAS oscillations with a period given by $\mathcal{B}_{\mathrm{osc}} \sim \phi_0/L^2$, superimposed with a smooth variation over a scale $\mathcal{B}_{\mathrm{damp}} \simeq \phi_0/wL_\varphi$. The phase coherence length can be extracted either from the amplitude of the oscillations or from the decay of the envelope of the MC curve. Which L_φ (L_N or L_c) is obtained from such a curve? According to Eq. (32) we see that $L_\varphi \to L_N$ in the pre-exponential factor, which mostly dominates the smooth envelope, while $L_\varphi \to L_c$ in the exponential decay, which dominates the damping of the rapid oscillations. In order to decouple the
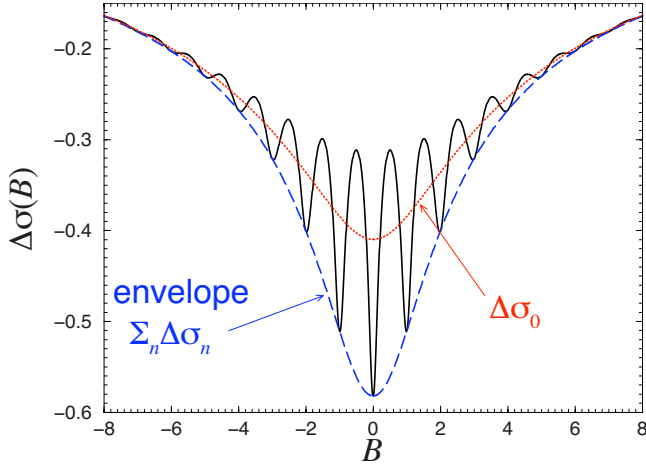
FIG. 4. (Color online) Typical shape of the MC curve of a network (here a chain of rings). Rapid oscillations are AAS oscillations. Damping of oscillations over large scale is due to the penetration of the magnetic field in the wires.

two effects the analysis of the experiments of Ref. 6 have been analyzed as follows:[16,67] the Fourier transform of the MC curve $\Delta\sigma(\mathcal{B})$ presents broadened Fourier peaks due to the penetration of the magnetic field in the wires. Integration of Fourier peaks eliminates this effect. Ratio of harmonics involve the length scale L_c. The length L_N was extracted from the smooth envelope $\Delta\tilde{\sigma}_{\mathrm{env}} = \Sigma_n \Delta\tilde{\sigma}_n \simeq \Delta\tilde{\sigma}_0$ for $L_N \ll L$. The temperature dependence of the phase coherence length was extracted in this way in Ref. 6. Results are plotted in Fig. 5, exhibiting clearly the two length scales in the regime $L_N \ll L$. We see that it is crucial to analyze the experiment in terms of the MC harmonics $\Delta\sigma_n$.

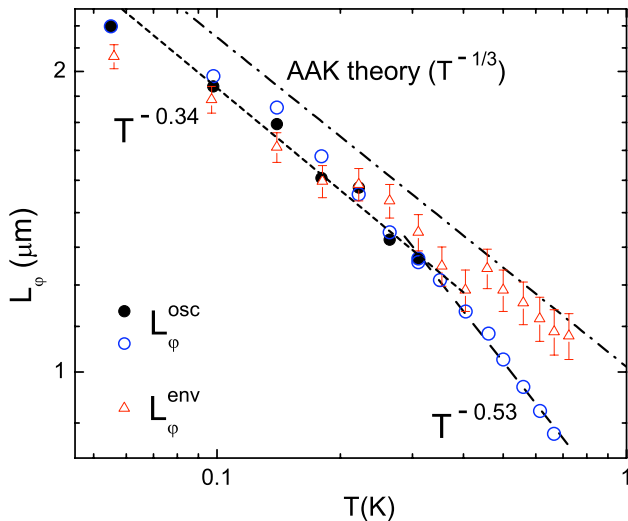*Isolated ring vs ring embedded in a network.* In transport

FIG. 5. (Color online) Phase coherence length as a function of the temperature obtained from measurements realized on a large square network[6] of lattice spacing $a=1$ μm (perimeter $L=4$ μm). The length scale $L_\varphi \to L_\varphi^{\mathrm{env}} \propto T^{-1/3}$ has been extracted from the smooth MC while the length $L_\varphi \to L_\varphi^{\mathrm{osc}} \propto T^{-1/2}$ has been extracted from ratio of harmonics. [Note that L_φ^{env} and L_φ^{osc} in Ref. 6 denote Eqs. (35) and (36) for $L_{\mathcal{B}} = \infty$.]

experiments the ring is never isolated: it is at least connected to contacts through which current is injected. Moreover the samples are often made of a large number of loops, in order to realize disorder averaging. The results obtained for the isolated ring are fortunately relevant to describe a more complex network of equivalent rings (Figs. 1 and 9) when the rings can be considered as *independent*, i.e., when interference phenomena do not involve several rings; this occurs when $L_\varphi \ll L$ (or $L_N \ll L$), in practice in a high-temperature regime. This temperature dependence of harmonics is rather difficult to extract from measurements since harmonics are suppressed exponentially. This has been done only very recently in Ref. 6. Another difficulty is that the "high-temperature regime" $L_N \ll L$ is in practice quite narrow in these samples due to fact that electron-phonon interaction dominates the decoherence above 1 K (in the sample of Refs. 11 and 51 L_N is much larger and when $L_N \ll L$ the role of electron-electron interaction is negligible).

It is an important issue to obtain the expression of the WL correction for a broader temperature range, that is, to study the regime $L \lesssim L_N$. This regime is reached in several experiments.[11,16,51] In this case diffusive interfering trajectories responsible for AAS harmonics are not constrained to remain inside a unique ring, but explore the surrounding network (see Figs. 1, 6, and 9). This affects both the winding properties and the nature of decoherence. The MC oscillations are therefore network dependent. In the following sections we discuss the behavior of the MC harmonics in the limit $L \lesssim L_\varphi$ (or $L \lesssim L_N$) for different networks: a ring connected to long arms, a necklace of rings, and a large square network. The case of a long hollow cylinder will also be discussed.

V. CONNECTED RING

In this section we consider the case of a single ring connected to two wires supposed much longer than L_φ (Fig. 6). This problem has already been considered in Refs. 5 and 7.

A. Model A

(i) Let us consider first the case $L_\varphi \ll L$. The Cooperon is constructed in Appendix F, Sec. 1 (see Ref. 7) and we obtain

$$\Delta\tilde{\sigma}_n(x \in \mathrm{ring}) \simeq -\left(\frac{2}{3}\right)^{2n} L_\varphi e^{-nL/L_\varphi}, \qquad (37)$$

where x is any position inside the ring far from the vertices (at distance larger than L_φ).

(ii) Now we turn to the regime $L_\varphi \gg L$. The Cooperon is uniform inside the ring and is computed in Appendix F, Sec. 1. We have[7]
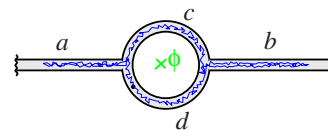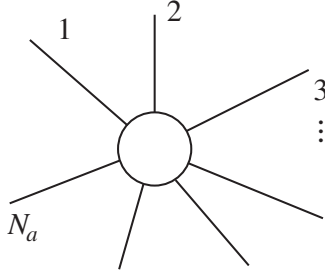

FIG. 6. (Color online) A ring connected to reservoirs through long wires a and b. In the regime $L_\varphi \gtrsim L$, the WL correction is dominated by trajectories exploring the arms, as represented here.

FIG. 7. A ring connected to N_a wires.

$$\Delta\tilde{\sigma}_n(x) \simeq -\sqrt{\frac{L_\varphi L}{2}} e^{-n\sqrt{2L/L_\varphi}} \quad \text{for } L \ll L_\varphi, \qquad (38)$$

where x is any position inside the ring, or in the arms at a distance to the ring smaller than L_φ. We emphasize that this behavior, quite different from Eq. (3), is due to the fact that the diffusive trajectories spend most of the time in the wires[7] (the distribution of the time spent by winding trajectories in the arm was analyzed in Ref. [62]).

Winding probability in a ring connected to N_a arms. We now derive the winding probability for a ring connected to N_a infinitely long arms (Fig. [7]) from the inverse Laplace transform of the Cooperon $P_c^{(n)}(x,x) = -\frac{1}{2}\Delta\tilde{\sigma}_n(x)$. At small time, Eq. (37) gives

$$\mathcal{P}_n(x,x;t) \simeq \left(\frac{2}{3}\right)^{N_a n} \frac{1}{\sqrt{4\pi t}} e^{-(nL)^2/4t} \quad \text{for } t \ll L^2, \quad (39)$$

where x is inside the ring, far from a vertex (at distance larger than $\sqrt{t}$).

At large time scales, $t \gg L^2$, the arms strongly modify the winding properties around the ring: the time dependence of the typical winding number becomes subdiffusive $n_t \sim t^{1/4}$, to be compared with the behavior for the isolated ring $n_t \sim t^{1/2}$ reflected by Eq. (12). For a ring connected to N_a infinite wires, Eq. (12) is replaced by the probability[7]

$$\mathcal{P}_n(x,x;t) \simeq \frac{\sqrt{L/N_a}}{2t^{3/4}} \Psi\left(\frac{n\sqrt{N_a L}}{t^{1/4}}\right) \quad \text{for } t \gg L^2, \qquad (40)$$

where N_a is the number of arms (as far as x is inside the ring or at a distance to the ring smaller than $t^{1/2} \sim 1/\sqrt{\gamma} = L_\varphi$, the Cooperon, or the corresponding probability is almost independent on x). The function $\Psi(\xi)$, given by[7,62]

$$\Psi(\xi) = \frac{2}{\pi} \text{Re}\left[e^{-i\pi/4} \int_0^\infty du \sqrt{u} e^{-u^2 - \sqrt{u}\xi e^{-i\pi/4}} \right], \qquad (41)$$

is studied in Appendix B and plotted in the conclusion (Fig. [17]).

From the conductivity to the conductance. In the geometry of Fig. [6], the conductance is not simply related to the conductivity. The classical conductance of the connected ring is given by $g = \alpha_d N_c \ell_e / \mathcal{L}$ with $\mathcal{L} = l_a + l_{c\|d} + l_b$, where l_i is the length of the wire i. $l_{c\|d}^{-1} = l_c^{-1} + l_d^{-1}$ is the equivalent length. From Eq. (8)

$$\Delta g_n = \frac{1}{(l_a + l_{c\|d} + l_b)^2}$$

$$\times \left[\int_a + \frac{l_d^2}{(l_c + l_d)^2} \int_c + \frac{l_c^2}{(l_c + l_d)^2} \int_d + \int_b \right] dx \, \Delta\tilde{\sigma}_n(x). \qquad (42)$$

The Cooperon $\Delta\tilde{\sigma}_n(x) = -2P_c^{(n)}(x,x)$ has been constructed for different positions of the coordinate x in Appendix F, Sec. 1. Depending on the ratio L_φ/L, the WL correction Δg_n is dominated by different terms.

(i) For $L_\varphi \ll L$, Eq. (F6) shows that harmonics of the Cooperon decay exponentially in the arms (Fig. [24]); inside the ring, the Cooperon (F8) is almost uniform, apart for small variations near the nodes. Therefore Δg_n is dominated by integrals $\int_c$ and $\int_d$ in the ring and we have

$$\Delta g_n \simeq \frac{l_{c\|d}}{\mathcal{L}^2} \Delta\tilde{\sigma}_n(x \in \text{ring}) \quad \text{for } L_\varphi \ll L, \qquad (43)$$

where x is any position inside the ring far from the vertices (at distance larger than L_φ).

(ii) For $L_\varphi \gg L$, using Eqs. (F6) and (F8) we see that the terms $\int_c$ and $\int_d$ bring a contribution proportional to the perimeter L whereas the terms $\int_a$ and $\int_b$ bring larger contributions proportional to L_φ: $\int_a dx P_c^{(n)}(x,x) \simeq \frac{1}{2}L_\varphi P_c^{(n)}(0,0)$; therefore

$$\Delta g_n \simeq \frac{L_\varphi}{\mathcal{L}^2} \Delta\tilde{\sigma}_n(x \in \text{ring}) \quad \text{for } L \ll L_\varphi. \qquad (44)$$

The general expression describing the crossover between Eqs. (43) and (44) can be obtained easily using the formalism of Ref. [30].

B. Model B

We now compute the harmonics of the conductivity within model B. We have now to consider Eqs. (13), (15), and (18). The function $W(x,x')$ has been constructed in Ref. [5]. In the limit $l_a, l_b \gg L$ and if x and x' belong to the connecting wires for x, x' (i.e., $L_N \ll l_a, l_b$), the function coincides with the one of the infinite wire $W(x,x') \simeq \frac{1}{2}|x - x'|$. Therefore, since in the limit $L \ll L_N$ the diffusive trajectories spend most of the time in the wires[62] (Fig. [6]), the dephasing mostly occurs in the wires and the relaxation of the phase coherence is similar to the one for the wire, Eq. (24), irrespective of the winding: $\langle e^{i\Phi_V[\mathcal{C}_t^n]}\rangle_{V,\mathcal{C}_t^n} \rightarrow f_{\text{wire}}(t/L_N^2)$.

Introducing Eq. (24) in Eq. (13) and performing the change in variable $|u_m|t/\tau_N = v^2$, we obtain for the correction to the conductivity

$$\Delta\tilde{\sigma}_n(x) \simeq -\sqrt{2\pi L_N L} \sum_{m=1}^\infty \frac{1}{|u_m|^{7/4}}$$

$$\times \int_0^\infty dv \sqrt{v} \Psi\left(|u_m|^{1/4} n \sqrt{\frac{2L}{v L_N}}\right) e^{-v^2}, \quad (45)$$

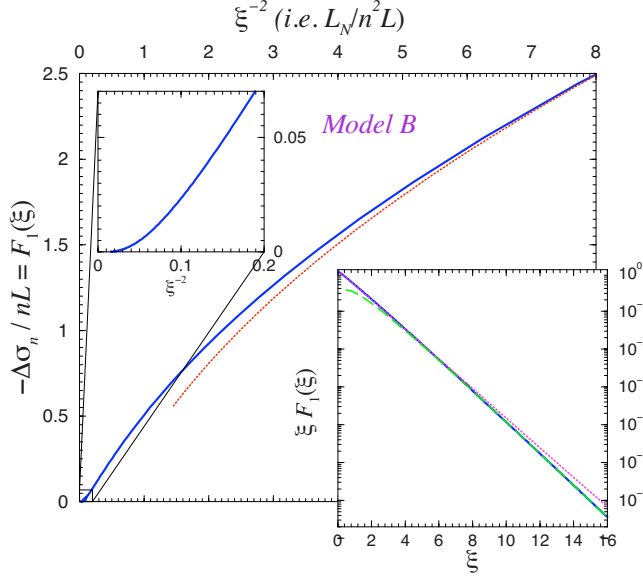where x is any position inside the ring. Using Eq. (41) we

FIG. 8. (Color online) $\Delta\tilde{\sigma}_n \propto F_1(\xi)$ (continuous blue line) as a function of $1/\xi^2 \propto L_N/n^2L$. Comparison with the limiting behavior $F_1(\xi \ll 1) \simeq 1.191/\xi - 0.877$ (red dotted line). Inset: $\xi F_1(\xi)$ in semi-log scale. For moderate values of ξ, the function is well fitted by $1.21 e^{-0.9\xi}$ (magenta dots). Green dashed curve is the asymptotic expression, Eq. (51).

rewrite the double integral in polar coordinates and perform integration over the radial coordinate. We find

$$\Delta\tilde{\sigma}_n(x) \simeq -Ln\, F_1(n\sqrt{2L/L_N}) \qquad (46)$$

with

$$F_1(\xi) = \frac{2\sqrt{2}}{\xi} \sum_{m=1}^{\infty} \frac{1}{|u_m|^{7/4}} g(|u_m|^{1/4}\xi) \qquad (47)$$

and

$$g(\Lambda) = \mathrm{Re}\left[\frac{e^{-i\pi/4}}{4}\int_0^{\pi/2} d\theta \sqrt{\sin 2\theta}\, e^{-\Lambda\sqrt{\cot\theta}\,e^{-i\pi/4}}\right], \quad (48)$$

$$g(\Lambda) = \frac{1}{\sqrt{2}} \mathrm{Re}\left[e^{-i\pi/4}\int_0^{\infty} dt\, \frac{t^2 e^{-\Lambda t e^{-i\pi/4}}}{(t^4+1)^{3/2}}\right]. \qquad (49)$$

A convenient representation can be obtained by a rotation of $\pi/4$ of the axis of integration in the complex plane. We get

$$g(\Lambda) = \frac{e^{-\Lambda}}{\sqrt{2}}\int_0^{\infty} dt\left(\frac{1}{8t^{3/2}} - \frac{(t+1)^2 e^{-\Lambda t}}{[(t+1)^4-1]^{3/2}}\right). \qquad (50)$$

The function $F_1(\xi)$ is plotted in Fig. 8. We now analyze the limiting behaviors.

We first consider the limit $L_N \ll n^2L$. Equation (50) gives $g(\Lambda \gg 1) \simeq \frac{1}{\sqrt{2}} e^{-\Lambda}\int_0^{\infty}\frac{dx}{8x^{3/2}}(1-e^{-\Lambda x}) = \frac{1}{4\sqrt{2}}\sqrt{\pi\Lambda}e^{-\Lambda}$; therefore $F_1(\xi \gg 1) \simeq \frac{1}{2}|u_1|^{-13/8}\sqrt{\pi}/\xi\, e^{-|u_1|^{1/4}\xi}$ and

$$\Delta\tilde{\sigma}_n(x) \simeq -\frac{Ln\sqrt{\pi}}{2^{5/4}|u_1|^{13/8}}\left(\frac{L_N}{n^2L}\right)^{1/4} e^{-\kappa_2 n\sqrt{L/L_N}} \qquad (51)$$

$$\sim T^{-1/12}e^{-nL^{1/2}T^{1/6}} \quad \text{for } L \ll L_N \ll n^2L, \quad (52)$$

where $\kappa_2 = \sqrt{2}|u_1|^{1/4} \simeq 1.421$.

For the lowest temperature $n^2L \ll L_N$, Eq. (49) gives $g(0) = \frac{1}{4\sqrt{\pi}}\Gamma(3/4)^2$. Therefore $F_1(\xi \ll 1) \simeq A_1/\xi$ with $A_1 = \frac{1}{2}\sqrt{2/\pi}\Gamma(3/4)^2\sum_{m=1}^{\infty}|u_m|^{-7/4} \simeq 1.191$ (the sum is $\sum_{m=1}^{\infty}|u_m|^{-7/4} \simeq 1.989$),

$$\Delta\tilde{\sigma}_n(x) \simeq -A_1\sqrt{\frac{L_N L}{2}} \quad \text{for } n^2L \ll L_N. \qquad (53)$$

Comparison between models A and B. We have seen that for the wire, the MC obtained from the two models are related through $L_{\varphi} \to \sqrt{2}L_N$ (cf. Sec. IV). It is tempting to look for a similar relation for the connected ring in the limit $L \ll L_N$.

Let us compare the results for the two models of decoherence. In the limit $n^2L \ll L_N$ the expression (53) is very close to Eq. (38) because in this case, the harmonics involve an integral over time of the function $\langle e^{i\Phi}\rangle_{V,\mathcal{C}_t}$. Therefore harmonics are insensitive to the details of this function but only to the scale over which it decays. In the other limit $L_N \ll n^2L$, the calculation of the harmonics rather involves the tail of the function $\langle e^{i\Phi}\rangle_{V,\mathcal{C}_t}$. Equation (51) presents an exponential decays similar to Eq. (38), with a different pre-exponential power law since the decay $\langle e^{i\Phi}\rangle_{V,\mathcal{C}_t} \propto \sqrt{t/\tau_N}e^{-|u_1|t/\tau_N}$ is different from the simple exponential decay $e^{-t/\tau_{\varphi}}$ for model A. The additional $\sqrt{t}$ in model B explains the different pre-exponential terms in Eqs. (38) and (51).

The similarities between results of model A and B are not surprising because decoherence occurring mostly in the wire is independent on the winding number. Could we map the results of the two models through a simple substitution of phase coherence length, as for the infinite wire? In the regime $L \ll L_N \ll n^2L$ we should compare the exponentials of Eqs. (38) and (51) what leads to $L_{\varphi} \to L_N/\sqrt{|u_1|} \simeq 0.99L_N$; however pre-exponential factors cannot be matched, obviously. In the regime $L_N \gg n^2L$ we rather compare the square roots (38) and (53) and therefore $L_{\varphi} \to A_1^2 L_N \simeq 1.418L_N$. Despite the fact that there is no unique simple substitution, we get in both cases $L_{\varphi} \sim L_N$.

Conductivity vs conductance. We discuss the relation to the conductance. In the regime $L_N \gg L$ discussed in this section, we expect

$$\Delta g_n \sim \frac{L_N}{\mathcal{L}^2}\Delta\tilde{\sigma}_n(x) \qquad (54)$$

for $x \in$ ring, for the same reason as for model A, Eq. (44) [the factor L_N comes from the fact that the integral (8) is dominated by regions of typical size L_N in the arms].

VI. CHAIN OF RINGS

Let us consider now a chain of rings separated by arms of lengths l_a [Fig. 9(a)]. The case where the phase coherence length remains smaller than the arms ($L_{\varphi} \lesssim l_a$) can be obtained from the results of the previous section since the rings can be considered as independent. The conductance of a
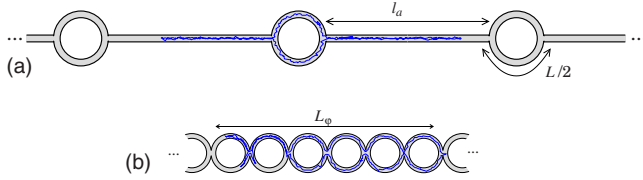
FIG. 9. (Color online) Chains of rings. If we consider the regime $l_a \gg L_\varphi$(or L_N)$\gg L$ the rings of figure (a) can be considered as independent. On the other hand, in the regime L_φ(or L_N)$\gg l_a, L$ interferences occur between trajectories encircling several rings; the latter cannot be considered anymore as independent in this case, as illustrated by the trajectory in the network (b).

chain of such N_r rings is given by performing the substitution $\frac{1}{\mathcal{L}^2} \to \frac{N_r}{[(N_r+1)l_a + N_r l_{c\|d}]^2}$ in the expression of Δg_n for one ring, Eqs. (43), (44), and (54).

When arms separating the rings are smaller than the phase coherence length ($l_a \lesssim L_\varphi$), coherent trajectories enclose magnetic fluxes in several rings. In order to study how the MC harmonics are affected by this effect we consider the limit when rings are directly attached to each other [Fig. 9(b)].

A. Model A

Considering the conductance of the symmetric chain of Fig. 9(b), the weights of the wires involved in Eq. (8) are all equal. This justifies a uniform integration of the Cooperon in the chain. In this case we can use the relation between the WL correction and the spectral determinant[27–29] (Appendix D). The spectral determinant of the infinite chain is given in Appendix F, Sec. 2. Averaging the Cooperon in the chain, $\Delta \widetilde{\sigma}(\theta) \equiv \int_{\text{chain}} \frac{dx}{\text{Vol}} \Delta \widetilde{\sigma}(x, \theta)$, and using Eqs. (D5) and (F10), we finally obtain[26]

$$\Delta \widetilde{\sigma}(\theta) = -\frac{L_\varphi}{2}\left(\coth(L/2L_\varphi) - \frac{2L_\varphi}{L}\right.$$
$$\left. + \frac{\sinh(L/2L_\varphi)}{\sqrt{\cosh^2(L/2L_\varphi) - \cos^2(\theta/2)}}\right), \quad (55)$$

where $\theta = 4\pi\phi/\phi_0$ is the reduced flux per ring. We now study the harmonics $n \neq 0$,

$$\Delta \widetilde{\sigma}_n = -\frac{L_\varphi}{\sqrt{2}} \int_0^{2\pi} \frac{d\theta}{2\pi} \frac{\sinh(L/2L_\varphi)e^{in\theta}}{\sqrt{\cosh(L/L_\varphi) - \cos(\theta)}}$$
$$= -L_\varphi \sinh(L/2L_\varphi)\oint_{\text{circle}} \frac{dz}{2i\pi} \frac{z^{n-1}}{\sqrt{(e^{L/L_\varphi} - z)(z - e^{-L/L_\varphi})/z}}. \quad (56)$$

The integration in the complex plane is performed along the unit circle in the clockwise direction. The segment of the real axis $[0, e^{-L/L_\varphi}]$ is a branch cut. The contour of integration is deformed to follow closely this segment. We obtain

$$\Delta \widetilde{\sigma}_n = -\frac{L}{2\pi}\frac{\sinh(L/2L_\varphi)}{L/2L_\varphi}e^{-(n-1/2)L/L_\varphi}\int_0^1 du \frac{(1-u)^{n-1/2}}{\sqrt{u^2 + \varepsilon u}}, \quad (57)$$

with $\varepsilon = e^{2L/L_\varphi} - 1$. We recognize the integral representation (C1) of the hypergeometric function[69] F,

$$\Delta \widetilde{\sigma}_n = -\frac{L}{2\pi}\frac{\sinh(L/2L_\varphi)}{L/2L_\varphi}e^{-(n+1/2)L/L_\varphi}B\left(\frac{1}{2}, n+\frac{1}{2}\right)$$
$$\times F\left(\frac{1}{2}, n+\frac{1}{2}; n+1; e^{-2L/L_\varphi}\right), \quad (58)$$

where $B(x, y)$ is the Euler β function.

Weakly coherent limit. We consider the limit $L_\varphi \ll L$. Using $F(\alpha, \beta; \gamma; \xi \to 0) \to 1$, we obtain

$$\Delta \widetilde{\sigma}_n \simeq -\frac{(2n-1)!!}{2^{n+1}n!}L_\varphi e^{-nL/L_\varphi} \quad \text{for } L_\varphi \ll L, \quad (59)$$

a result reminiscent of the result of the isolated ring (3), with a different prefactor originating from the probability to cross the vertices of coordination number 4 (note that $\frac{(2n-1)!!}{2^{n+1}n!} = \frac{\Gamma(n+1/2)}{2\sqrt{\pi}n!} \simeq \frac{1}{\sqrt{4\pi n}}$ for $n \gg 1$).

Large coherence length. In the opposite limit $L_\varphi \gg L$. Equation (C4) gives

$$\Delta \widetilde{\sigma}_n \simeq -\sqrt{\frac{L_\varphi L}{8\pi n}}e^{-nL/L_\varphi} \quad \text{for } L \ll L_\varphi \ll nL. \quad (60)$$

We have recovered an exponential damping of the harmonics, reminiscent of Eqs. (3) and (59), but with a different L_φ dependence of the pre-exponential factor.

On the other hand, for harmonics with $nL \ll L_\varphi$, the harmonics can be expanded by using Eq. (C3). Let us introduce $b_n = \ln n - \psi(n + \frac{1}{2}) + \psi(1)$. These coefficients converge to a finite limit at large n: $b_n = -\text{C} - \frac{1}{24n^2} + O(\frac{1}{n^4})$, where $\text{C} = -\psi(1) = 0.577215\ldots$ is the Euler constant. Finally we obtain

$$\Delta \widetilde{\sigma}_n \simeq -\frac{L}{2\pi}[\ln(2L_\varphi/nL) + b_n] \quad \text{for } nL \ll L_\varphi. \quad (61)$$

It is useful to remark that expressions (60) and (61) coincide with the limiting behaviors of the modified Bessel function $K_0(z)$ for large n (the proof is given in Appendix C),

$$\Delta \widetilde{\sigma}_n \simeq -\frac{L}{2\pi}K_0(nL/L_\varphi) \quad \text{for } L \ll L_\varphi. \quad (62)$$

Up to a factor $1/2$ interpreted below, this expression coincides with the MC harmonics for a long hollow cylinder,[14] Eq. (102) recalled in Sec. VIII. We compare this approximation with the exact expression (58) in Fig. 10. We see that the approximation is already good for $n = 1$, provided $L_\varphi \gtrsim L$. The difference rapidly diminishes as n increases.

Logarithmic divergence of the harmonics for $L_\varphi \to \infty$. We see from Eq. (61) that the harmonics are weakly dependent on n (for $n \ll L_\varphi/L$). This logarithmic behavior reflects the singular behavior $\Delta \widetilde{\sigma}_{\text{osc}}(\theta) \sim 1/\theta$, with a cutoff at $\theta \sim L/L_\varphi$: $\Delta \widetilde{\sigma}_n \sim \int_{L/L_\varphi}^{1/n} \frac{d\theta}{\theta} = \ln[L_\varphi/(nL)]$. The harmonics are therefore almost independent on n as soon as n is small enough com-
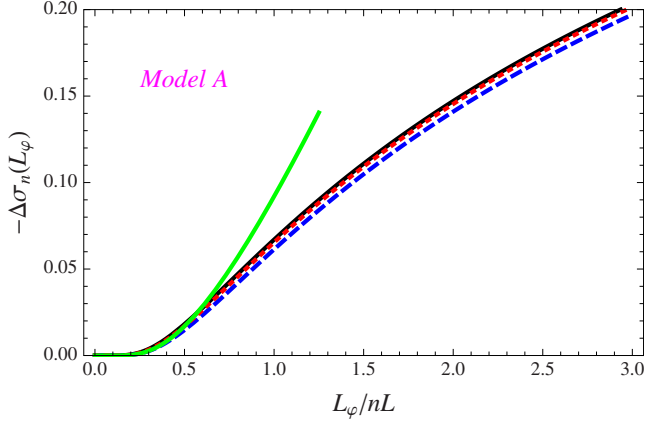
FIG. 10. (Color online) Comparison between exact result (58) for $n=1$ (dashed blue line) and 2 (dotted red line) and the approximation (62) (black continuous line). The interrupted green curve is (59). Even for small $n(=2)$ Eq. (62) is a very good approximation of Eq. (58).
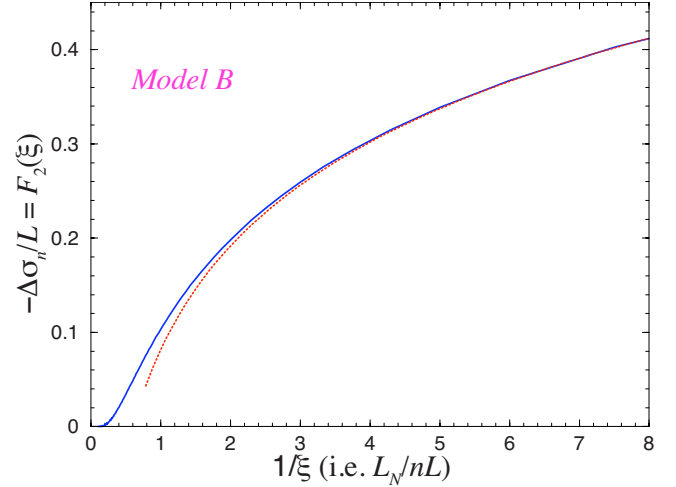

FIG. 11. (Color online) $\Delta\tilde{\sigma}_n \propto F_2(\xi)$ as a function of $1/\xi \propto L_N/nL$ (blue continuous line). Comparison with the limiting behavior (red dotted line) $\frac{1}{2\pi}[\ln(1/\xi) + C_{\text{cyl}}]$ with $C_{\text{cyl}} \simeq 0.51$.

pared to L_φ/L. Note that in practice, this logarithmic divergence of the harmonics is limited: for a chain of N_r rings contacted at two reservoirs, when the phase coherence length exceeds the total length of the chain $L_\varphi \gtrsim N_r L$, the cutoff is provided by $N_r L$. Therefore, for $L_\varphi \to \infty$, harmonics reach a finite limit $\Delta\tilde{\sigma}_n \simeq -\frac{L}{2\pi}\ln(N_r/n)$.

Winding probability. We now extract the probability $\mathcal{P}_n(x,x;t)$ from these results. First of all the behavior (59) is related to

$$\mathcal{P}_n(x,x;t) \simeq \frac{(2n-1)!!}{2^{n+1}n!}\frac{1}{\sqrt{4\pi t}}e^{-(nL)^2/4t} \quad \text{for } t \ll L^2. \quad (63)$$

We have recovered Eq. (12) with an additional dimensionless factor coming from the probability to cross the vertices of coordination number 4 (this factor can be understood when one writes the trace formula for the heat kernel in the network[29,70]).

The regime $L_\varphi \gtrsim L$ for the WL correction probes the regime $t \gtrsim L^2$ for the winding probability. We use the approximation (62) in order to perform the inverse Laplace transform. Using the integral representation of the modified Bessel function,[69] we get

$$\mathcal{P}_n(x,x;t) \simeq \frac{L}{8\pi t}e^{-(nL)^2/4t} \quad \text{for } t \gg L^2. \quad (64)$$

We may check that Eqs. (60) and (61) coincide with the limiting behaviors of this probability. It is interesting to point that this probability is similar to the one found for an infinitely long hollow cylinder, apart for a factor $1/2$. This additional factor can be understood from the fact that, starting from a given ring, it is equiprobable to return in one of its two arms.

Let us give a heuristic argument to recover roughly (64), which will be useful for the following. Arriving at a vertex, the diffusive particle equiprobably chooses one of the four arms. Therefore it is equiprobable to wind a ring or not, while diffusing along the chain. This suggests that the wind-

ing probability is almost independent on n, up to $n \sim \sqrt{t}/L$, the maximum number of rings explored for a time t. This rough approximation would be $\mathcal{P}_n(x,x;t) \sim \mathcal{N}_t\theta(\sqrt{t}/L - |n|)$. The normalization is estimated easily: since diffusion along the chain is one dimensional, we expect $\sum_n \mathcal{P}_n(x,x;t) \sim 1/\sqrt{t}$ so that $\mathcal{P}_n(x,x;t) \sim L/t$ for $|n| \lesssim \sqrt{t}/L$ and 0 otherwise. This is a crude estimate of Eq. (64).

B. Model B

In order to compute the MC harmonics we first need to construct the function W entering in Eq. (15). Following Appendix F, we introduce a coordinate $\tilde{x}=(x,f)$ to locate a point in the chain (the continuous variable x measures the distance along the chain while the discrete index $f \in \{u,d\}$ indicates the arm, up or down). If $\tilde{x}$ and $\tilde{x}'$ do not belong to the same ring we have

$$W(\tilde{x},\tilde{x}') = \frac{1}{4}|x - x'| = \frac{1}{2}W_{\text{wire}}(x,x'). \quad (65)$$

Remembering that $W(x,x')$ is proportional to the resistance between points x and x' this equation has a clear meaning: when two consecutive nodes are linked by two wires instead of one, the resistance is diminished by a factor of 2. In the limit $t \gg L_N^2$ the trajectories contributing to

$$\langle e^{i\Phi_{\sqrt{}}[\mathcal{C}_t^n]}\rangle_{V,\mathcal{C}_t^n} = \left\langle \exp\left[-\frac{2}{L_N^3}\int_0^t d\tau\, W(x(\tau),x(t-\tau))\right]\right\rangle_{\mathcal{C}_t^n} \quad (66)$$

are trajectories extending over distances $L_N \gg L$ along the chain. In this case we can neglect the contributions to the integral where the two arguments of $W(\tilde{x},\tilde{x}')$ are in the same ring. We have seen that for $nL \lesssim \sqrt{t}$ the measure of the Brownian paths weakly depends on n; therefore we expect that $\langle e^{i\Phi}\rangle_{V,\mathcal{C}_t^n} \simeq \langle e^{i\Phi}\rangle_{V,\mathcal{C}_t}$, where the average of the left-hand side is realized among Brownian curves of definite winding,

whereas the average of the right-hand side is among all Brownian curves. The argument shows that the function describing decoherence corresponds to the result of the infinite wire in which $L_N^3 \rightarrow 2L_N^3$. This factor 2 stands from the ratio between the resistance of a wire and of a chain of rings of the same length. Finally

$$\langle e^{i\Phi_V[\mathcal{C}_t^n]} \rangle_{V,\mathcal{C}_t^n} \simeq f_{\text{wire}}(t/2^{2/3}\tau_N). \qquad (67)$$

We can use Eq. (24) in order to compute $\Delta\tilde{\sigma}_n$ $\simeq -2\int_{L^2}^{\infty} dt \frac{Le^{-(nL)^2/4t}}{8\pi t} f_{\text{wire}}(t/2^{2/3}L_N^2)$. The lower cutoff takes into account the fact that expression of $\mathcal{P}_n(x,x;t)$ is only valid for $t \gg L^2$. However, except if $n=0$, the cutoff is not important and can be replaced by 0. Using Eq. (24) we obtain (Fig. 11)

$$\Delta\tilde{\sigma}_n \simeq -L F_2(2^{-1/3}nL/L_N), \qquad (68)$$

where

$$F_2(\xi) = \frac{1}{4} \sum_{m=1}^{\infty} \frac{1}{|u_m|^{3/2}} e^{-\sqrt{|u_m|}\xi}. \qquad (69)$$

In the limit $L_N \ll nL$ the first term of the series dominates,

$$\Delta\tilde{\sigma}_n \simeq -\frac{L}{4|u_1|^{3/2}} e^{-\kappa_3 nL/L_N} \qquad (70)$$

$$\sim e^{-nLT^{1/3}} \quad \text{for } L \ll L_N \ll nL, \qquad (71)$$

where $\kappa_3 = 2^{-1/3}|u_1|^{1/2} \simeq 0.801$.

In the opposite limit, for $nL \ll L_N(\xi \rightarrow 0)$, we can replace the sum by an integral and use the asymptotic behavior $u_m \simeq -[\frac{3\pi}{2}(m-\frac{3}{4})]^{2/3}$,

$$F_2(\xi) \simeq_{\xi \rightarrow 0} \frac{1}{6\pi} \int_1^{\infty} \frac{dm}{m} e^{-\xi[3\pi m/4]^{1/3}}, \qquad (72)$$

$$F_z(\xi) \simeq \frac{1}{6\pi} \int_1^{1/\xi^3} \frac{dm}{m} + \text{cste} = \frac{1}{2\pi}[\ln(1/\xi) + C_{\text{cyl}}]. \qquad (73)$$

Finally we find a result similar to the one obtained for exponential relaxation of phase coherence,

$$\Delta\tilde{\sigma}_n \simeq -\frac{L}{2\pi}[\ln(L_N/nL) + C_{\text{chain}}] \quad \text{for } nL \ll L_N. \qquad (74)$$

The constant is estimated numerically: we find $C_{\text{cyl}} \simeq 0.51$, hence $C_{\text{chain}} \simeq 0.74$. This result could also have been more simply obtained by noticing that $f_{\text{wire}}(t/2^{2/3}L_N^2)$ cuts the tail of $\mathcal{P}_n(x,x;t)$ on a scale L_N^2: $\langle\Delta\tilde{\sigma}_n\rangle \simeq -2\int_{(nL)^2}^{L_N^2} dt \frac{L}{8\pi t}$.

Comparison between models A and B. As we have done for the infinite wire and the connected ring, we establish some correspondence between the results for the two models when $L_N \gg L$. In the regime $L \ll L_N \ll n^2L$ the exponentials of Eqs. (60) and (70) may be matched if $L_\varphi \rightarrow L_N/\kappa_3 \simeq 1.25L_N$. In the regime $L_N \gg n^2L$ the logarithmic behaviors (61) and (74) coincide for $L_\varphi \rightarrow 1.87L_N$.

For not too large n, the two curves $\Delta\tilde{\sigma}_n^{(B)}(L_N)$ $\approx \Delta\tilde{\sigma}_n^{(A)}(L_\varphi \simeq 1.87L_N)$ are very close, apart for $L_N \ll L$ for which there is a qualitative difference between Eqs. (3) and (27).

From the conductivity to the conductance. The weights in Eq. (8) are all equal and conductance is related to an uniform integration of $\Delta\tilde{\sigma}(x)$ in the chain. The dimensionless conductance is given by $\Delta g = \frac{4}{N_r L}\Delta\tilde{\sigma}$, where N_r is the number of rings of the chain.

VII. SQUARE NETWORK

The easiest way to realize disorder averaging experimentally is to use networks with a large number of rings, like 2D networks (square,[6,11,15,16,67,68] honeycomb,[15,19,20] dice[11,51]). The "high-temperature" regime ($L_N \ll L$) is now well understood theoretically and experimentally,[6] but low-temperature experimental results are still unexplained.[51] Therefore understanding the magnetoconductance of large networks when decoherence is dominated by *e-e* interaction still deserves some clarification. In this section we study the case of an infinite square network of lattice spacing *a* (Fig. 1).

A. Model A

The weak localization correction was derived analytically by Douçot and Rammal for rational fluxes $\theta_{p,q} = 2\pi p/q$ with $p,q \in \mathbb{N}$ (reduced flux is defined as $\frac{\theta}{2\pi} = 2\phi/\phi_0$). They obtained[26]

$$\Delta\tilde{\sigma}(\theta_{p,q}) = -\frac{L_\varphi}{2}\left[\coth\frac{a}{L_\varphi} - \frac{L_\varphi}{a} + \frac{8\sinh\frac{a}{L_\varphi}}{\pi q}\frac{P'_{p,q}\left(4\cosh\frac{a}{L_\varphi}\right)}{P_{p,q}\left(4\cosh\frac{a}{L_\varphi}\right)}\right.$$
$$\left. \times K\left(\frac{4}{P_{p,q}\left(4\cosh\frac{a}{L_\varphi}\right)}\right)\right], \qquad (75)$$

where $P_{p,q}(\varepsilon)$ is a polynomial of degree q defined in Appendix G, Sec. 3 where derivation of Eq. (75) is recalled. $K(x)$ is the elliptic integral of the first kind.[69]

Weakly coherent network. The harmonics are suppressed exponentially as $\Delta\tilde{\sigma}_n \propto -L_\varphi e^{-4na/L_\varphi}$. Despite the fact that there is no close expression of the remaining dimensionless *n*-dependent factor, a systematic expansion of the spectral determinant can be written thanks to the trace formula of Ref. 70 (the first terms of this expansion are available in Ref. 16).

Large coherence length. The rest of the section is devoted to the large coherence length regime $L_\varphi \gg a$.

Continuum limit. In the limit of small flux, $\theta \ll 1$, and large coherence length, $L_\varphi \gg a$, the discrete character of the network disappears and one should recover the results for the 2D plane in a uniform magnetic field. Informations can be extracted from the study of this limit.

The zero-field WL correction is obtained from Eq. (75) with $p=q=1$, using $P_{1,1}(x)=-x$. Using the expansion of the elliptic integral,[69,71] we find[16,72]

$$\Delta\widetilde{\sigma}(0) \simeq -\frac{a}{\pi}\left[\ln(4L_{\varphi}/a) + \frac{\pi}{6}\right]. \qquad (76)$$

This result is reminiscent of the WL correction of the film (91), but here, the cutoff at small scales is naturally provided by the lattice spacing a.

The limit of small fluxes is studied in detail in Appendix G, Sec. 2. Using that $\theta = 4\pi\phi/\phi_0 = 4\pi\mathcal{B}a^2/\phi_0$, Eq. (G4) reads

$$\Delta\widetilde{\sigma}(\theta \ll 1) - \Delta\widetilde{\sigma}(0) \simeq \frac{a}{2\pi}\left[\psi\left(\frac{1}{2} + \frac{a^2}{\theta L_{\varphi}^2}\right) - \ln\left(\frac{a^2}{\theta L_{\varphi}^2}\right)\right]. \qquad (77)$$

This expression gives a quadratic behavior for small flux[86]

$$\Delta\widetilde{\sigma}(\theta) - \Delta\widetilde{\sigma}(0) \simeq \frac{a}{48\pi}\left(\frac{\theta L_{\varphi}^2}{a^2}\right)^2 \quad \text{for } \theta \ll \frac{a^2}{L_{\varphi}^2} \qquad (78)$$

and a logarithmic behavior for intermediate fluxes[86]

$$\Delta\widetilde{\sigma}(\theta) \simeq \frac{a}{2\pi}[\ln\theta + C_{\mathrm{sn}}] \quad \text{for } \frac{a^2}{L_{\varphi}^2} \ll \theta \ll 1, \qquad (79)$$

where $C_{\mathrm{sn}} = -\mathrm{C} - 3\ln 2 - \frac{\pi}{3} \simeq -3.704$.

We now turn to the analysis of the MC harmonics. A first simple remark allows to get the scaling of harmonics with time: the reduced flux θ is the variable conjugated to the harmonic number n; therefore the structure $\Delta\widetilde{\sigma}(\theta) = \mathrm{fct}(a/\sqrt{\theta}L_{\varphi})$ corresponds to $\Delta\widetilde{\sigma}_n = \mathrm{fct}(\sqrt{n}a/L_{\varphi})$. We now extract this function. Using the path integral formulation it is straightforward to get the structure

$$\Delta\widetilde{\sigma}(\theta) - \Delta\widetilde{\sigma}(0) = -2\int_0^{\infty} dt\, \mathcal{P}(x,x;t)(\langle e^{i\theta\mathcal{N}[\mathcal{C}_t]}\rangle_{\mathcal{C}_t} - 1)e^{-t/L_{\varphi}^2}, \qquad (80)$$

where $\mathcal{N}[\mathcal{C}_t]$ is the winding number of the closed trajectory. At large times the return probability coincides with the one of a plane, $\mathcal{P}(x,x;t) \simeq \frac{a}{4\pi t}$ (Appendix F, Sec. 3); it can be obtained from Eq. (76) thanks to an inverse Laplace transform. Using[69] $\int_0^{\infty} dt\left(\frac{1}{t} - \frac{\lambda}{\sinh\lambda t}\right)e^{-\gamma t} = \psi\left(\frac{1}{2} + \frac{\gamma}{2\lambda}\right) - \ln\left(\frac{\gamma}{2\lambda}\right)$, we deduce that expression (77) corresponds to $\langle e^{i\theta\mathcal{N}[\mathcal{C}_t]}\rangle_{\mathcal{C}_t} \simeq \frac{\theta t}{2a^2 \sinh(\theta t/2a^2)}$. A Fourier transform[69] gives the distribution of the winding number, plotted in Fig. 17,

$$Q_t(\mathcal{N}) \simeq \frac{\pi a^2}{2t \cosh^2(\pi a^2\mathcal{N}/t)}. \qquad (81)$$

We have recovered the well-known Levy law for the distribution of the algebraic area $\mathcal{A} = \mathcal{N}a^2$ enclosed by a planar Brownian motion.[73–76] For $t \gg a^2$ and $n \gg 1$, the return probability conditioned to wind n fluxes is therefore expected to behave as $\mathcal{P}_n(x,x;t) \simeq \mathcal{P}(x,x;t)Q_t(n)$,

$$\mathcal{P}_n(x,x;t) \simeq \frac{a^3}{8t^2}\frac{1}{\cosh^2(\pi na^2/t)}. \qquad (82)$$

A Laplace transform gives the corresponding harmonics,

$$\Delta\widetilde{\sigma}_n \simeq -\frac{a}{4\pi n}\mathcal{F}_3(\pi na^2/L_{\varphi}^2), \qquad (83)$$

where

$$\mathcal{F}_3(\xi) = \int_0^{\infty} dy\, \frac{e^{-\xi/y}}{\cosh^2 y}. \qquad (84)$$

We extract the following limiting behaviors:

$$\mathcal{F}_3(\xi) \underset{\xi \ll 1}{\simeq} 1 - \xi\ln(\xi_0/\xi), \qquad (85)$$

$$\mathcal{F}_3(\xi) \underset{\xi \gg 1}{\simeq} \sqrt{4\pi}(2\xi)^{1/4}e^{-\sqrt{8\xi}}. \qquad (86)$$

The constant ξ_0 is estimated numerically: $\xi_0 \simeq 1.239$. The tail of the distribution corresponds to

$$\Delta\widetilde{\sigma}_n \simeq -\frac{a}{(2n)^{3/4}}\sqrt{\frac{a}{\pi L_{\varphi}}}e^{-\sqrt{8}\pi na/L_{\varphi}} \qquad (87)$$

for $L_{\varphi} \ll \sqrt{n}a$. The saturation of the harmonics for $L_{\varphi} \rightarrow \infty$ is given by

$$\Delta\widetilde{\sigma}_n \simeq -\frac{a}{4\pi n}\left[1 - \frac{\pi na^2}{L_{\varphi}^2}\ln\left(\frac{L_{\varphi}^2\xi_0}{\pi na^2}\right)\right] \qquad (88)$$

for $\sqrt{n}a \ll L_{\varphi}$.

Harmonics reach a finite limit for $L_{\varphi} \rightarrow \infty$. It is interesting to compare the MC of the chain and the MC of the square network. For the chain, the behavior of the MC near zero flux $\Delta\widetilde{\sigma}^{(\mathrm{chain})}(\theta) \sim 1/\theta + \mathrm{cste}$, Eq. (55), is related to a weak logarithmic divergence of the harmonics $\Delta\widetilde{\sigma}_n^{(\mathrm{chain})} \sim \ln(L_{\varphi}/nL)$, Eq. (61). For planar networks the WL correction presents a weaker divergence at zero magnetic field $\Delta\widetilde{\sigma}(\theta) \sim \ln\theta$. Therefore $\int_0^{2\pi} d\theta\, \Delta\widetilde{\sigma}(\theta) < \infty$ and the harmonics reach a finite value in the limit $L_{\varphi} \rightarrow \infty$. Let us compute this value. The singular behavior $\Delta\widetilde{\sigma}(\theta) \simeq \mathrm{Cste} + \frac{a}{2\pi}\ln|\theta|$ near zero flux is expected to dominate the harmonics behavior $\Delta\widetilde{\sigma}_n \sim \int_0 d\theta\ln\theta\cos(n\theta)$. The typical scale over which $\ln\theta$ varies is $\theta\ln 1/\theta$. If we define θ_c by $\theta_c\ln 1/\theta_c = 1/n$, we see that the integral is dominated by the interval $[0, \theta_c]$. We have $\theta_c \simeq 1/(n\ln n)$, whence $\Delta\widetilde{\sigma}_n \sim \int_0^{1/(n\ln n)} d\theta\ln\theta \simeq -1/n$. More precisely, we have obtained above: $\Delta\widetilde{\sigma}_n \simeq -\frac{a}{4\pi n}$ for $n \gg 1$.

Numerical calculations. The MC is computed numerically as a function of the reduced flux θ for rational fluxes $\theta = 2\pi p/q$. As recalled in Appendix G, Sec. 3 the computation of the MC is related to the study of the spectrum of a tight binding Hamiltonian on a square lattice submitted to a magnetic field, the so-called Hofstadter problem. For rational flux $\theta = 2\pi p/q$, this spectrum presents q bands determined by the polynomials $P_{p,q}(\varepsilon)$. For example, band edges correspond to roots of $P_{p,q}(\varepsilon) = \pm 4$. For small q (in practice we choose ≤ 8) the MC is computed by using Eq. (75). For large q (large number of Hofstadter bands), we use a more efficient procedure and rather follow Ref. 77: we neglect the dispersion of Hofstadter bands, according to which Eq. (G10) reduces to $\frac{1}{N_x N_y}\mathrm{Tr}\{\frac{1}{N(\gamma,\theta_{p,q})}\} \simeq \frac{1}{q}\sum_{r=1}^q \frac{1}{4\cosh(\sqrt{\gamma}a) + \bar{\varepsilon}_r}$, where $\bar{\varepsilon}_r$ designates the position of the band. The weak localization correction is represented in Fig. 12 as a function of the reduced flux θ for three values of the ratio L_{φ}/a. As this latter
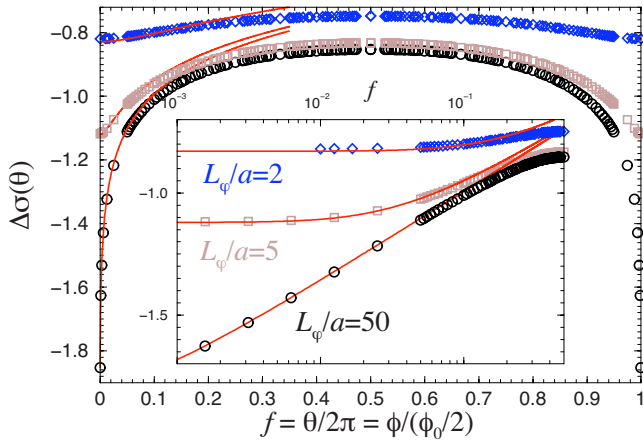
FIG. 12. (Color online) WL correction for $L_\varphi/a=2$ (blue diamonds), $L_\varphi/a=5$ (brown squares), and $L_\varphi/a=50$ (black circles). The red continuous lines correspond to the continuum limit, Eqs. (76) and (77).

increases, the MC becomes sharper around zero flux, according to the above discussion, and the harmonic content becomes richer. The MC is computed in this way for different values of the phase coherence length ranging from $L_\varphi/a=0.5$ to 50. For each curve the first ten harmonics are extracted and plotted as a function of L_φ/a in Fig. 13.

In order to analyze the numerical results, we use the discussion of the above paragraph on the continuum limit. In the limit $L_\varphi \gg a$ we expect the scaling $n_t \sim t/a^2$. In Fig. 14, we plot $\frac{4\pi n}{a}\Delta\tilde\sigma_n$ as a function of $1/\sqrt{\xi}=L_\varphi/a\sqrt{\pi n}$ (note that the scaling $n_t \sim t/a^2$ is only expected for $L_\varphi \gtrsim a$ when we reach a "two-dimensional limit;" for $L_\varphi \lesssim a$ we rather expect the scaling corresponding to the isolated ring $n_t \sim \sqrt{t}/a$).

After rescaling, all curves of Fig. 13 collapse onto each other as we can see in Fig. 14 (at least in the domain $L_\varphi \gtrsim a$). Some significant deviation from expression (83) occurs only for $n=1$. In order to analyze the behavior for largest L_φ more precisely, harmonics are replotted as functions of the variable $\xi \ln(\xi_0/\xi)$ in the inset of Fig. 14: we check the linear
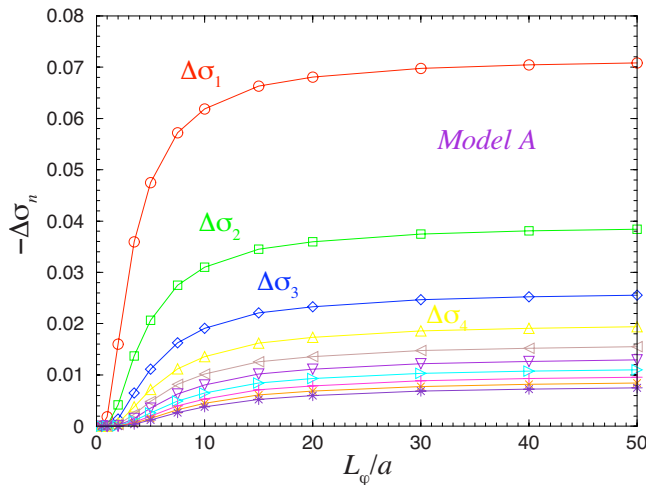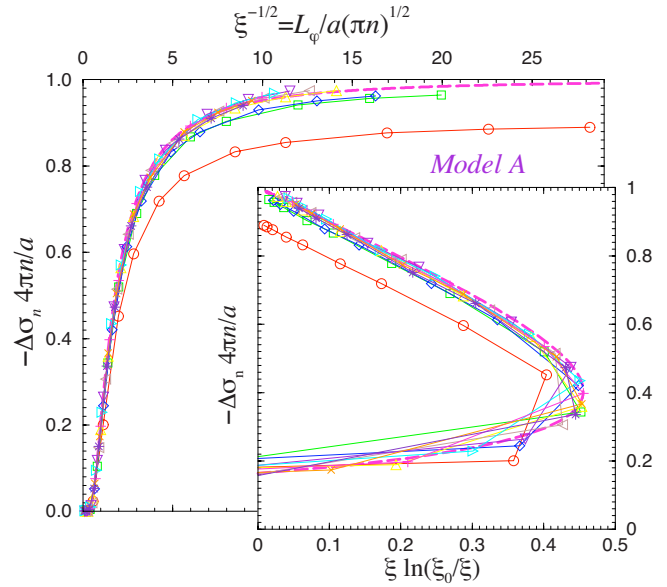

FIG. 14. (Color online) The harmonics represented in Fig. 13 are plotted here as a function of the variable $\sqrt{\xi}=L_\varphi/a\sqrt{\pi n}$. The magenta dashed line corresponds to the continuum limit: function $\mathcal{F}_3(\xi)$. Inset: Same functions as a function of $\xi \ln(\xi_0/\xi)$ with $\xi_0 \simeq 1.239$.

behavior with this variable. Surprisingly, the continuum limit can be considered as a very good approximation already for $n \geq 2$.

Remark: Brownian path/random walk. We have shown that the distribution of the number $n \in \mathbb{Z}$ of cells enclosed by a Brownian path in the square lattice is very close from the Levy law describing the distribution of the algebraic area enclosed by a planar Brownian motion (continuum limit) already for $n \geq 2$. It is interesting to point out that this remark also holds for the number of cells enclosed by a *discrete* random walk jumping between the different nodes of the square lattice.[78,79]

FIG. 13. (Color online) Numerical calculation of ten first MC harmonics $\Delta\tilde\sigma_n$ for a square network, computed for L_φ/a between 0.5 and 50.

B. Model B

1. Two-dimensional limit

The thin film. Let us first recall some known results for the plane (or thin film of thickness b).[3,33,35] In two dimensions the diffuson presents a logarithmic behavior. The function W behaves in the same way, with a cutoff at small scales at the thermal length L_T:[3,33,52,80] $W(\vec{r},\vec{r}')=\frac{1}{2\pi}\ln(\|\vec{r}-\vec{r}'\|/L_T)$ for $\|\vec{r}-\vec{r}'\| \gtrsim L_T$. Therefore the functional governing decoherence behaves as

$$\Gamma[\mathcal{C}_t]t \equiv \frac{1}{2}\langle\Phi_V[\mathcal{C}_t]^2\rangle_V \sim \frac{2e^2T}{\sigma_0 b}t\frac{1}{2\pi}\ln\frac{\sqrt{Dt}}{L_T}. \quad (89)$$

We recognize the sheet resistance[82] $R_\square=1/(b\sigma_0)$ of the film of thickness b. The phase coherence (Nyquist) time is evaluated from $\Gamma[\mathcal{C}_t]t \sim 1$. We obtain the temperature dependence[3,33,35]

$$\frac{1}{\tau_N^{\text{film}}} = \frac{R_\square}{h/e^2} T \ln\left[\frac{h/e^2}{2R_\square} \right], \tag{90}$$

valid for $L_T \gg b$. This behavior was observed experimentally for thin metallic film[83] and two-dimensional electron gas.[84] We recall that 2D magnetoconductance is given by:[2,13,85]

$$\Delta\sigma^{\text{film}}(\mathcal{B}) = \frac{2e^2}{h} \frac{1}{2\pi b}\left[\psi\left(\frac{1}{2} + \frac{\tau_\mathcal{B}}{\tau_N^{\text{film}}} \right) - \ln\left(\frac{\tau_\mathcal{B}}{\tau_e} \right) \right] + \text{cste}, \tag{91}$$

where $\tau_\mathcal{B} = \phi_0/(8\pi D\mathcal{B})$ and $\psi(z)$ is the Digamma function[86] [the additional factor $1/2$ in the Digamma function, compared to Eq. (77), is explained in Appendix G, Sec. 2]. We may simply write $\Delta\sigma \simeq -\frac{2e^2}{h}\frac{1}{2\pi b}\ln[\min(\tau_N^{\text{film}}, \tau_\mathcal{B})/\tau_e] + \text{cste}$. The small time cutoff τ_e in Eq. (91) is introduced by hand to account for the fact that the diffusion approximation only holds for times[87] $t \gtrsim \tau_e$.

The square network. For large time scale ($\tau_\varphi \sim t \gg a^2$) and small magnetic fields (such that $\phi \ll \phi_0$) the result for the network should coincide with the one for a plane. In this case the function W entering the decoherence rate is $W(x,x') \simeq \frac{a}{2\pi} \ln(\|x-x'\|/a)$, where $\|x-x'\|$ is the distance between the two points of the network. The logarithmic behavior is now cut off naturally at the scale a. Because the function W presents a smooth logarithmic behavior, we extract the relevant time scale (phase coherence time) by following the same lines as for the plane. We write

$$\Gamma[\mathcal{C}_t] t \equiv \frac{1}{2}\langle \Phi_V[\mathcal{C}_t]^2 \rangle_V \sim \frac{2D}{L_N^3} t \frac{a}{2\pi} \ln\frac{\sqrt{Dt}}{a} = \frac{2e^2 T}{\sigma_0 s} t \frac{a}{2\pi} \ln\frac{\sqrt{Dt}}{a}, \tag{92}$$

where $s = wb$ is the section of the wires of width w and thickness b (Fig. 1). From this expression we extract a time scale reminiscent of Eq. (90) for the film,

$$\frac{1}{\tau_N^{\text{net}}} = \frac{R_\square^{\text{net}}}{h/e^2} T \ln\left[\frac{L_T^2}{a^2} \frac{h/e^2}{2R_\square^{\text{net}}} \right]. \tag{93}$$

This result is valid for $L_T \lesssim a$. The opposite limit $L_T \gtrsim a$ is similar to the case of a thin film. The cutoff in the function W is given by the thermal length[52] L_T, and therefore $1/\tau_N^{\text{net}} = \frac{R_\square^{\text{net}}}{h/e^2} T \ln[\frac{h/e^2}{2R_\square^{\text{net}}}]$. However this latter regime seems less relevant from the experimental point of view.[36] The sheet resistance of the network is

$$R_\square^{\text{net}} = \frac{a}{wb\sigma_0} = \frac{a}{s\sigma_0} = R_\square \frac{a}{w}. \tag{94}$$

This characteristic time is reduced by a factor w/a, compared to the Nyquist time (90) obtained for a film of same thickness: $\tau_N^{\text{net}} \sim \frac{w}{a}\tau_N^{\text{film}}$. We can also introduce a Nyquist length for the network $L_N^{\text{net}} = \sqrt{D\tau_N^{\text{net}}}$, related to the Nyquist length of the wire L_N by,[90]

$$\frac{1}{L_N^{\text{net}}} = \frac{1}{L_T} \sqrt{\frac{R_\square^{\text{net}}}{h/e^2} \ln\left[\frac{L_T^2}{a^2} \frac{h/e^2}{2R_\square^{\text{net}}} \right]} = \sqrt{\frac{3a}{2\pi L_N^3}} \ln(L_N/a). \tag{95}$$

We expect that the MC presents the logarithmic behavior $\Delta\widetilde{\sigma} \simeq \frac{a}{2\pi}[\ln\theta + C_{\text{sn}}]$, which is cut off at very low magnetic field: $\Delta\widetilde{\sigma} \simeq -\frac{a}{\pi}\ln[\min(L_N^{\text{net}}, L_\mathcal{B})/a]$, where $L_\mathcal{B} = \sqrt{\phi_0/(4\pi\mathcal{B})}$ is the 2D cutoff.

2. MC harmonics

In the network, the diffuson behaves logarithmically at large distances $P_d(x,x') \simeq -\frac{a}{2\pi}\ln(\|x-x'\|/a)$. Therefore we expect that the relaxation of phase coherence is controlled by

$$\frac{1}{2}\langle \Phi_V[\mathcal{C}_t]^2 \rangle_{V,\mathcal{C}_t} \sim \frac{a}{\pi L_N^3} t \ln(\sqrt{t}/a) \rightarrow \frac{3a}{2\pi L_N^3} t \ln(L_N/a). \tag{96}$$

As for the plane we use the fact that the functional describing decoherence weakly depends on trajectories since $W(x,x') \sim \ln\|x-x'\|$. This suggests that the result for model B is given by performing, in the result for model A, the substitution

$$\frac{1}{L_\varphi^2} \rightarrow \frac{3a}{2\pi L_N^3}\ln(L_N/a), \quad \text{i.e.,} \quad L_\varphi \rightarrow L_N^{\text{net}}, \tag{97}$$

where the Nyquist length for the network is given by Eq. (95). Using Eq. (87), we get for the tail

$$\Delta\widetilde{\sigma}_n \sim (L_N^{\text{net}})^{-1/2} e^{-\sqrt{8\pi n}\, a/L_N^{\text{net}}}$$
$$\sim L_N^{-3/4} \ln^{1/4}\left(\frac{L_N}{a} \right) e^{-\sqrt{n}(a/L_N)^{3/2}\ln^{1/2}(L_N/a)}, \tag{98}$$

$$\Delta\widetilde{\sigma}_n \sim (T\ln 1/T)^{1/4} e^{-n^{1/2}a^{3/2}(T\ln 1/T)^{1/2}}. \tag{99}$$

A similar substitution in Eq. (88) leads to

$$\Delta\widetilde{\sigma}_n \sim -\frac{a}{4\pi n}\left[1 - \frac{9na^3}{2L_N^3}\ln^2(L_N/a) \right] \tag{100}$$

to describe the saturation of the harmonics at large L_N/a (small temperature).

We insist that since $\int_0 d\theta \Delta\sigma(\theta) < \infty$ the harmonics reach a limit for $L_\varphi \rightarrow \infty$ (or $L_N \rightarrow \infty$), which is independent on the decoherence mechanism. In other terms the magnetoconductance curve $\Delta\widetilde{\sigma}(\theta)$ reaches a limit apart in a very narrow region of width $\delta\theta \sim (a/L_\varphi)^2$ around zero flux (Fig. 12).

VIII. HOLLOW CYLINDER

We have noticed that a network made of a large number of rings realizes disorder averaging. Another natural way to realize this averaging is to consider a long hollow cylinder of perimeter L (longer than L_φ) submitted to a magnetic field along its axis.[14,15,17,18] We study below how the original result of AAS (Ref. 14) obtained within model A is modified when decoherence is dominated by electron-electron interac-
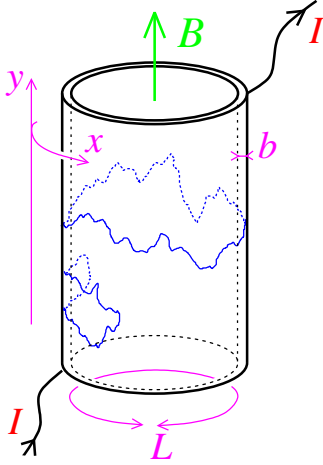
FIG. 15. (Color online) A metallic film is deposited on an insulating wire. This allows to study quantum transport in a long hollow cylinder.[17] Two diffusive trajectories are represented with winding $n=0$ and $n=1$.

tion. In this section, it is natural to define the reduced dimensionless conductivity $\widetilde{\sigma}$ as $\sigma = \frac{2e^2}{hb}\widetilde{\sigma}$, where b is the thickness of the metallic film.

A. Model A

Let us first recall the well-known result for the weak localization correction computed within model A.[12,14] We denote by $y \in \mathbb{R}$ the coordinate along the axis of the cylinder and $x \in [0,L]$ the coordinate in the perpendicular direction. The WL correction is written as a path integral over Brownian paths $\vec{r}(\tau) = [x(\tau), y(\tau)]$ in the cylinder, where $x(\tau)$ describes a Brownian path on the circle and $y(\tau)$ on $\mathbb{R}$ (Fig. 15),

$$\Delta\widetilde{\sigma}_n^{\text{AAS}} = -2\int_0^\infty dt\, e^{-t/\tau_\varphi}$$
$$\times \int_{\vec{r}(0)=\vec{r}}^{\vec{r}(t)=\vec{r}} \mathcal{D}\vec{r}(\tau)\, \delta_{n,\mathcal{N}[x(\tau)]} \exp\left(-\int_0^t d\tau\, \frac{1}{4}\dot{\vec{r}}^2\right),$$
(101)

$$\Delta\widetilde{\sigma}_n^{\text{AAS}} = -2\int_0^\infty dt\, e^{-t/\tau_\varphi}\frac{e^{-(nL)^2/4t}}{4\pi t} = -\frac{1}{\pi}K_0\left(\frac{nL}{L_\varphi}\right),$$
(102)

where $K_0(x)$ is a modified Bessel function. Therefore

$$\Delta\widetilde{\sigma}_n^{\text{AAS}} \simeq -\sqrt{\frac{L_\varphi}{2\pi nL}}\, e^{-nL/L_\varphi} \quad \text{for } L_\varphi \ll |nL|, \quad (103)$$

$$\Delta\widetilde{\sigma}_n^{\text{AAS}} \simeq -\frac{1}{\pi}\ln(L_\varphi/nL) \quad \text{for } |nL| \ll L_\varphi. \quad (104)$$

These results are very similar to the one obtained for the chain of rings [Eqs. (60)–(62)]. This is due to the similar winding properties, what was already noticed after Eq. (64).

B. Model B: *e-e* interaction

We now have to consider the path integral

$$\Delta\widetilde{\sigma}_n = -2\int_0^\infty dt\int_{\vec{r}(0)=0}^{\vec{r}(t)=0} \mathcal{D}\vec{r}(\tau)\, \delta_{n,\mathcal{N}[x(\tau)]}$$
$$\times \exp\left\{-\int_0^t d\tau\left[\frac{1}{4}\dot{\vec{r}}^2 + 2e^2 TR_\square W(\vec{r}(\tau),0)\right]\right\},$$
(105)

where we have used translation invariance along the two perpendicular directions in order to deal with a path integral with action local in time, in a similar way as for the ring: Eq. (A1).

1. Function W

The cylinder is translation invariant in the two directions, therefore we may write $W(\vec{r},\vec{r}') = W(\vec{r}-\vec{r}',0)$ with $W(\vec{r},0) = P_d(\vec{r}_c,0) - P_d(\vec{r},0)$, where $\vec{r}_c$ is a short distance cutoff of order L_T (we will see that the direction of the vector $\vec{r}_c$ plays no role).[52]

In order to avoid the divergent contribution of the zero mode of the Laplace operator, we start by considering the solution of $(\gamma - \Delta)P = \delta$,

$$P(\vec{r},0) = \frac{1}{L}\sum_{n\in\mathbb{Z}}\int_{-\infty}^{+\infty}\frac{dk}{2\pi}\frac{e^{2i\pi nx/L+iky}}{\gamma + \left(\frac{2\pi n}{L}\right)^2 + k^2}, \quad (106)$$

$$P(\vec{r},0) = \frac{1}{2L}\sum_{n\in\mathbb{Z}}\frac{1}{\sqrt{\gamma + \left(\frac{2\pi n}{L}\right)^2}}e^{2i\pi nx/L-\sqrt{\gamma+(2\pi n/L)^2}|y|}.$$
(107)

Next we take the limit $\gamma \to 0$ in

$$W(\vec{r},0) = \lim_{\gamma\to 0}[P(\vec{r}_c,0) - P(\vec{r},0)], \quad (108)$$

$$W(\vec{r},0) = \frac{|y|}{2L} + \frac{1}{2\pi}\sum_{n=1}^\infty \frac{1}{n}\left(\cos\frac{2\pi nx_c}{L}e^{-2\pi ny_c/L}\right.$$
$$\left. - \cos\frac{2\pi nx}{L}e^{-2\pi n|y|/L}\right). \quad (109)$$

We finally obtain

$$W(\vec{r},0) = \frac{|y|}{2L} + \frac{1}{2\pi}\,\text{Re}\left[\ln\left(\frac{1-e^{-2\pi(ix+|y|)/L}}{2\pi L_T/L}\right)\right], \quad (110)$$

where we used that $\|\vec{r}_c\| = L_T \ll L$. We can check that this expression reproduces known results in two limits: for $|y| \gg L$, we recover the 1D form $W \simeq |y|/(2L)$. For $|y| \ll L$ we obtain the 2D result $W \simeq \frac{1}{2\pi}\ln(\|\vec{r}\|/L_T)$.

2. Harmonics

The first term of Eq. (110) originates from the 1D motion along the cylinder. To this 1D motion, we can associate a 1D
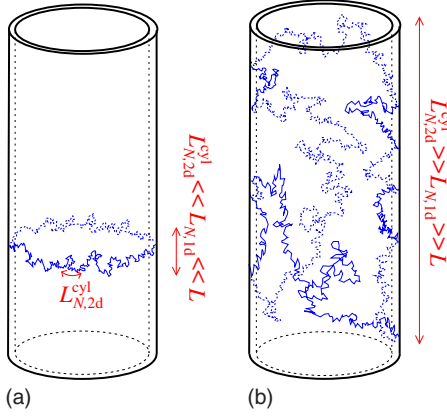
FIG. 16. (Color online) Trajectories contributing to first harmonic for "high temperature" (left) and "low temperature" (right).

Nyquist time similar to the one obtained for the wire, Eq. (5),

$$\frac{1}{\tau_{N,1\mathrm{D}}} = \left(\frac{e^2 R_\square \sqrt{DT}}{L}\right)^{2/3} = \left(\frac{e^2\sqrt{DT}}{\sigma_0 bL}\right)^{2/3} \quad (111)$$

that coincides with Eq. (5) in which the section is taken as $s = bL$.

We consider first the high-temperature limit $L \gg L_{N,1\mathrm{D}} = \sqrt{D\tau_{N,1\mathrm{D}}} = (\frac{\sigma_0 DbL}{e^2 T})^{1/3}$. We remark that for the harmonic $n = 0$, trajectories very unlikely wind around the cylinder and we can use $W \simeq \frac{1}{2\pi} \ln(\|\vec{r}\|/L_T)$ for $y \ll L$. Therefore the calculation of the path integral (105) corresponds to the one for the film, $\Delta\sigma_0 \simeq \Delta\sigma^{\mathrm{film}}$, with the time scale (90).

Next we consider nonzero harmonics $n \neq 0$. In this case the trajectories have a small extension along the wire $|y| \lesssim L_{N,1\mathrm{D}} \ll L$ and we can neglect the $|y|$ in the exponential in Eq. (110) (see Fig. 16). Therefore we perform the substitution

$$W(\vec{r},0) \rightarrow \frac{|y|}{2L} + \widetilde{W}(x) \quad (112)$$

with

$$\widetilde{W}(x) = \frac{1}{2\pi} \ln \frac{|\sin(\pi x/L)|}{\pi L_T/L}. \quad (113)$$

This approximation allows us to factorize the path integral as

$$\Delta\widetilde{\sigma}_n \simeq -2\int_0^\infty dt \int_{x(0)=0}^{x(t)=0} \mathcal{D}x(\tau)\,\delta_{n,\mathcal{N}[x(\tau)]}$$
$$\times \exp\left\{-\int_0^t d\tau\left[\frac{1}{4}\dot{x}^2 + 2e^2 TR_\square \widetilde{W}(x)\right]\right\}$$
$$\times \int_{y(0)=0}^{y(t)=0} \mathcal{D}y(\tau)\exp\left(-\int_0^t d\tau\left[\frac{1}{4}\dot{y}^2 + \frac{|y|}{L_{N,1\mathrm{D}}^3}\right]\right). \quad (114)$$

The first path integral runs over trajectories encircling the cylinder. Therefore we can replace $\widetilde{W}(x)$ by its average $\int_0^L \frac{dx}{L}\widetilde{W}(x)$. This approximation is justified by the fact that $\widetilde{W}$ has only a logarithmic dependence. This simplify the calcu-

lation by substituting the functional by a constant,

$$2e^2 TR_\square \int_0^t d\tau \widetilde{W}(x(\tau)) \rightarrow \frac{t}{\tau_{N,2\mathrm{D}}^{\mathrm{cyl}}}, \quad (115)$$

where we have introduced the time scale

$$\frac{1}{\tau_{N,2\mathrm{D}}^{\mathrm{cyl}}} = \frac{R_\square}{h/e^2} T \ln\left(\frac{L^2}{L_T^2}\right). \quad (116)$$

This time is reminiscent of the Nyquist time for the film, Eq. (90), but the two times differ by the argument of the logarithm.

The second path integral precisely coincides with the one for a wire: $\frac{1}{\sqrt{4\pi t}}\langle e^{i\Phi}\rangle_{V,\mathcal{C}_t}$ given by Eq. (24). Finally

$$\Delta\widetilde{\sigma}_n \simeq -2\int_0^\infty dt\,\frac{1}{\sqrt{4\pi t}} e^{-(nL)^2/4t} e^{-t/\tau_{N,2\mathrm{D}}^{\mathrm{cyl}}}$$
$$\times \frac{1}{\sqrt{4\pi t}}\sqrt{\frac{\pi t}{\tau_{N,1\mathrm{D}}}}\sum_{m=1}^\infty \frac{1}{|u_m|} e^{-|u_m|t/\tau_{N,1\mathrm{D}}}, \quad (117)$$

which leads to the series (for $n \neq 0$)

$$\Delta\widetilde{\sigma}_n \simeq -\frac{1}{2\sqrt{\tau_{N,1\mathrm{D}}}}\sum_{m=1}^\infty \frac{\sqrt{\tau_m}}{|u_m|} e^{-nL/\sqrt{\tau_m}}, \quad (118)$$

where the times τ_m are defined as

$$\frac{1}{\tau_m} = \frac{|u_m|}{\tau_{N,1\mathrm{D}}} + \frac{1}{\tau_{N,2\mathrm{D}}^{\mathrm{cyl}}} \quad (119)$$

(we recall that u_m's are zeros of Airy function Ai′).

This expression assumes that $L \gg L_{N,1\mathrm{D}}$. We show that Eq. (118) is also valid for the other regime $L \ll L_{N,1\mathrm{D}}$: in this case the path integral runs over trajectories such that $|y| \gg L$ (see Fig. 16); therefore, in Eq. (110), the exponential damping suppresses the x and y dependence in the logarithmic of W what leads to the same conclusion for the two regimes since $W \rightarrow \frac{|y|}{2L} + \frac{1}{2\pi}\ln(L/2\pi L_T)$.

In order to analyze the two limiting cases into more details it is convenient to relate the two times as

$$\frac{\tau_{N,1\mathrm{D}}}{\tau_{N,2\mathrm{D}}^{\mathrm{cyl}}} = \frac{1}{\pi}\left(\frac{L}{L_{N,1\mathrm{D}}}\right)\ln\left(\frac{L}{L_T}\right). \quad (120)$$

Since the two lengths $L_{N,2\mathrm{D}}^{\mathrm{cyl}}$ and $L_{N,1\mathrm{D}}$ are related, we just have to consider two different regimes. As it is clear from Eq. (119), the harmonics are always controlled by the smallest scale among $L_{N,2\mathrm{D}}^{\mathrm{cyl}}$ and $L_{N,1\mathrm{D}}$.

(i) *High-temperature* $L_{N,1\mathrm{D}} \ll L$ (then $L_{N,2\mathrm{D}}^{\mathrm{cyl}} \ll L_{N,1\mathrm{D}}$). The WL correction is dominated by nonwinding trajectories, in this case

$$\Delta\widetilde{\sigma} \simeq \Delta\widetilde{\sigma}_0 \simeq -\frac{1}{2\pi}\ln\left(\frac{\tau_N^{\mathrm{film}}}{\tau_e}\right) + \mathrm{cste} \quad (121)$$

involves the 2D Nyquist time (90). Considering the oscillating part of the MC, only the first term of the series dominates. The harmonics are governed by the smallest length among $L_{N,2\mathrm{D}}^{\mathrm{cyl}}$ and $L_{N,1\mathrm{D}}$,

$$\Delta\tilde{\sigma}_n \simeq -\frac{L_{N,2D}^{\text{cyl}}}{2|u_1|L_{N,1D}}e^{-nL/L_{N,2D}^{\text{cyl}}} \sim e^{-nL(T\ln T)^{1/2}} \quad (122)$$

for $L_{N,1D} \ll L$. Note that this result is reminiscent of the result (27) for a ring $\Delta\tilde{\sigma}_n^{\text{ring}} \sim e^{-nL^{3/2}T^{1/2}}$: up to some logarithmic correction it presents a similar $T^{1/2}$ in the exponential for the similar reason (related to potential fluctuations seen by winding trajectories). However the L dependence differs from the one of the ring.

(ii) *Low-temperature* $L \ll L_{N,1D}$ (then $L_{N,1D} \ll L_{N,2D}^{\text{cyl}}$). The harmonics involve $L_{N,1D}$, the smallest length among $L_{N,2D}^{\text{cyl}}$ and $L_{N,1D}$. Equation (118) coincides with the one obtained for the chain of rings (68)

$$\Delta\tilde{\sigma}_n \simeq -2F_2(nL/L_{N,1D}). \quad (123)$$

For intermediate coherence length, $L \ll L_{N,1D} \ll nL$, Eq. (118) gives

$$\Delta\tilde{\sigma}_n \simeq -\frac{1}{|u_1|^{3/2}}e^{-|u_1|^{1/2}nL/L_{N,1D}} \sim e^{-nLT^{1/3}}. \quad (124)$$

For largest phase coherence length $nL \ll L_{N,1D}$, we may use the form derived in Sec. VI,

$$\Delta\tilde{\sigma}_n \simeq -\frac{1}{\pi}\left[\ln\left(\frac{L_{N,1D}}{nL}\right) + C_{\text{cyl}}\right], \quad (125)$$

where the constant, $C_{\text{cyl}} \simeq 0.51$, was introduced in Sec. VI.

Discussion. It is worth emphasizing the similarity between the results for the cylinder and for the networks.

In Sec. IV we have seen that the MC harmonics of a weakly coherent ring probe two length scales $L_N \propto T^{-1/3}$ or $L_c \propto T^{-1/2}$. For the lowest temperatures the surrounding network matters and another length scale emerges: the MC of the square network involves a unique time scale $1/\tau_N^{\text{net}} \sim T\ln 1/T$, Eq. (95), reminiscent of the 2D Nyquist time (90).
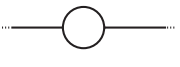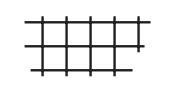
For a cylinder the MC also probes several time scales. At high temperature the zero harmonic related to non-winding trajectories probes the 2D Nyquist time $\frac{1}{\tau_N^{\text{film}}} = \frac{R_\square}{h/e^2}T\ln[h/e^2 2R_\square]$, whereas the nonzero harmonics probe the time $\frac{1}{\tau_{N,2D}^{\text{cyl}}} = \frac{R_\square}{h/e^2}T\ln[L^2/L_T^2]$. The main dependence of the corresponding length $L_{N,2D}^{\text{cyl}} \propto T^{-1/2}$ has the same origin as for a single ring and reflects that winding trajectories feel fluctuations of the potential over length scale given by the perimeter (Fig. 16, left). For lower temperature, trajectories diffuse along the cylinder over length scale much larger than the perimeter and the WL correction is controlled by a unique length $L_{N,1D}$, corresponding to the usual 1D Nyquist time $\tau_{N,1D} \propto T^{-2/3}$.

IX. CONCLUSION

We have studied the weak localization correction in metallic networks and in a hollow cylinder. This study relies on a detailed analysis of the winding properties of closed Brownian trajectories in these systems. We now summarize our results.

We first recall the behavior of the probability to return to the starting point after a time t for trajectories conditioned to

TABLE I. Return probability and distribution $Q_t(n) = \frac{\mathcal{P}_n(x,x;t)}{\mathcal{P}(x,x;t)}$ of the winding number in the large time limit $t \gg L^2$. The function $\Psi(\xi)$ is defined in Eq. (41).

Network	$\mathcal{P}(x,x;t)$	$Q_t(n)$	$q(x)$
![ring]	$\frac{1}{N_a\sqrt{\pi t}}$	$\frac{\sqrt{N_aL}}{(4\pi t)^{1/4}}q\left(\frac{n\sqrt{N_aL}}{(4\pi t)^{1/4}}\right)$	$\frac{\pi^{3/4}}{\sqrt{2}}\Psi((4\pi)^{1/4}x)$
![chain]	$\frac{1}{4\sqrt{\pi t}}$	$\frac{L}{\sqrt{2t}}q\left(\frac{nL}{\sqrt{2t}}\right)$	$\frac{1}{\sqrt{2\pi}}e^{-x^2/2}$
![grid]	$\frac{a}{4\pi t}$	$\frac{2\sqrt{3}a^2}{t}q\left(\frac{n2\sqrt{3}a^2}{t}\right)$	$\frac{\pi}{4\sqrt{3}}\frac{1}{\cosh^2\left(\frac{\pi x}{2\sqrt{3}}\right)}$

wind n rings. In the short time limit $t \ll L^2$, we have $\mathcal{P}_n(x,x;t) \simeq p_n\frac{1}{\sqrt{4\pi t}}e^{-(nL)^2/4t}$, where p_n depends on the network: $p_n=1$ for the isolated ring, $p_n=(\frac{2}{3})^{nN_a}$ for the ring connected to N_a long wires and $p_n=\frac{(2n-1)!!}{2^{n+1}n!}$ in the chain of rings. For the square network, there is no close expression but a systematic expansion may be found in Ref. 16 with the trace formula of Ref. 70.

At large times $t \gg L^2$ the typical winding number scales as $n_t \sim (t/L^2)^\alpha$, where α is a network-dependent exponent. Introducing the return probability $\mathcal{P}(x,x;t)=\Sigma_n\mathcal{P}_n(x,x;t)$, we may write the winding probability as

$$\mathcal{P}_n(x,x;t) \simeq \frac{\mathcal{P}(x,x;t)}{c_2(t/L^2)^\alpha}q\left(\frac{n}{c_2(t/L^2)^\alpha}\right), \quad (126)$$

where $\int dx\, q(x)=1$. The dimensionless number c_2 ensures that $\int dx\, x^2 q(x)=1$. Since $\mathcal{P}(x,x;t) \sim t^{-d/2}$, where d is the effective dimensionality of the network, we may also write

$$\mathcal{P}_n(x,x;t) \sim \frac{1}{t^{\alpha+d/2}}q\left(\frac{n}{t^\alpha}\right) \quad (127)$$

(L may be reintroduced by dimensional analysis). The function $q(x)$ is given for the various networks in Table I, and represented in Fig. 17. Surprisingly the functions for the connected ring and the plane are very close; they only differ in the wings when functions are exponentially small.

We have analyzed in details the harmonics of the magneto-conductance oscillations obtained when decoherence is described by a simple exponential relaxation (model A). In the limit of large coherence length compared to the perimeter of the rings, the scaling of the harmonics can be easily understood from the Laplace transform $\Delta\tilde{\sigma}_n \sim \int_0^\infty dt\mathcal{P}_n(x,x;t)e^{-t/L_\varphi^2}$. We see that the time scale coincides with $t \sim L_\varphi^2$. We deduce from Eq. (127) that harmonics are of the form

$$\Delta\tilde{\sigma}_n \sim \frac{1}{L_\varphi^{d-2+2\alpha}}\Phi\left(\frac{n}{L_\varphi^{2\alpha}}\right), \quad (128)$$

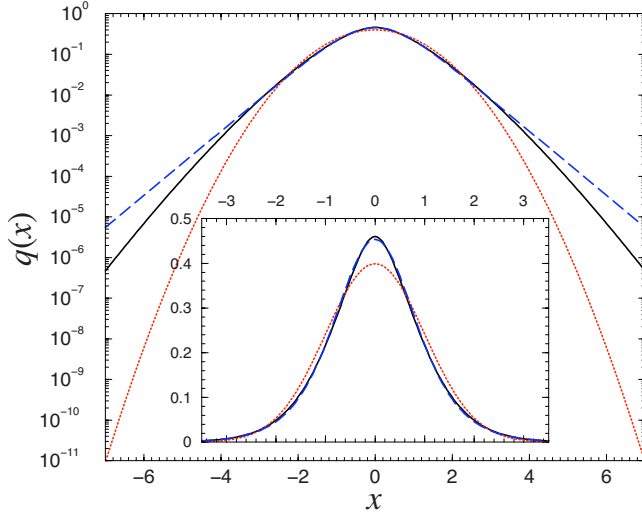where $\Phi(x)$ is a dimensionless network-dependent function

FIG. 17. (Color online) Rescaled distribution of the winding number [function $q(x)$] for the connected ring (black continuous line), the chain of rings (red dotted line), and square network (blue dashed line) in semilog scale. Inset: Same functions in linear scale.

(the perimeter L is easily reintroduced by reminding that $\Delta\tilde{\sigma}$ has dimension of a length). We may then summarize the following for each geometry:

(i) For the isolated ring ($d=0$, $\alpha=1/2$), the form of the harmonics $\Delta\tilde{\sigma}_n \sim L_\varphi \Phi_{\text{i.r.}}(nL/L_\varphi)$ is related to the scaling $n_t \sim t^{1/2}$.

(ii) For the connected ring ($d=1$, $\alpha=1/4$): $\Delta\tilde{\sigma}_n \sim \sqrt{L_\varphi L}\Phi_{\text{c.r.}}(n\sqrt{L/L_\varphi})$ can be understood from $n_t \sim t^{1/4}$.

(iii) For the chain of rings ($d=1$, $\alpha=1/2$): $\Delta\tilde{\sigma}_n \sim \Phi_{\text{chain}}(nL/L_\varphi)$ reflects $n_t \sim t^{1/2}$.

(iv) For the square network ($d=2$, $\alpha=1$): $\Delta\tilde{\sigma}_n \sim \frac{L}{n}\tilde{\Phi}_{\text{s.n.}}(nL^2/L_\varphi^2)$ originates from $n_t \sim t$ [here the harmonics were not written exactly under the form (128), but in terms of the function $\tilde{\Phi}(x)=x\Phi(x)$ in order to emphasize that harmonics reach a finite value for $L_\varphi \to \infty$].

The precise behaviors for the harmonics Δg_n are summarized in Table II (we recall that $\Delta g_n \sim \Delta\sigma_n$ apart for the connected ring for which $\Delta g_n \sim \frac{L_\varphi}{l_a}\Delta\sigma_n$, where l_a is the length of the connecting wires).

For each situation we have also discussed the effect of decoherence due to electron-electron interaction (model B), the dominant phase breaking mechanism at low temperature. As recalled at the beginning of the paper, this mechanism requires a refined description: the simple exponential decay of phase coherence is replaced by a functional of the trajectories, Eqs. (15) and (18). In networks of quasi-1D wires the decoherence due to e-e interaction is controlled by the Nyquist length $L_N \propto T^{-1/3}$.

In the "high-temperature" limit $L_N \ll L$ the fact that trajectories with finite winding number and trajectories with winding $n=0$ do probe different length scales is responsible for the emergence of two length scales $L_N \propto T^{-1/3}$ and $L_c \propto T^{-1/2}$ [or $L_N^{\text{film}} \propto T^{-1/2}$ and $L_{N,\text{2D}}^{\text{cyl}} \propto (T \ln T)^{-1/2}$ for the cylinder]. The models A and B give different dependences in the phase coherence length: $\Delta\tilde{\sigma}^{(A)} \sim -L_\varphi e^{-nL/L_\varphi}$ and $\Delta\tilde{\sigma}^{(B)} \sim -L_N e^{-n(L/L_N)^{3/2}}$. The exponential decay of harmonics is almost independent of the network.
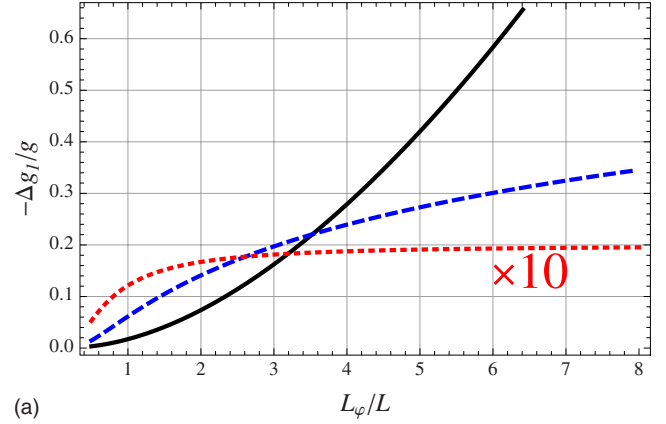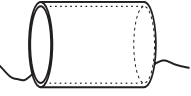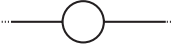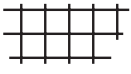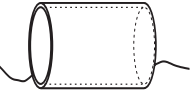

(a)
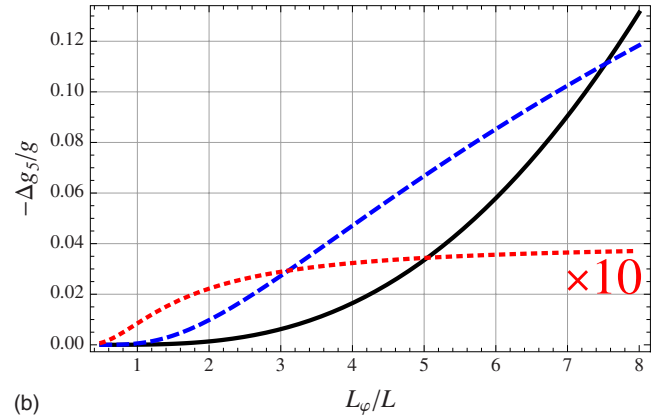
(b)

FIG. 18. (Color online) Comparison between harmonics $\Delta g_n/g$ for different networks in the low temperature regime $L_\varphi \gtrsim L$ with $n=1$ and $n=5$. For the connected ring (continuous black line) we choose $l_a/L=10$. The blue dashed line corresponds to the chain of rings. The result for the square network (dotted red line) has been multiplied by a factor 10 for visibility.

In the "low-temperature" limit $L_N \gg L$, all trajectories probe the same typical scale, irrespective of the winding. However this length scale depends on the geometry: $L_N \propto T^{-1/3}$ for the chains of rings and the hollow cylinder, and $L_N^{\text{net}} = (\frac{2\pi L_N^3}{3a})^{1/2}\ln^{-1/2}(L_N/a) \sim (T \ln 1/T)^{-1/2}$ for the square network. As a function of the phase coherence length, models A and B predict harmonics of similar form strongly network dependent. We have compared harmonics as a function of the phase coherence length for the different networks in Fig. 18 (for model A).

All results are summarized in Table II. We have plotted the WL correction to conductances for the three different networks in Fig. 18.

An experimental verification of these predictions would be interesting and would confirm our understanding of decoherence due to electron-electron interaction in complex geometries. In particular an interesting and clear experimental test would be to compare the MC harmonics for the chain of rings for independent rings and coherent rings (networks of Fig. 9) in the "low-temperature" limit $L_N \gg L$. The experimental analysis of the MC harmonics for the square network in this limit seems more difficult due to the fact that harmonics reach a value independent on the phase breaking mecha-

TABLE II. Harmonics of MC $\Delta g_n/g$ for different networks. In the high-temperature regime $L_\varphi \ll L$, winding trajectories cannot explore more than a single ring and harmonics do not depend on the network. Dimensionless constants are $\kappa_1 = \pi^2/8 \simeq 1.234$, $\kappa_2 = \sqrt{2}|u_1|^{1/4} \simeq 1.421$, $\kappa_3 = 2^{-1/3}|u_1|^{1/2} \simeq 0.801$, and $\kappa_4 = |u_1|^{1/2} \simeq 1.009$. The various Nyquist lengths are $L_N \sim T^{-1/3}$, $L_N^{\mathrm{net}} \sim (T \ln 1/T)^{-1/2}$, and $L_{N,\mathrm{2D}}^{\mathrm{cyl}} \sim (T \ln T)^{-1/2}$.

	Model A (exp. relax.)		Model B (e-e inter.)	
	Regime $L_\varphi \ll L$:			
	$L_\varphi e^{-nL/L_\varphi}$		$L_N e^{-\kappa_1 n(L/L_N)^{3/2}}$	for $L_N \ll L$
	$L_\varphi^{1/2} e^{-nL/L_\varphi}$		$\dfrac{L_{N,\mathrm{2D}}^{\mathrm{cyl}}}{L_{N,\mathrm{1D}}} e^{-nL/L_{N,\mathrm{2D}}^{\mathrm{cyl}}}$	for $L_{N,\mathrm{2D}}^{\mathrm{cyl}} \ll L_{N,\mathrm{1D}} \ll L$
	Regime $L_\varphi \gg L$:			
	$L_\varphi^{3/2}$	for $n^2 \ll L_\varphi/L$	$L_N^{3/2}$	for $n^2 \ll L_N/L$
	$L_\varphi^{3/2} e^{-n\sqrt{2L/L_\varphi}}$	for $n^2 \gg L_\varphi/L$	$L_N^{5/4} e^{-\kappa_2 n\sqrt{L/L_N}}$	for $n^2 \gg L_N/L$
	$\ln(L_\varphi/nL)$	for $n \ll L_\varphi/L$	$\ln(L_N/nL)$	for $n \ll L_N/L$
	$L_\varphi^{1/2} e^{-nL/L_\varphi}$	for $n \gg L_\varphi/L$	$e^{-\kappa_3 nL/L_N}$	for $n \gg L_N/L$
	$\dfrac{1}{n}\left[1 - \dfrac{\pi n L^2}{16 L_\varphi^2} \ln\left(\dfrac{L_\varphi^2}{nL^2} \right) \right]$	for $\sqrt{n} \ll L_\varphi/L$	idem for $L_\varphi \to L_N^{\mathrm{net}}$	
	$L_\varphi^{-1/2} e^{-\sqrt{(\pi/2)nL/L_\varphi}}$	for $\sqrt{n} \gg L_\varphi/L$	idem for $L_\varphi \to L_N^{\mathrm{net}}$	
	$\ln(L_\varphi/nL)$	for $n \ll L_\varphi/L$	$\ln(L_{N,\mathrm{1D}}/nL)$	for $n \ll L_{N,\mathrm{1D}}/L$
	$L_\varphi^{1/2} e^{-nL/L_\varphi}$	for $n \gg L_\varphi/L$	$e^{-\kappa_4 nL/L_{N,\mathrm{1D}}}$	for $n \gg L_{N,\mathrm{1D}}/L$

nism. Therefore, contrarily to the chains of rings, the MC harmonics for the square network are less sensitive to the model of decoherence for large phase coherence length.

APPENDIX A: A USEFUL PROPERTY OF WINDING BROWNIAN TRAJECTORIES

The difficulty for computing the path integral (19) lies in the time nonlocality of the action. In this appendix we show how it is possible to get rid of time nonlocality in certain cases, as explained in Refs. 5 and 62. For that purpose we demonstrate the identity

$$
\int_{x(0)=x}^{x(t)=x} \mathcal{D}x \, \delta_{n,\mathcal{N}[x]}
$$
$$
\times \exp\left[-\frac{1}{2}\int_0^t d\tau \, \dot{x}^2 - \int_0^t d\tau \, V(x(\tau) - x(t-\tau)) \right]
$$
$$
= \int_{x(0)=0}^{x(t)=0} \mathcal{D}x \, \delta_{n,\mathcal{N}[x]} \exp\left[-\frac{1}{2}\int_0^t d\tau \, \dot{x}^2 - \int_0^t d\tau \, V(x(\tau)) \right],
$$
$$\text{(A1)}$$

where $x(\tau)$ is a Brownian path on the circle (here identified with the interval $[0,1]$). The identity is valid for any symmetric and periodic function: $V(-x) = V(x)$ and $V(x+n) = V(x)$ for $n \in \mathbb{Z}$.

Demonstration for $n=0$ was given in Refs. 5 and 62, where we pointed that, for a Brownian bridge on $\mathbb{R}[x(\tau)]$, $0 \leq \tau \leq t \,|\, x(0) = x(t) = 0]$, we have the following equality in law:[91]

$$x(\tau) - x(t-\tau) \overset{(law)}{=} x(2\tau) \quad \text{for } 0 \leqslant \tau \leqslant t/2. \quad (A2)$$

The proof lies in the fact that we can relate the bridge to a free Brownian motion (Wiener process) $[W(\tau), 0 \leqslant \tau \leqslant t,$ $W(0) = 0]$: $x(\tau) \overset{(law)}{=} W(\tau) - \frac{\tau}{t}W(t)$.

Here we generalize this relation when $x(\tau)$ lives on the circle $[0,1]$ and when we constrain the winding number. Let us unfold the ring in order to work on $\mathbb{R}$. A close path winding n times around the ring is related to the following path living on the real axis: $[x_n(\tau), 0 \leqslant \tau \leqslant t | x_n(0) = 0; x_n(t) = n]$ that can be written as

$$x_n(\tau) \overset{(law)}{=} W(\tau) + \frac{\tau}{t}[n - W(t)] \overset{(law)}{=} x_0(\tau) + n\frac{\tau}{t}. \quad (A3)$$

$x_0(\tau)$ is the Brownian bridge. It is now easy to show that[92]

$$x_n(\tau) - x_n(t-\tau) \overset{(law)}{=} x_n(2\tau) - n \quad \text{for } 0 \leqslant \tau \leqslant t/2. \quad (A4)$$

Since $x_n(\tau) - x_n(t-\tau)$ is the argument of the periodic function, the integer shift can be forgotten. The symmetry $V(x) = V(-x)$ ensures the equality of contributions of intervals $\int_0^{t/2}$ and $\int_{t/2}^t$. It follows that

$$\int_0^t d\tau\, V(x_n(\tau) - x_n(t-\tau)) \overset{(law)}{=} \int_0^t d\tau\, V(x_n(\tau)), \quad (A5)$$

which demonstrates Eq. (A1).

Infinite wire. Using Eq. (A1), we see that the path integral (20) involves an action local in time,

$$P_c(x,x) \equiv -\frac{1}{2}\Delta\tilde{\sigma}(x) = \int_0^\infty dt\, e^{-\gamma t}$$
$$\times \int_{x(0)=0}^{x(t)=0} \mathcal{D}x(\tau)\exp\left\{-\int_0^t d\tau\left[\frac{1}{4}\dot{x}^2 + \frac{1}{L_N^3}|x(\tau)|\right]\right\}, \quad (A6)$$

that can now be computed. We obtain $P_c(0,0) = -L_N \frac{\mathrm{Ai}(\gamma L_N^2)}{2\mathrm{Ai}'(\gamma L_N^2)}$ derived in Ref. 3 (numerical factors are incorrect in this reference).

Isolated ring. The function $W(x,x')$ is given by Eq. (E9). The path integral (19) can be rewritten as

$$\int_0^\infty dt\, e^{-\gamma t} \int_{x(0)=0}^{x(t)=0} \mathcal{D}x\, \delta_{n,\mathcal{N}[x]}$$
$$\times \exp\left\{-\int_0^t d\tau\left[\frac{\dot{x}^2}{4} + \frac{|x|}{L_N^3}\left(1 - \frac{|x|}{L}\right)\right]\right\} \quad (A7)$$

that can be expressed in terms of Hermite functions.[5]

APPENDIX B: THE FUNCTION $\Psi(\xi)$

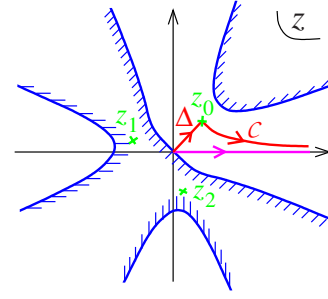We analyze several properties of the function (41), which we rewrite

FIG. 19. (Color online) Appropriate contour deformation in order to estimate (B1). The dashed area corresponds to the region where $\mathrm{Re}[\varphi(z)] < 0$.

$$\Psi(\xi) = \frac{4}{\pi}\Lambda^{3/4}\,\mathrm{Re}\left[e^{-i\pi/4}\int_{\mathbb{R}^+} dz\, z^2 e^{-\Lambda\varphi(z)}\right], \quad (B1)$$

where $\varphi(z) = z^4 + 4z e^{-i\pi/4}$ and $\Lambda = (\xi/4)^{4/3}$. The value of the function at the origin is $\Psi(0) = \frac{\Gamma(3/4)}{\pi\sqrt{2}}$.

The asymptotic behavior for $\xi \gg 1$ may be studied by the steepest descent method. $\varphi'(z) = 0$ has three solutions $z_n = e^{i\pi/4 + 2in\pi/3}$, with $n = 0,1,2$ (Fig. 19). An appropriate contour deformation in the complex plane of the variable z must remain in the region, where $\mathrm{Re}[\varphi(z)] > 0$. This domain can be easily determined by performing a rotation $z = w e^{i\pi/4}$: writing $w = u + iv$ we have $\mathrm{Re}[\varphi(z)] = -u^4 + 6u^2 v^2 - v^4 + 4u$ that vanishes for $v = \pm\sqrt{3u^2 \pm 2\sqrt{2u^4 + u}}$. The domain where $\mathrm{Re}[\varphi(z)] > 0$ is represented in Fig. 19. This shows that the contour can only visit $z_0 = e^{i\pi/4}$. The integration over $\mathbb{R}^+$ is replaced by integration over the segment Δ from the origin to z_0 and the contour $\mathcal{C}$ issuing from z_0 and going to infinity (Fig. 19). Noticing that $\int_\Delta dz\, z^2 e^{-\Lambda\varphi(z)}$ is purely imaginary, we are left with the contribution of the contour $\mathcal{C}$ only. We now use the steepest descent method $\Psi(\xi) = \frac{4}{\pi}\Lambda^{3/4}\,\mathrm{Re}[e^{-i\pi/4}\int_\mathcal{C} dz\, z^2 e^{-\Lambda\varphi(z)}] \simeq \frac{4}{\pi}\Lambda^{3/4}\,\mathrm{Re}[e^{-i\pi/4}\frac{1}{2}\sqrt{\frac{2\pi}{\Lambda\varphi''(z_0)}}e^{-\Lambda\varphi(z_0)}]$, where the $1/2$ is due to the fact that the contour issues from the stationary point; hence

$$\Psi(\xi \gg 1) \simeq \frac{2}{\sqrt{6\pi}}(\xi/4)^{1/3} e^{-3(\xi/4)^{4/3}} \quad (B2)$$

(note that a factor $1/2$ is missing in Ref. 7).

Finally the relation to the function $q(x)$ introduced in the conclusion requires the two integrals $\int_0^\infty d\xi\, \Psi(\xi) = 1/\sqrt{\pi}$ and $\int_0^\infty d\xi\, \xi^2 \Psi(\xi) = 2$.

APPENDIX C: HYPERGEOMETRIC FUNCTION $F(\frac{1}{2}, n+\frac{1}{2}; n+1; \xi)$

This appendix is devoted to the study of the hypergeometric function $F(\frac{1}{2}, n+\frac{1}{2}; n+1; \xi)$. Our starting point is the integral representation[69]

$$B\left(\frac{1}{2}, n+\frac{1}{2}\right) F\left(\frac{1}{2}, n+\frac{1}{2}; n+1; \xi\right) = \int_0^1 dt \frac{t^{n-1/2}}{\sqrt{(1-t)(1-\xi t)}}. \tag{C1}$$

We recall that the hypergeometric function is regular at the origin $F(\alpha, \beta; \gamma; 0) = 1$. Note that the Euler β function $B(\frac{1}{2}, n+\frac{1}{2}) = \sqrt{\pi}\Gamma(n+\frac{1}{2})/n!$ is well approximated by $B(\frac{1}{2}, n+\frac{1}{2}) \simeq \sqrt{\pi/n}$ in the large n limit.

In order to analyze the behavior of the hypergeometric function for $\xi \to 1$ we rewrite the integral of Eq. (C1) as

$$\int_0^1 dt \frac{(1-t)^{n-1/2}}{\sqrt{t(1-\xi+\xi t)}}$$
$$= \frac{1}{\sqrt{\xi}}\left(\int_0^1 dt \frac{1}{\sqrt{t^2+\varepsilon t}} + \int_0^1 dt \frac{(1-t)^{n-1/2}-1}{\sqrt{t^2+\varepsilon t}}\right), \tag{C2}$$

where $\varepsilon = 1/\xi - 1$. The first integral is $2\,\mathrm{argsh}(1/\sqrt{\varepsilon}) = \ln(4/\varepsilon) + O(\varepsilon)$. The second integral reaches a finite limit for $\varepsilon \to 0$, expressed in terms of the Digamma function[69] $\int_0^1 du \frac{u^{n-1/2}-1}{1-u} = \psi(1) - \psi(n+\frac{1}{2})$. We can show that correction to this constant is of order $\varepsilon \ln(\varepsilon)$; therefore,

$$F\left(\frac{1}{2}, n+\frac{1}{2}; n+1; \xi\right)$$
$$\underset{\xi \to 1}{=} \frac{1}{B\left(\frac{1}{2}, n+\frac{1}{2}\right)}$$
$$\times \left[\ln\left(\frac{4}{1-\xi}\right) + \psi(1) - \psi\left(n+\frac{1}{2}\right) + O(\varepsilon \ln \varepsilon)\right]. \tag{C3}$$

The behavior (C3) only holds for n not too large, $n \ll (1-\xi)^{-1}$. In the opposite case $n \gg (1-\xi)^{-1} \gg 1$, the factor $(1-t)^{n-1/2} \simeq e^{-(n-1/2)t}$ in Eq. (C2) selects an interval of width $1/n \ll (1-\xi)$ and we can neglect the quadratic term ξt^2 below the square root. Therefore Eq. (C2) is $\simeq \int_0^\infty dt \frac{1}{\sqrt{(1-\xi)t}} e^{-(n-1/2)t}$. Finally

$$F\left(\frac{1}{2}, n+\frac{1}{2}; n+1; \xi\right) \underset{\xi \to 1}{\simeq} \frac{1}{\sqrt{1-\xi}} \tag{C4}$$

for $n \gg (1-\xi)^{-1} \gg 1$.

We now prove a useful relation between the hypergeometric function and the MacDonald function (modified Bessel function). If $\xi = e^{-2z/n} \simeq 1 - 2z/n$, the integral (C2) may be rewritten as

$$\int_0^n \frac{dt}{n} \frac{\left(1-\frac{t}{n}\right)^{n-1/2}}{\sqrt{\frac{t}{n}\left(\frac{2z}{n}+\frac{t}{n}\right)}} \xrightarrow[n\to\infty]{} \int_0^\infty dt \frac{e^{-t}}{\sqrt{t(2z+t)}}. \tag{C5}$$

We recognize an integral representation of the MacDonald function.[69] Therefore, for $z \ll n$, we can write
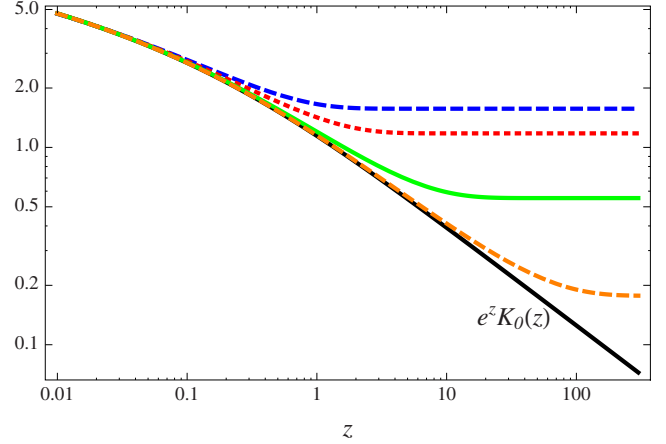

FIG. 20. (Color online) Comparison between the two sides of Eq. (C6) for $n = 1, 2, 10$, and 100.

$$B\left(\frac{1}{2}, n+\frac{1}{2}\right) F\left(\frac{1}{2}, n+\frac{1}{2}; n+1; e^{-2z/n}\right) \simeq e^z K_0(z). \tag{C6}$$

The right-hand side describes the crossover between Eqs. (C3) and (C4). We compare the two sides of Eq. (C6) for different values of n in Fig. 20.

APPENDIX D: LAPLACE EQUATION IN NETWORKS (SPECTRAL DETERMINANT)

In this appendix we introduce an important tool, the spectral determinant, used to study some properties of the equation

$$(\gamma - \Delta) P(x, x') = \delta(x - x') \tag{D1}$$

in networks.

The spectral determinant is formally defined as $S(\gamma) = \det(\gamma - \Delta) = \Pi_n(\gamma + E_n)$, where $\{E_n\}$ is the spectrum of the Laplace operator $-\Delta$ (in the presence of a magnetic field, $\Delta \to [\nabla - 2ieA(x)]^2$). Despite the fact that this operator acts in a space of infinite dimension, the spectral determinant can be related to the determinant of a finite size matrix, of dimension equal to the number of vertices. This matrix encodes all informations on the network (topology, lengths of the wires, magnetic field, boundary conditions describing connections to reservoirs). Let us label vertices with greek letters. $l_{\alpha\beta}$ designates the length of the wire $(\alpha\beta)$ and $\theta_{\alpha\beta}$ the circulation of the vector potential along the wire. The topology is encoded in the adjacency matrix: $a_{\alpha\beta} = 1$ if α and β are linked by a wire, $a_{\alpha\beta} = 0$ otherwise. We consider the case where Laplace operator acts on functions $\varphi(x)$ (i) continuous at the vertices satisfying (ii) $\Sigma_\beta a_{\alpha\beta}\varphi'_{\alpha\beta}(0) = \lambda_\alpha \varphi_\alpha$, where $\varphi_{\alpha\beta}(x)$ designates the component of the function on the wire $(\alpha\beta)$ and φ_α its value at the vertex. Self-adjointness of the Laplace operator is ensured if $\lambda_\alpha \in \mathbb{R}$ (more details may be found in Refs. 29 and 62). $\lambda_\alpha = \infty$ corresponds to Dirichlet boundary condition at the vertex and describe the case where α touches a reservoir through which current is injected in the network. $\lambda_\alpha = 0$ for internal vertices. The interest of mixed boundary conditions (finite λ_α) is illustrated in Appendix F. We introduce the matrix

$$\mathcal{M}_{\alpha\beta} = \delta_{\alpha\beta}\left(\lambda_\alpha + \sqrt{\gamma}\sum_\mu a_{\alpha\mu}\coth\sqrt{\gamma}l_{\alpha\mu}\right) - a_{\alpha\beta}\sqrt{\gamma}\frac{e^{-i\theta_{\alpha\beta}}}{\sinh\sqrt{\gamma}l_{\alpha\beta}},$$

(D2)

where the $a_{\alpha\mu}$ constrains the sum to run over neighboring vertices. Then[28,29]

$$S(\gamma) = \prod_{(\alpha\beta)}\frac{\sinh\sqrt{\gamma}l_{\alpha\beta}}{\sqrt{\gamma}}\det\mathcal{M},$$

(D3)

where the product runs over all wires. Despite the spectral determinant encodes the spectral information, it is also possible to extract some local information, like $P(x,x)$, by small modifications of the matrix. This has been used in Ref. 7 and is briefly discussed in Appendix F.

It is useful to remark that the matrix $\mathcal{M}$ can be used to express $P(x,x')$ when x and x' coincides with nodes (this is always possible to introduce a vertex anywhere without changing the properties of the network)

$$P(\alpha,\beta) = (\mathcal{M}^{-1})_{\alpha\beta}.$$

(D4)

WL correction in regular networks. In large regular networks connected in such a way that currents are uniformly distributed in the wires, we can assume that weights attributed to the wires of the networks in Eq. (8) are equal. In this case, a uniform integration of the Cooperon $P_c(x,x) = \langle x|\frac{1}{\gamma-\Delta}|x\rangle$ in the network leads to a meaningful quantity (relevant experimentally). The Cooperon integrated uniformly is directly related to the spectral determinant[27,29]

$$\int_{\text{network}} dx\,\Delta\tilde{\sigma}(x) = -2\frac{\partial}{\partial\gamma}\ln S(\gamma).$$

(D5)

This equation provides a very efficient way for calculating the WL correction in arbitrary networks, when uniform integration of Cooperon is justified.

WL correction in arbitrary networks. In the most general case, Eq. (8) requires one to construct the Cooperon in each wire. A general expression was provided in Ref. 30, however it is useful to notice that $P_c(x,x) = -\frac{1}{2}\Delta\tilde{\sigma}(x)$ can also be obtained from a spectral determinant for a modified boundary condition at point x. It was shown in Refs. 7 and 62 that if we introduce mixed boundary conditions with a parameter λ_x at x, then

$$\Delta\tilde{\sigma}(x) = -2\frac{\partial}{\partial\lambda_x}\ln S^{(\lambda_x)}(\gamma)\big|_{\lambda_x=0}.$$

(D6)

APPENDIX E: CLASSICAL RESISTANCE/CONDUCTANCE

We calculate the resistance between two vertices of an arbitrary network. We consider a network of wires of lengths $l_{\mu\nu}$ with same sections s. In this case the conductance of the wire $\mu\nu$ is given by $\sigma_0 s/l_{\mu\nu}$. We introduce the matrix
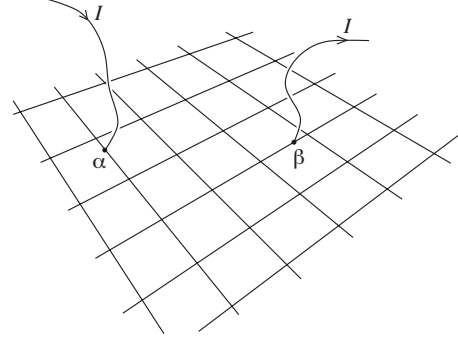

FIG. 21. Injection of current in a network (here a regular square network).

$$(\mathcal{M}_0)_{\mu\nu} = \delta_{\mu\nu}\sum_\rho\frac{a_{\mu\rho}}{l_{\mu\rho}} - \frac{a_{\mu\nu}}{l_{\mu\nu}},$$

(E1)

whose matrix elements coincide with the conductances of the wires (up to the factor $\sigma_0 s$). This matrix coincides with the matrix (D2) if all fluxes are set to zero and the limit $\gamma\to 0$ is taken and moreover with $\lambda_\mu=0$, $\forall\mu$ for an isolated network.

We now consider the situation where we inject a current at the vertex α. This current exits at vertex β (see Fig. 21). If we denote by V_μ the potential at μ, Kirchhoff law at vertex μ takes the form

$$\sigma_0 s\sum_\nu(\mathcal{M}_0)_{\mu\nu}V_\nu = I[\delta_{\mu,\alpha} - \delta_{\mu,\beta}].$$

(E2)

Potential is therefore given by

$$V_\mu = \frac{I}{\sigma_0 s}[(\mathcal{M}_0^{-1})_{\mu\alpha} - (\mathcal{M}_0^{-1})_{\mu\beta}].$$

(E3)

Note that the matrix $\mathcal{M}_0$ is not inversible; it is explained below how to give a precise meaning to this expression. We define the resistance between points α and β as $\mathcal{R}_{\alpha\beta} = (V_\alpha - V_\beta)/I$. Therefore

$$\mathcal{R}_{\alpha\beta} = \frac{2}{\sigma_0 s}\left[\frac{(\mathcal{M}_0^{-1})_{\alpha\alpha} + (\mathcal{M}_0^{-1})_{\beta\beta}}{2} - (\mathcal{M}_0^{-1})_{\alpha\beta}\right]. \quad (E4)$$

Using Eq. (D4) we see that we can express the resistance in terms of the solution P_d of the equation $-\Delta P_d = \delta$,

$$\mathcal{R}(x,x') = \frac{2}{\sigma_0 s}\left[\frac{P_d(x,x) + P_d(x',x')}{2} - P_d(x,x')\right]$$

$$= \frac{2}{\sigma_0 s}W(x,x').$$

(E5)

This demonstrates that the function $W(x,x')$ defined by Eq. (17) is indeed the equivalent resistance between points x and x'.

Remark: $\mathcal{M}_0$ is not inversible. It is easy to check that

$$\sum_\mu(\mathcal{M}_0)_{\mu\nu} = 0.$$

(E6)

Kernel of the matrix is the vector $(1,1,\ldots,1)$. Physically Eq. (E6) ensures: (i) that sum of all currents arriving at vertex ν is zero, (ii) currents are zero if all potentials are equal (equi-

librium). This problem can be overcome easily by noticing that only *differences* of inverse matrix elements have appeared, in Eqs. (E3) and (E4). We can always inverse the matrix $\mathcal{M}_0$ in the space orthogonal to the vector $(1,1,\ldots,1)$ and compute differences of such matrix elements. This is how Eqs. (E3)–(E5) must be understood.

In practice, an easier way to compute such differences is to regularize the calculation by computing the inverse of matrix $\mathcal{M}$ for finite γ (or at least one finite λ_α) and take the limit $\gamma \to 0$ (or $\lambda_\alpha \to 0$) after having computed the difference of inverse matrix elements,

$$(\mathcal{M}_0^{-1})_{\mu\alpha} - (\mathcal{M}_0^{-1})_{\mu\beta} = \lim_{\gamma \to 0}[\mathcal{M}_{\mu\alpha}^{-1} - \mathcal{M}_{\mu\beta}^{-1}]. \quad \text{(E7)}$$

Note that $\det \mathcal{M} \neq 0$ for $\gamma \in \mathbb{R}^{+*}$ since $\mathrm{Spec}(\Delta) \subset \mathbb{R}^-$.

This point is related to the fact that was already mentioned in the continuum limit in order to construct the function $W(x,x')$ (in Sec. VIII B 1 or in Appendix F): Equation (E7) is the analog of Eq. (108). In the continuum this problem is related to the fact that the Laplace operator is not inversible in the space of functions satisfying Neumann boundary conditions corresponding to an isolated conductor.

Example: function W in an isolated ring. The relation between the function W and the resistance may be used in order to construct easily W. Let us consider the case of a ring of perimeter L. When the ring is connected at two wires at x and x', the resistance $\mathcal{R}(x,x')$ corresponds to the one of two wires of lengths $|x-x'|$ and $L-|x-x'|$ put in parallel. We straightforwardly recover the function obtained in Ref. 5,

$$W_{\text{ring}}(x,x') = \frac{1}{2}\frac{1}{\dfrac{1}{|x-x'|} + \dfrac{1}{L-|x-x'|}}, \quad \text{(E8)}$$

$$W_{\text{ring}}(x,x') = \frac{1}{2}|x-x'|\left(1 - \frac{|x-x'|}{L}\right). \quad \text{(E9)}$$

Note that if we consider a ring connected at reservoirs through arms of finite length, the function $W(x,x')$ inside the ring is modified,[4,5] since its construction needs to consider a four-terminal device. In the limit of infinitely long arms we can neglect currents flowing through the leads and we recover the result of the isolated ring (appendix of Ref. 5).

Classical conductance. It is interesting to compare the formula obtained for the resistance with the one obtained for the conductance matrix of a multiterminal network.[30] We first stress that we consider two different situations. Equations (E4) and (E5) give the *potentials* when the *currents* injected at vertex α and extracted at vertex β are fixed (Fig. 21). On the other hand, a conductance matrix allows to determine the *currents* through contacts when the *potentials* at these contacts are fixed (Fig. 22).

We consider a multiterminal network, connected to external contacts through which current is injected at a set of vertices indicated with primes: $\alpha', \beta', \ldots$. The connection is accounted for by introducing parameters $\lambda_{\alpha'} = \infty$ added to the matrix $\mathcal{M}_0$, which now become inversible. These parameters describe Dirichlet conditions for the diffusion equation and
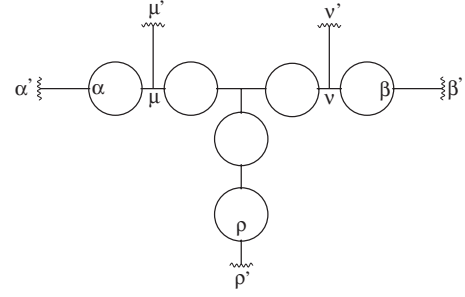

FIG. 22. A multiterminal network. Wavy lines represent contacts through which current is injected. Contacts correspond to vertices with primed labels.

permit to inverse the Laplace operator. The transport through the network is characterized by a conductance matrix whose elements are given by[30]

$$\mathcal{G}_{\alpha'\beta'} = -\frac{\sigma_0 s}{l_{\alpha\alpha'} l_{\beta\beta'}}(\mathcal{M}_0^{-1})_{\alpha\beta} = -\frac{\sigma_0 s}{l_{\alpha\alpha'} l_{\beta\beta'}}P_d(\alpha,\beta). \quad \text{(E10)}$$

At first sight diffuson $P_d(\alpha,\beta)$ [i.e., inverse matrix element $(\mathcal{M}_0^{-1})_{\alpha\beta}$] is related to both the conductance and the resistance. Note however that the matrix $\mathcal{M}_0$ [and the corresponding diffuson $P_d(x,x')$] in Eq. (E10) does account for the boundary conditions (Dirichlet boundary conditions at contacts, i.e., primed vertices) whereas $\mathcal{M}_0$ [and $P_d(x,x')$] in Eqs. (E4) and (E5) describe the isolated network.

APPENDIX F: SOLUTION OF THE DIFFUSION EQUATION IN SOME PARTICULAR NETWORKS

We consider the solution of the diffusion Eq. (D1) for the networks studied in this article.

1. The ring with one or several arms

We consider a ring of perimeter L attached to an arm of length b connected to a reservoir (i.e., with Dirichlet boundary condition at its end) and submitted to a magnetic field. The spectral determinant is[7]

$$S(\gamma) = \frac{2}{\sqrt{\gamma}} \sinh \sqrt{\gamma}b \left[\cosh \sqrt{\gamma}L_{\text{eff}} - \cos \theta\right], \quad \text{(F1)}$$

where the effective perimeter is given by

$$\cosh \sqrt{\gamma}L_{\text{eff}} = \cosh \sqrt{\gamma}L + \frac{1}{2}\coth \sqrt{\gamma}b \sinh \sqrt{\gamma}L. \quad \text{(F2)}$$

A systematic way for obtaining the spectral determinant of two subgraphs glued at one vertex from the spectral determinants of the subgraphs has been derived in Ref. 93. This allow recovering easily Eq. (F1).

(i) Introducing mixed boundary conditions at the node (vertex 0) we easily obtain $S^{(\lambda_0)}(\gamma) = \frac{\lambda_0}{\gamma}\sinh \sqrt{\gamma}L \sinh \sqrt{\gamma}b + S(\gamma)$ from Eq. (D3). Using Eq. (D6), and performing a Fourier transform, we get the Cooperon $P_c^{(n)}(0,0) = -\frac{1}{2}\Delta\tilde{\sigma}_n(0)$ at the node[7]
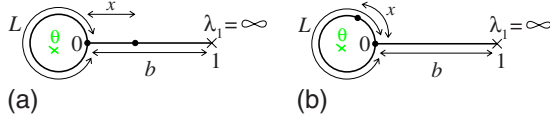
FIG. 23. (Color online) A ring with one wire. We choose a Dirichlet boundary condition at the vertex 1 for simplicity ($\lambda_1 = \infty$).

$$P_c^{(n)}(0,0) = \frac{1}{2\sqrt{\gamma}} \frac{\sinh\sqrt{\gamma}L}{\sinh\sqrt{\gamma}L_{\text{eff}}} e^{-n\sqrt{\gamma}L_{\text{eff}}}. \tag{F3}$$

In the weakly coherent limit we find $L_{\text{eff}} \simeq L + L_\varphi \ln(3/2)$, whence $P_c^{(n)}(0,0) \simeq \frac{1}{2\sqrt{\gamma}}(\frac{2}{3})^{n+1} e^{-n\sqrt{\gamma}L}$.

In the limit $\sqrt{\gamma}L \ll 1$ the effective perimeter is $L_{\text{eff}} \simeq \gamma^{-1/4}L^{1/2}$. We have[7,62]

$$P_c^{(n)}(0,0) \simeq \frac{\sqrt{L}}{2\gamma^{1/4}} e^{-n\sqrt{L}\gamma^{1/4}}. \tag{F4}$$

(ii) In order to calculate the harmonics of the Cooperon in the arm [x is the distance from the ring, see Fig. 23(a)], we have to consider the spectral determinant for the graph with mixed boundary conditions at x, with parameter λ_x,

$$S^{(\lambda_x)}(\gamma) = S(\gamma) + \frac{\lambda_x}{\gamma}\left[\sinh L \frac{\sinh^2(b-x)}{\sinh b} \right.$$
$$\left. + 2\sinh x \sinh(b-x)(\cosh L_{\text{eff}} - \cos\theta) \right] \tag{F5}$$

(for shorter notations we have omitted $\sqrt{\gamma}$ in hyperbolic functions). From Eq. (D6) we obtain

$$P_c^{(n)}(x,x) = \delta_{n,0} \frac{1}{\sqrt{\gamma}} \frac{\sinh\sqrt{\gamma}x \sinh\sqrt{\gamma}(b-x)}{\sinh\sqrt{\gamma}b}$$
$$+ \left(\frac{\sinh\sqrt{\gamma}(b-x)}{\sinh\sqrt{\gamma}b} \right)^2 P_c^{(n)}(0,0) \tag{F6}$$

for $x \in$ arm [Fig. 23(a)]. We recognize the first term as the result obtained for a wire of length b connected to reservoirs (i.e., with Dirichlet boundaries). In the limit $b \to \infty$ we have $P_c^{(n)}(x,x) \simeq P_c^{(n)}(0,0)e^{-2\sqrt{\gamma}x}$ (for $n \neq 0$).

(iii) If x is inside the ring [Fig. 23(b)] the modified spectral determinant reads

$$S^{(\lambda_x)}(\gamma) = S(\gamma) + \frac{\lambda_x}{\gamma}[\sinh x \sinh(L-x)\cosh b + \sinh b \sinh L] \tag{F7}$$

and from Eq. (D6) the Cooperon is therefore

$$P_c^{(n)}(x,x) = \left[1 + \coth\sqrt{\gamma}b \frac{\sinh\sqrt{\gamma}x \sinh\sqrt{\gamma}(L-x)}{\sinh\sqrt{\gamma}L} \right] P_c^{(n)}(0,0) \tag{F8}$$
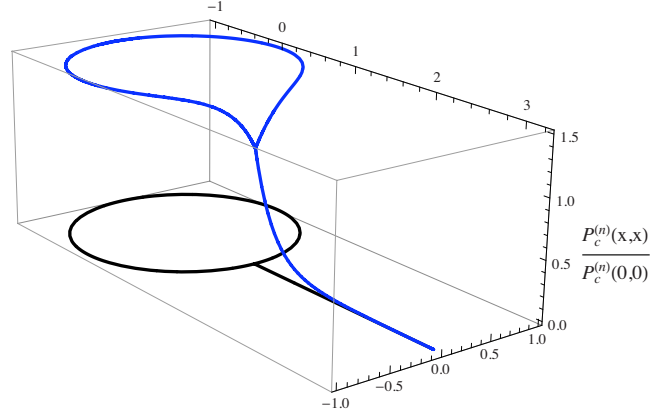
for $x \in$ ring [Fig. 23(b)].

FIG. 24. (Color online) x dependence of the Cooperon $P_c^{(n)}(x,x)$ in the connected ring for $L_\varphi \ll L$.

If $L_\varphi \ll L$ we have $P_c^{(n)}(x,x) \simeq [\frac{3}{2} - \frac{1}{2}e^{-2\sqrt{\gamma}x}]P_c^{(n)}(0,0)$ for $x < L/2$. In the bulk (for x and $L-x \gg L_\varphi$) we have $P_c^{(n)}(x,x) \simeq \frac{3}{2}P_c^{(n)}(0,0)$ (Fig. 24), where the factor $\frac{3}{2}$ corresponds to the ratio of coordination numbers at 0 and at x.

In the opposite limit $L \ll L_\varphi \ll b$ the Cooperon is homogeneous inside the ring, as expected.

From one to N_a arms. In the regime $L_\varphi \ll L$, we have seen that the presence of one arm is responsible for factor $(\frac{2}{3})^n$ originating from the n crossings of the vertex. We immediately deduce that the Cooperon in the ring is $P_c^{(n)}(x,x) \simeq \frac{1}{2\sqrt{\gamma}}(\frac{2}{3})^{nN_a}e^{-n\sqrt{\gamma}L}$.

In order to study the regime $L_\varphi \gg L$, instead of considering the network of Fig. 7 we discuss the case where all arms are attached at the same point in the ring. The calculation is more simple in this case. The two situations were studied in Ref. 7, where it was shown that the Cooperons for the two networks only slightly differ in the regime $L_\varphi \ll L$ and are equal in the regime $L_\varphi \gg L$ of interest now. The effective length is now given by $\cosh\sqrt{\gamma}L_{\text{eff}} = \cosh\sqrt{\gamma}L + \frac{N_a}{2}\sinh\sqrt{\gamma}L \coth\sqrt{\gamma}b$. The structure (F3) still holds. When $L \ll L_\varphi \ll b$ we find $L_{\text{eff}} \simeq \gamma^{-1/4}\sqrt{N_a L}$; therefore $P_c^{(n)}(x,x) \simeq \frac{1}{2}\sqrt{L_\varphi L/N_a}e^{-n\sqrt{N_a L}/L_\varphi}$, whose inverse Laplace transform leads to Eq. (40). This N_a dependence may be more simply obtained by noticing that, given the winding probability $\mathcal{P}_n(x,x;t)$ for one arm, the one for N_a arms is obtained thanks to the substitution $n \to nN_a$ and $L \to L/N_a$.

2. Necklace of rings

We analyze the solution of the diffusion equation in a chain of N_r identical rings of perimeter L. Rings are attached in such a way that the two arms joining two vertices are symmetric. The chain is closed in order to form a necklace for simplicity; as soon as the total length is smaller than L_φ, the results are insensitive to boundary conditions: periodic (isolated necklace) or Dirichlet (chain connected to external contacts). Let us label the vertices joining consecutive rings with greek letters $\alpha, \beta \in \{1, \ldots, N_r\}$. The matrix introduced in Appendix D has the simple form $\mathcal{M}_{\alpha\beta} = \frac{2\sqrt{\gamma}}{\sinh(\sqrt{\gamma}L/2)}[\delta_{\alpha\beta}2\cosh(\sqrt{\gamma}L/2) - a_{\alpha\beta}\cos(\theta/2)]$, where θ is the reduced flux per ring. With our convention the adjacency
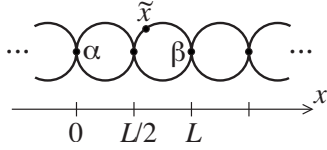
FIG. 25. Infinite chain of rings.

matrix reads $a_{\alpha\beta} = \delta_{\alpha,\beta+1} + \delta_{\alpha,\beta-1}$. Its spectrum of eigenvalues is $2\cos(2n\pi/N_r)$ with $n \in \{1, \ldots, N_r\}$, therefore the spectral determinant reads

$$S(\gamma) = \left(\frac{4\sinh(\sqrt{\gamma}L/2)}{\sqrt{\gamma}} \right)^{N_r}$$

$$\times \prod_{n=1}^{N_r} \left(\cosh(\sqrt{\gamma}L/2) - \cos(\theta/2)\cos\frac{2\pi n}{N_r} \right). \quad \text{(F9)}$$

We replace the product by a sum by considering the logarithm. The sum can then be computed in the limit $N_r \to \infty$,

$$S(\gamma) \underset{N_r \to \infty}{=} \left(\frac{2|\cos(\theta/2)|\sinh(\sqrt{\gamma}L/2)}{\sqrt{\gamma}} e^{\text{argch}[\cosh(\sqrt{\gamma}L/2)/|\cos(\theta/2)|]} \right)^{N_r}.$$

$$\text{(F10)}$$

We now consider $P(x,x')$ when arguments coincide with vertices,

$$P(\alpha,\beta) = (\mathcal{M})^{-1}_{\alpha\beta} = \frac{\sinh\sqrt{\gamma}L/2}{N_r 4\sqrt{\gamma}} \sum_{n=1}^{N_r} \frac{e^{2i\pi n/N_r(\alpha-\beta)}}{\cosh\sqrt{\gamma}L/2 - \cos\frac{2\pi n}{N_r}}$$

$$\underset{N_r \to \infty}{=} \frac{1}{4\sqrt{\gamma}} e^{-|\alpha-\beta|\sqrt{\gamma}L/2}. \quad \text{(F11)}$$

We introduce the notation $\tilde{x} \equiv (x,f)$ to locate points in the chain, where x is the coordinate along the axis (see Fig. 25); in the nth ring $x \in [nL/2, (n+1)L/2]$. The discrete index $f \in \{u,d\}$ indicates whether the point is in the upper branch or the lower branch.

If $\tilde{x}$ and $\tilde{x}'$ are arbitrary positions we can consider the following several situations:

(i) $\tilde{x}$ and $\tilde{x}'$ belong to different rings. The Cooperon is

$$P(\tilde{x},\tilde{x}') \simeq \frac{1}{4\sqrt{\gamma}} e^{-\sqrt{\gamma}|x-x'|}, \quad \text{(F12)}$$

which is *half* of the result for the infinite line.

(ii) $\tilde{x}$ and $\tilde{x}'$ belong to the same ring,

$$P(\tilde{x},\tilde{x}') \underset{\gamma \to 0}{\simeq} \frac{1}{4\sqrt{\gamma}}. \quad \text{(F13)}$$

We conclude that in time representation

$$\mathcal{P}(\tilde{x},\tilde{x}';t) \underset{t \gg L^2}{\simeq} \frac{1}{2} \frac{1}{\sqrt{4\pi t}} e^{-(x-x')^2/4t} \quad \text{(F14)}$$

(the relation is exact when $\tilde{x}$ and $\tilde{x}'$ belong to different rings). The $1/2$ corresponds to the probability to end in one of

the two arms of the rings. It ensures normalization: $\int d\tilde{x}\, \mathcal{P}(\tilde{x},\tilde{x}';t) \equiv \Sigma_{f=u,d} \int dx\, \mathcal{P}(\tilde{x},\tilde{x}';t) = 1$.

The function $W(x,x')$. Expression (F11) can be used to construct $P_d(x,x')$ by taking the limit $\gamma \to 0$. We find for the function entering into description of dephasing

$$W(x,x') = \frac{1}{4}|x-x'| = \frac{1}{2}W_{\text{wire}} \quad \text{(F15)}$$

for x,x' in different rings, and

$$W(x,x') = \frac{1}{2}|x-x'|\left(1 - \frac{|x-x'|}{L}\right) = W_{\text{ring}} \quad \text{(F16)}$$

for $x,x' \in$ same ring. In Eq. (F15) positions are measured along an axis along the chain; the result is *half* of the result for a wire. As it has been already noticed this result can be understood thanks to the relation (E5): when the number of wires between each node is doubled, the resistance is divided by a factor of 2. In Eq. (F16) coordinates are relative to a unique axis inside the ring (it is understood that the expression is periodic); the result is exactly the result obtained for an isolated ring. Once again interpretation is easy: for an infinitely long necklace, when two external wires are plugged inside a ring, no current can flow out of the ring and resistance $\mathcal{R}(x,x')$ is not affected by the remaining rings.

3. Square network

We construct the solution of the diffusion equation in the square network. We use Eq. (D4) to express $P(x,x')$ when the two coordinates coincide with nodes of the network. In this paragraph, nodes are labelled with a couple of integers $\alpha \to (n,m) \equiv \vec{R}$. The matrix $\mathcal{M}$ has the structure

$$(\mathcal{M})_{\vec{R},\vec{R}'} = \frac{\sqrt{\gamma}}{\sinh\sqrt{\gamma}a}[4\cosh\sqrt{\gamma}a\,\delta_{\vec{R},\vec{R}'} - a_{\vec{R},\vec{R}'}]. \quad \text{(F17)}$$

This matrix is easily inverted

$$(\mathcal{M}^{-1})_{\vec{R},\vec{R}'} = \frac{\sinh\sqrt{\gamma}a}{2\sqrt{\gamma}}$$

$$\times \int_{\text{BZ}} \frac{d\vec{Q}}{(2\pi)^2} \frac{e^{i\vec{Q}\cdot(\vec{R}-\vec{R}')}}{2\cosh\sqrt{\gamma}a - \cos Q_x - \cos Q_y}, \quad \text{(F18)}$$

where integral runs over wavevectors of the Brillouin zone. If we are interested in $\mathcal{P}(x,x';t)$ in the large time limit, $t \gg a^2$, this corresponds to consider $\gamma a^2 \ll 1$. In this regime the above integral is dominated by small $\vec{Q}$ and we get

$$P(\vec{R},\vec{R}') = (\mathcal{M}^{-1})_{\vec{R},\vec{R}'} \simeq \frac{a}{2} \int \frac{d\vec{Q}}{(2\pi)^2} \frac{e^{i\vec{Q}\cdot(\vec{R}-\vec{R}')}}{\gamma a^2 + \frac{1}{2}\vec{Q}^2}$$

$$= \frac{a}{2} \int_0^\infty dt\, e^{-\gamma t} \frac{1}{2\pi t} e^{-(a^2/2t)(\vec{R}-\vec{R}')^2}, \quad \text{(F19)}$$

where integral over $\vec{Q}$ has been extended to $\mathbb{R}^2$. We expect

$\mathcal{P}(x,x';t)$ to vary smoothly on the scale of the lattice spacing; therefore we may write

$$\mathcal{P}(x,x';t) \underset{t \gg a^2}{\simeq} \frac{a}{2} \frac{1}{2\pi t} e^{-\|x-x'\|^2/2t}, \qquad \text{(F20)}$$

where $\|x-x'\|$ designates the distance in $\mathbb{R}^2$ between the two points x and x' of the square network. This result calls for two remarks. First, we see that the fact that the diffusion is constrained in the 1D wires forming the square network leads to a continuum limit with a renormalized diffusion constant $D^* = 1/2$, if the diffusion constant is $D = 1$ in the wire (more generally $D^* = 1/d$, where d is the effective dimensionality of the network). Second, the probability presents a prefactor $1/2$ of similar origin than the one in Eq. (F14), ensuring normalization condition. Each elementary plaquette, labeled by $\vec{R} \equiv (n,m)$, contains two wires. Therefore each wire of the network can be labelled with $\vec{R}$ and an index f taking two values (for horizontal or vertical wires). We check that Eq. (F21) is correctly normalized: $\int_{\text{network}} dx \, \mathcal{P}(x,x';t) = \sum_{\vec{R}} \sum_f \int_{\text{wire}(\vec{R},f)} dx \, \mathcal{P}(x,x';t) \simeq \sum_{\vec{R}} 2a \mathcal{P}(x,x';t) \simeq 2a \sum_{\vec{R}} \frac{a}{2} \frac{1}{2\pi t} e^{-(a^2/2t)(\vec{R}-\vec{R}')^2} \simeq 1.$

The generalization of Eqs. (F18)–(F20) to the other regular planar networks can be done. We obtain

$$\mathcal{P}(x,x';t) \underset{t \gg a^2}{\simeq} \frac{1}{2} \tan\left(\frac{\pi}{z}\right) \frac{a}{2\pi t} e^{-(1/2t)\|x-x'\|^2}, \qquad \text{(F21)}$$

where the dimensionless factor $\frac{1}{2} \tan \frac{\pi}{z}$, where z is the coordination number of the lattice, has the interpretation of the area of the Wigner-Seitz elementary cell $\mathcal{A}_z(1+\delta_{z,6})$, where $\mathcal{A}_z$ is defined in the next appendix, divided by the number of bonds per cell.

APPENDIX G: MC OF PLANAR REGULAR NETWORKS

1. Planar regular networks

We apply the formulas (D3) and (D5) to the case of infinite planar regular networks. Let us denote by z the coordination number of the network. The plane can be covered by only three different tillings: the triangular lattice ($z=6$), the square lattice ($z=4$), and the honeycomb lattice ($z=3$).

Let us mention a few properties of regular tillings of flat surfaces.

(i) The lattice of coordination number z is a tilling by regular polygons with p sides. p is related to the coordination number by[94] $(z-2)(p-2)=4$.

(ii) The area of a regular p gone of side a is $\mathcal{A}_z = a^2 \frac{1}{4} p \cot(\pi/p) = a^2 \frac{z}{2(z-2)} \tan(\pi/z)$.

(iii) If boundary effects are neglected, the number of bonds B and the number of vertices V of the planar network are related by $2B = zV$ (z bonds issue from each vertex and each bond touch two vertices).

The matrix (D2) takes the form $\mathcal{M} = \frac{\sqrt{\gamma}}{\sinh \sqrt{\gamma} a} N$, where the matrix N is given by

$$N_{\alpha\beta} = \delta_{\alpha\beta} z \cosh \sqrt{\gamma} a - a_{\alpha\beta} e^{-i\theta_{\alpha\beta}}, \qquad \text{(G1)}$$

where reduced fluxes $\theta_{\alpha\beta}$ describe a uniform magnetic field $\mathcal{B}$. We use Eqs. (D3) and (D5) to express the WL correction

$\Delta\tilde{\sigma} = -\frac{2}{\text{Vol}} \frac{\partial}{\partial \gamma} \ln S(\gamma)$, where the volume is related to the number of bonds Vol$=Ba$,

$$\Delta\tilde{\sigma}(\theta) = \left(\frac{2}{z}-1\right) L_\varphi \left(\coth \frac{a}{L_\varphi} - \frac{L_\varphi}{a}\right)$$
$$- \frac{z}{B} L_\varphi \sinh \frac{a}{L_\varphi} \text{Tr}\left\{\frac{1}{N(\gamma,\theta)}\right\}. \qquad \text{(G2)}$$

$\theta = 4\pi\phi/\phi_0$ is the reduced flux per elementary plaquette. The computation of this expression requires the knowledge of the spectrum of the matrix N, i.e., of $a_{\alpha\beta} e^{-i\theta_{\alpha\beta}}$ (Hofstadter problem[95]).

2. Continuum limit

We study the continuum limit: for $L_\varphi \gg a$ the WL correction probes large scales. Moreover when the flux per cell is much smaller that the flux quantum, $\phi \ll \phi_0$, the result for the planar network coincide with the result for a plane. Let us show that this is indeed the case. We note that the action of the adjacency matrix $a_{\alpha\beta}$ on a smooth function can be replaced by the Laplacian: $a_{\alpha\beta} \to \frac{1}{4} z a^2 \Delta + z$. Therefore in the presence of a weak magnetic field $a_{\alpha\beta} e^{-i\theta_{\alpha\beta}} \to \frac{1}{4} z a^2 (\nabla - 2ieA)^2 + z$ involves the covariant derivative. The spectrum of this operator is the Landau spectrum shifted by $-z$: Spec$(-a_{\alpha\beta} e^{-i\theta_{\alpha\beta}}) \simeq \{z a^2 e\mathcal{B}(n+1/2) - z \,|\, n \in \mathbb{N}\}$, where each Landau level has a degeneracy $d_{\text{LL}} = \frac{1}{\pi} e\mathcal{B} \text{Area}$, "Area" being the total area occupied by the planar network.

In the limit $L_\varphi \gg a$ and $\theta \ll 1$, Eq. (G2) is dominated by the trace which is itself dominated by the bottom of the spectrum of $-a_{\alpha\beta} e^{-i\theta_{\alpha\beta}}$ and it rewrites

$$\Delta\tilde{\sigma} \simeq -a \frac{z}{B} \frac{e\mathcal{B}\text{Area}}{\pi} \sum_{n=0}^{N_c} \frac{1}{\frac{a^2}{2L_\varphi^2} + z a^2 e\mathcal{B}(n+1/2)} + \text{cste},$$

$$\text{(G3)}$$

where we have introduced a cutoff N_c corresponding to the number of the Landau level for which continuum limit fails: $z a^2 e\mathcal{B}(N_c+1/2) \sim z$, the width of the spectrum of the adjacency matrix. This gives $N_c \sim 1/(a^2 e\mathcal{B}) \sim \phi_0/(\mathcal{B}a^2)$. Using that the total number of bonds is related to the number of elementary plaquettes by $B = \frac{2z}{z-2} \frac{1}{2} \times$ (no. of plaquettes) we find Area $= \frac{a^2}{2} \tan(\pi/z) B$. Finally the WL correction may be expressed with the Digamma function[69]

$$\Delta\tilde{\sigma}(\theta \ll 1) \simeq \frac{a}{2\pi} \tan\left(\frac{\pi}{z}\right) \left[\psi\left(\frac{1}{2} + \frac{\phi_0}{4\pi\mathcal{B}L_\varphi^2}\right) - \ln\left(\frac{\phi_0}{\mathcal{B}a^2}\right) \right]$$
$$+ \text{cste}. \qquad \text{(G4)}$$

This result indeed coincides with the result for a plane, Eq. (91), apart for a factor 2 in the argument of Digamma functions. We think that it is worth devoting a small paragraph to this point since it is related to some interesting property of the continuum limit of the result for the networks.

The additional factor of 2 and the continuum limit. As mentioned in Sec. VII the WL correction in the network can be written with a path integral as

$$\Delta\tilde{\sigma}(\theta) = -2\int_0^\infty dt\, e^{-t/L_\varphi^2}$$

$$\times \int_{x(0)=x}^{x(t)=x} \mathcal{D}x(\tau)\exp\left\{-\frac{1}{4}\int_0^t d\tau\,\dot{x}^2 + i\theta\mathcal{N}[x(\tau)]\right\},$$

$$(G5)$$

where $\mathcal{N}[x(\tau)]$ is the (algebraic) number of elementary plaquettes surrounded the trajectories. When one is interested in large time scale properties $(t \gg a^2)$, Eq. (F21) shows that the path integral over Brownian paths $x(\tau)$ in the square network can be replaced by a path integral over planar Brownian curves $\vec{r}(\tau)$ as

$$\int_{x(\tau)\in\text{network}} \mathcal{D}x(\tau)\exp\left(-\frac{1}{4}\int d\tau\,\dot{x}^2\right)$$

$$\rightarrow a\frac{1}{2}\tan\left(\frac{\pi}{z}\right)\int_{\vec{r}(\tau)\in\text{plane}} \mathcal{D}\vec{r}(\tau)\exp\left(-\frac{1}{2}\int d\tau\,\dot{\vec{r}}^2\right).$$

$$(G6)$$

$\theta\mathcal{N}[x(\tau)] = 2e\mathcal{B}\mathcal{A}[x(\tau)]$ coincides with the magnetic flux enclosed by the trajectory multiplied by $2e$, where $\mathcal{A}[x(\tau)]$ is the algebraic area enclosed by the curve $(\mathcal{A}[x(\tau)] = a^2\mathcal{N}[x(\tau)]$ for the square network). Finally we can rewrite Eq. (G5) as

$$\Delta\tilde{\sigma}(\theta \ll 1)$$

$$\simeq -a\tan\left(\frac{\pi}{z}\right)\int_{a^2}^\infty dt\, e^{-t/L_\varphi^2}$$

$$\times \int_{\vec{r}(0)=\vec{r}}^{\vec{r}(t)=\vec{r}} \mathcal{D}\vec{r}(\tau)\exp\left\{-\frac{1}{4D^*}\int_0^t d\tau\,\dot{\vec{r}}^2 + 2ie\mathcal{B}\mathcal{A}[\vec{r}(\tau)]\right\}$$

$$(G7)$$

with $D^* = 1/2$. Then we can use the well-known result[2,13] (91) to get $\Delta\tilde{\sigma}(\theta \ll 1) \simeq \frac{a}{2\pi}\tan(\frac{\pi}{z})[\psi(\frac{1}{2} + \frac{\phi_0}{8\pi\mathcal{B}D^*L_\varphi^2}) - \ln(\frac{\phi_0}{\mathcal{B}a^2})]$ +cste, which precisely coincides with Eq. (G4).

3. Square network

The WL correction can be expressed more explicitly for rational fluxes. We recall briefly a derivation due to Douçot and Rammal[26] for the case of a square network of dimension $V = N_x \times N_y$. We start from

$$\Delta\tilde{\sigma}(\theta) = -\frac{L_\varphi}{2}\left[\coth(\sqrt{\gamma}a) - \frac{1}{\sqrt{\gamma}a}\right.$$

$$\left. + 4\sinh(\sqrt{\gamma}a)\frac{1}{N_xN_y}\text{Tr}\left\{\frac{1}{N(\gamma,\theta)}\right\}\right].$$

$$(G8)$$

We label the vertices $\alpha \equiv (n,m)$, n for the position along the

horizontal direction and m along the vertical direction. We can choose a Landau gauge: $\theta_{\alpha\beta} = m\theta$ for horizontal wires, $\alpha \equiv (n,m)$ and $\beta \equiv (n+1,m)$, and $\theta_{\alpha\beta} = 0$ for vertical wires.

The computation of the MC for a square network submitted to a magnetic field requires to consider the problem of determination of the spectrum of $H_{\alpha\beta} = -a_{\alpha\beta}e^{-i\theta_{\alpha\beta}}$ (Hofstadter problem). In the Landau gauge where the flux is put along the n axis the solution of $H\psi = \varepsilon\psi$ can be written as $\psi_{n,m} = \Phi_m e^{ik_x n}$. We obtain the Harper equation $\Phi_{m-1} + [\varepsilon + 2\cos(k_x + m\theta)]\Phi_m + \Phi_{m+1} = 0$.

If the flux is rational $\theta_{p,q} = 2\pi p/q$ with $p,q \in \mathbb{N}$, the Harper equation is periodic with periodicity q. Therefore, writing $m = r + qs$ with $s \in \mathbb{Z}$ and $r \in \{1,\ldots,q\}$ we can look for solutions of the form $\Phi_m = \varphi_r e^{ik_y s}$. The wave function φ_r is solution of a linear system $D_q\varphi = 0$ where the hermitian $q \times q$-matrix D_q is defined by

$$\begin{cases} D_{r,r} = \varepsilon + 2\cos\left(k_x + 2\pi\frac{rp}{q}\right), & \text{for } r = 1,\ldots,q, \\ D_{r+1,r} = 1, & \text{for } r = 1,\ldots,q-1, \\ D_{q,1} = e^{ik_y}. \end{cases}$$

$$(G9)$$

The secular equation $\det D_q = 0$ gives the q energy bands denoted $\varepsilon_r(\vec{k})$. Interestingly the secular equation can be rewritten as $\det D_q = (-1)^q[P_{p,q}(\varepsilon) - 2(\cos qk_x + \cos k_y)] = 0$, where $P_{p,q}(\varepsilon)$ is a polynomial of degree[96] q. For example, $P_{1,1}(\varepsilon) = -\varepsilon$, $P_{1,2}(\varepsilon) = \varepsilon^2 - 4$, $P_{1,3}(\varepsilon) = -\varepsilon^3 + 6\varepsilon$, etc.

The weak localization correction involves

$$\frac{1}{N_xN_y}\text{Tr}\left\{\frac{1}{N(\gamma,\theta_{p,q})}\right\} = \int_0^{2\pi} \frac{d^2\vec{k}}{(2\pi)^2}\frac{1}{q}\sum_{r=1}^q \frac{1}{4\cosh(\sqrt{\gamma}a) + \varepsilon_r(\vec{k})}$$

$$(G10)$$

therefore

$$\frac{1}{N_xN_y}\text{Tr}\left\{\frac{1}{N(\gamma,\theta_{p,q})}\right\}$$

$$= \frac{1}{q}\int_0^{2\pi} \frac{d^2\vec{k}}{(2\pi)^2}\frac{P'_{p,q}(4\cosh(\sqrt{\gamma}a))}{P_{p,q}(4\cosh(\sqrt{\gamma}a)) - 2\cos k_x - 2\cos k_y},$$

$$(G11)$$

where we have used the equality $\sum_{r=1}^q \frac{1}{\varepsilon - \varepsilon_r} = \frac{P'(\varepsilon)}{P(\varepsilon)}$, valid for a polynomial of degree q: $P(\varepsilon) = \prod_{r=1}^q(\varepsilon_r - \varepsilon)$. Integration over $\vec{k}$ leads to the result (75) of Douçot and Rammal.

[1] S. Chakravarty and A. Schmid, Phys. Rep. **140**, 193 (1986).

[2] E. Akkermans and G. Montambaux, *Mesoscopic Physics of Electrons and Photons* (Cambridge University Press, Cambridge, 2007).

[3] B. L. Altshuler, A. G. Aronov, and D. E. Khmelnitsky, J. Phys. C **15**, 7367 (1982).

[4] T. Ludwig and A. D. Mirlin, Phys. Rev. B **69**, 193306 (2004).

[5] C. Texier and G. Montambaux, Phys. Rev. B **72**, 115327 (2005); Phys. Rev. B **74**, 209902(E) (2006).

[6] M. Ferrier, A. C. H. Rowe, S. Guéron, H. Bouchiat, C. Texier, and G. Montambaux, Phys. Rev. Lett. **100**, 146802 (2008).

[7] C. Texier and G. Montambaux, J. Phys. A **38**, 3455 (2005).

[8] G. Montambaux and E. Akkermans, Phys. Rev. Lett. **95**, 016403 (2005).

[9] C. P. Umbach, C. van Haesendonck, R. B. Laibowitz, S. Washburn, and R. A. Webb, Phys. Rev. Lett. **56**, 386 (1986).

[10] S. Washburn and R. A. Webb, Adv. Phys. **35**, 375 (1986).

[11] F. Schopfer, F. Mallet, D. Mailly, C. Texier, G. Montambaux, L. Saminadayar, and C. Bäuerle, Phys. Rev. Lett. **98**, 026807 (2007).

[12] B. L. Al'tshuler and A. G. Aronov, JETP Lett. **33**, 499 (1981).

[13] G. Bergmann, Phys. Rep. **107**, 1 (1984).

[14] B. L. Al'tshuler, A. G. Aronov, and B. Z. Spivak, JETP Lett. **33**, 94 (1981).

[15] A. G. Aronov and Yu. V. Sharvin, Rev. Mod. Phys. **59**, 755 (1987).

[16] M. Ferrier, L. Angers, A. C. H. Rowe, S. Guéron, H. Bouchiat, C. Texier, G. Montambaux, and D. Mailly, Phys. Rev. Lett. **93**, 246804 (2004).

[17] D. Yu. Sharvin and Yu. V. Sharvin, JETP Lett. **34**, 272 (1981).

[18] B. L. Al'tshuler, A. G. Aronov, B. Z. Spivak, D. Yu. Sharvin, and Yu. V. Sharvin, JETP Lett. **35**, 588 (1982).

[19] B. Pannetier, J. Chaussy, R. Rammal, and P. Gandit, Phys. Rev. Lett. **53**, 718 (1984).

[20] B. Pannetier, J. Chaussy, R. Rammal, and P. Gandit, Phys. Rev. B **31**, 3209 (1985).

[21] Amplitude of Aharonov-Bohm (AB) oscillations can be studied by analysis of the correlation function of the magnetoconductance. Therefore AB oscillations of the conductance (period ϕ_0) are related to universal conductance fluctuations (UCF), while AAS oscillations of the averaged conductance (period $\phi_0/2$) are oscillations of the WL correction. See discussion in the appendix of Ref. 5.

[22] F. Pierre and N. O. Birge, Phys. Rev. Lett. **89**, 206804 (2002).

[23] It was shown in Ref. 7 on the case of the ring connected to arms that the crossover between the "small coherence length regime" $L_\varphi/L \ll 1$ and the "large coherence length regime" $L_\varphi/L \gg 1$ occurs in practice already for $L_\varphi \gtrsim L$. The study of this regime is far from academic since in metallic samples L_φ can be made larger than 10 μm at $T \simeq 20$ mK, like in the experiment in Ref. 24.

[24] C. Bäuerle, F. Mallet, F. Schopfer, D. Mailly, G. Eska, and L. Saminadayar, Phys. Rev. Lett. **95**, 266805 (2005).

[25] B. Douçot and R. Rammal, Phys. Rev. Lett. **55**, 1148 (1985).

[26] B. Douçot and R. Rammal, J. Phys. (Paris) **47**, 973 (1986).

[27] M. Pascaud, Ph.D. thesis, Université Paris 11, 1998.

[28] M. Pascaud and G. Montambaux, Phys. Rev. Lett. **82**, 4512 (1999).

[29] E. Akkermans, A. Comtet, J. Desbois, G. Montambaux, and C. Texier, Ann. Phys. (N.Y.) **284**, 10 (2000).

[30] C. Texier and G. Montambaux, Phys. Rev. Lett. **92**, 186801 (2004).

[31] This question was first considered in a ring in Ref. 32 where the Cooperon was properly weighted in the wires. The rigorous proof and the generalization leading to a proper analysis of non-local effects was provided in Ref. 30.

[32] P. Santhanam, Phys. Rev. B **39**, 2541 (1989).

[33] B. L. Altshuler and A. G. Aronov, in *Electron-Electron Interactions in Disordered Systems*, edited by A. L. Efros and M. Pollak (North-Holland, Amsterdam, 1985), p. 1.

[34] Factors 2 are missing in the L_N given in AAK's original paper (Refs. 2 and 35).

[35] I. L. Aleiner, B. L. Altshuler, and M. E. Gershenson, Waves Random Media **9**, 201 (1999).

[36] Let us estimate this length for the samples of Ref. 11 made of pure silver wires of width $w=60$ nm and thickness $b=50$ nm. Fermi wavelength in silver is $k_F^{-1}=0.083$ nm (i.e., DoS is $2\rho_0 = 18$ eV^{-1}nm^{-3}). This corresponds to $N_c=33\,000$ channels. Diffusion constant was measured to be $D \simeq 0.01$ m^2/s corresponding to elastic mean-free path $\ell_e \simeq 23$ nm and leading to $L_T(T=1$ K$)=0.27$ μm. We get $L_N(T=1$ K$)=2.9$ μm.

[37] Let us remind that $\ell_{\text{loc}} \sim N_c \ell_e$ is the localization length of the infinitely long wire (Refs. 38–40). The perturbation theory is valid for Ref. 33 $L_N \ll \ell_{\text{loc}}$ (i.e., $L_T \ll L_N$), that is above the temperature $T^* \sim D/\ell_{\text{loc}}^2 \sim 1/(N_c^2 \tau_e d)$.

[38] O. N. Dorokhov, JETP Lett. **36**, 318 (1982).

[39] P. A. Mello, P. Pereyra, and N. Kumar, Ann. Phys. (N.Y.) **181**, 290 (1988).

[40] C. W. J. Beenakker, Rev. Mod. Phys. **69**, 731 (1997).

[41] F. Pierre, Ph.D. thesis, Université Paris 6, 2000; Ann. Phys. (Paris) **26** (4) (2001).

[42] M. H. Pedersen, S. A. van Langen, and M. Büttiker, Phys. Rev. B **57**, 1838 (1998).

[43] K. Kobayashi, H. Aikawa, S. Katsumoto, and Y. Iye, J. Phys. Soc. Jpn. **71**, 2094 (2002).

[44] G. Seelig, S. Pilgram, A. N. Jordan, and M. Büttiker, Phys. Rev. B **68**, 161310(R) (2003).

[45] C. L. Kane, R. A. Serota, and P. A. Lee, Phys. Rev. B **37**, 6701 (1988).

[46] S. Hershfield and V. Ambegaokar, Phys. Rev. B **38**, 7909 (1988).

[47] S. Hershfield, Ann. Phys. (N.Y.) **196**, 12 (1989).

[48] M. B. Hastings, A. D. Stone, and H. U. Baranger, Phys. Rev. B **50**, 8230 (1994).

[49] S. Hikami, A. I. Larkin, and Y. Nagaoka, Prog. Theor. Phys. **63**, 707 (1980).

[50] The experiment (Ref. 51) has investigated the regime $L_\varphi \gtrsim L$, where nonlocal effects are important, above 1 K, when decoherence is dominated by electron-phonon scattering. The experimental MC was perfectly fitted by the MC obtained for a simple exponential relaxation.

[51] F. Mallet, Ph.D. thesis, Université Joseph Fourier, Grenoble, 2006.

[52] Note that the function $W(r,r')=P_d(r,r)-P_d(r,r')$ involved in this functional may present a divergent behavior at short distance: this is the case for the metallic film or the hollow cylinder studied in the last section for which $P_d(r,r') \sim \ln\|r-r'\|$. In this case one must come back to the assumption of classical electric fluctuations: due to the Pauli principle, energy transfers between electrons are limited to $\omega \lesssim T$. This amounts to replace the Dirac of the correlator $\langle V(r,t)V(r',t')\rangle_V$ by a function of width $1/T$:

$\delta(t-t') \to \delta_T(t-t')$. The diverging term $\int d\tau P_d(r(\tau), r(\tau))$ should be replaced by a term (Ref. 53) $\int d\tau d\tau' \, \delta_T(\tau - \tau') P_d(r(\tau), r(\tau'))$. Therefore the δ_T function constrains the two trajectories to differ by at most the thermal length $\|r(\tau) - r(\tau')\| \lesssim L_T$. This is the reason why it is sufficient to cut off the divergence of $P_d(r, r)$ in $W(r, r')$ at scale L_T, according to Refs. 3 and 33.

[53] M. Treiber, O. Yevtushenko, F. Marquardt, J. von Delft, and I. Lerner, arXiv:0905.1213 (unpublished).

[54] Note that AAK's treatment (Ref. 3) of electron-electron interaction through some "influence functional" arising from the fluctuations of the classical electric field of the other electrons has initiated several works. A more sophisticated influence functional was constructed in Refs. 55 and 56, where the quantum nature of the environment and the Pauli principle were accounted for, that justifies more rigorously the cutoff procedure of AAK (the difficulty lies in the fact that the "bath"—the other electrons—is of the same nature than the "system"—a given electron). The revival of this question was initiated by the work of Golubev and Zaikin (GZ) (Refs. 57–59). These authors constructed an influence functional that correctly includes the Pauli principle,[55] however their calculation within this basis, which has led to a finite decoherence rate at zero temperature, was later strongly criticized by several authors (Refs. 35, 55, 56, 60, and 61). The discrepancy lies on the contribution of high-frequency processes to the decoherence rate, which are cut off by the temperature T due to Pauli blocking, whereas GZ's approach incorporates the contribution of higher frequencies up to $1/\tau_e$. See Refs. 55 and 61 for a detailed comparison of the different works within the influence functional approach.

[55] F. Marquardt, J. von Delft, R. A. Smith, and V. Ambegaokar, Phys. Rev. B **76**, 195331 (2007).

[56] J. von Delft, F. Marquardt, R. A. Smith, and V. Ambegaokar, Phys. Rev. B **76**, 195332 (2007).

[57] D. S. Golubev and A. D. Zaikin, Phys. Rev. Lett. **81**, 1074 (1998).

[58] D. S. Golubev and A. D. Zaikin, Phys. Rev. B **59**, 9195 (1999).

[59] D. S. Golubev and A. D. Zaikin, Phys. Rev. B **62**, 14061 (2000).

[60] Y. Imry, arXiv:cond-mat/0202044 (unpublished).

[61] J. von Delft, Int. J. Mod. Phys. B **22**, 727 (2008) (available as arXiv:cond-mat/0510563).

[62] A. Comtet, J. Desbois, and C. Texier, J. Phys. A **38**, R341 (2005).

[63] *Handbook of Mathematical Functions*, edited by M. Abramowitz and I. A. Stegun (Dover, New York, 1964).

[64] See also the related work on a ring made of an array of quantum dots: A. G. Semenov and A. D. Zaikin, Physica E (Amsterdam) (to be published). This paper recovers the results of Refs. 4 and 5, but with a saturation of L_φ at low T.

[65] C. Texier, Phys. Rev. B **76**, 153312 (2007).

[66] U. Sivan, Y. Imry, and A. G. Aronov, Europhys. Lett. **28**, 115 (1994).

[67] M. Ferrier, Ph.D. thesis, Université Paris-Sud, 2004.

[68] G. J. Dolan, J. C. Licini, and D. J. Bishop, Phys. Rev. Lett. **56**, 1493 (1986).

[69] I. S. Gradshteyn and I. M. Ryzhik, *Table of Integrals, Series and Products*, 5th ed. (Academic Press, New York, 1994).

[70] J.-P. Roth, C. R. Math. Acad. Sci. **296**, 793 (1983).

[71] $K(x \to 1) \simeq \ln(4/x')$ with $x' = \sqrt{1 - x^2}$.

[72] C. Texier and G. Montambaux, Phys. Rev. B **76**, 094202 (2007).

[73] D. C. Khandekar and F. W. Wiegel, J. Phys. A **21**, L563 (1988).

[74] M. Yor, J. Phys. A **22**, 3049 (1989).

[75] B. Duplantier, J. Phys. A **22**, 3033 (1989).

[76] A. Comtet, J. Desbois, and S. Ouvry, J. Phys. A **23**, 3563 (1990).

[77] G. Montambaux, Phys. Rev. Lett. **63**, 1657 (1989).

[78] J. Bellissard, C. J. Camacho, A. Barelli, and F. Claro, J. Phys. A **30**, L707 (1997).

[79] J. Desbois (unpublished).

[80] In Ref. 33 a distinction between inelastic and "quasielastic" processes is made. The former refer to high energy transfers (however limited by the Pauli principle) while the latter stands for low energy transfers. This separation is motivated by the low energy divergences in the usual perturbative treatment (Ref. 81). This has led AAK to propose the influence functional approach (Ref. 3). We however insist on the fact that the influence functional approach fully account for electron-electron interaction, what is clear on the more sophisticated version (Refs. 55 and 56), and not only to quasielastic processes.

[81] W. Eiler, J. Low Temp. Phys. **56**, 481 (1984).

[82] A quantity frequently introduced is $g = (h/e^2)/R_\square$, the "dimensionless conductance" (of a square connected at two opposite sides). In a plane (two-dimensional electron gas), the sheet resistance $R_\square^{\text{plane}} = 1/\sigma_0$ reads $(h/e^2)/R_\square^{\text{plane}} = \frac{2m*D}{\hbar} = k_F \ell_e$, where $m*$ is the effective mass of charge carriers. In a thin film of thickness b, it is given by $\frac{h/e^2}{R_\square} = 4\pi\hbar\rho_0 bD = \frac{2}{3\pi}k_F^2 b\ell_e$, where ρ_0 is the DoS per volume and per spin channel. Let us give order of magnitude: for a film of silver of thickness $b = 50$ nm with $\ell_e = 23$ nm we obtain $(h/e^2)/R_\square \simeq 34000$.

[83] P. M. Echternach, M. R. Thoman, C. M. Gould, and H. M. Bozler, Phys. Rev. B **46**, 10339 (1992).

[84] M. Eshkol, E. Eisenberg, M. Karpovski, and A. Palevski, Phys. Rev. B **73**, 115318 (2006).

[85] $\Delta\sigma = -\frac{2e^2}{\pi}\int_0^\infty dt \mathcal{P}(t)(e^{-t/\tau_\varphi} - e^{-t/\tau_e})$. The "return probability" is given by $\mathcal{P}(t) = \frac{1}{\text{Area}}\sum_n e^{-E_n t}$, where "energies" correspond to the spectrum of $-(\nabla - 2ieA)^2$: $E_n = 4e\mathcal{B}(n + 1/2)$ for a degeneracy $\frac{e\mathcal{B}\text{Area}}{\pi}$, therefore $\mathcal{P}(t) = \frac{e\mathcal{B}}{\pi \sinh(2e\mathcal{B}t)}$. Using formula [3.541] of Ref. 69, $\int_0^\infty dt \frac{\lambda}{\sinh \lambda t}(e^{-\gamma_1 t} - e^{-\gamma_2 t}) = \psi(\frac{1}{2} + \frac{\gamma_2}{2\lambda}) - \psi(\frac{1}{2} + \frac{\gamma_1}{2\lambda})$ gives Eq. (91).

[86] We recall limiting behaviors: (Ref. 69) $\psi(1/2 + x) = \ln x + 1/(24x^2) + O(1/x^4)$ for large x and $\psi(1/2 + x) = \psi(1/2) + \frac{\pi^2}{2}x + O(x^2)$ for small x; $\psi(1/2) = -C - 2\ln 2$.

[87] Note that this procedure can be avoided by computing the Cooperon beyond the diffusion approximation (by solving the Bethe-Salpether integral equation) as it has been discussed in Ref. 88 [these authors have extended a previous work (Ref. 89) where some contributions were forgotten].

[88] A. P. Dmitriev, V. Y. Kachorovskii, and I. V. Gornyi, Phys. Rev. B **56**, 9910 (1997).

[89] A. Cassam-Chenai and B. Shapiro, J. Phys. I **4**, 1527 (1994).

[90] for the silver samples of Refs. 11 and 51 the factor is $w/a \simeq 0.09$; therefore $(h/e^2)/R_\square^{\text{net}} \simeq 3200$ [compared to $(h/e^2)/R_\square \simeq 34000$ for the film]. From $D \simeq 0.01$ m^2/s we obtain $L_T \simeq 0.27$ μm at $T = 1$ K. Therefore the various Nyquist lengths are $L_N(T = 1\text{ K}) \simeq 2.9$ μm for the infinite wire, $L_N^{\text{film}}(T = 1\text{ K}) \simeq 16$ μm for the 2D film and $L_N^{\text{net}}(T = 1\text{ K}) \simeq 6.4$ μm for the square network.

[91] An equality in law relates two processes with similar statistical properties.

[92] Note that if $\xi_n(\tau) \overset{\text{def}}{=} x_n(\tau) - x_n(t - \tau)$ we have $\xi_n(0) = -n$ and $\xi_n(t) = n$.

[93] C. Texier, J. Phys. A **41**, 085207 (2008).

[94] J. Stillwell, *Geometry of Surfaces* (Springer-Verlag, Berlin, 1992).

[95] The Landau problem on a lattice was solved by Hofstadter (Ref. 97) on the square lattice, by Claro and Wannier (Ref. 98) on the triangular lattice and on the honeycomb lattice by Rammal (Ref. 99). Note however that Hofstadter butterflies were already plotted in an older paper by Langbein (Ref. 100) (see also Ref. 101).

[96] F. Claro and G. H. Wannier, Phys. Status Solidi B **88**, K147 (1978).

[97] D. R. Hofstadter, Phys. Rev. B **14**, 2239 (1976).

[98] F. H. Claro and G. H. Wannier, Phys. Rev. B **19**, 6068 (1979).

[99] R. Rammal, J. Phys. (Paris) **46**, 1345 (1985).

[100] D. Langbein, Phys. Rev. **180**, 633 (1969).

[101] E. Gerlach and D. Langbein, Phys. Rev. **145**, 449 (1966).